Department of Chemical Engineering

Comparison of Turbulence Models for the Prediction of Hydrodynamics of Packed Beds under Supercritical Fluid Condition

Jameson Malang

This thesis is presented for the Degree of
Master of Philosophy (Chemical Engineering)
of
Curtin University

November 2017

STATEMENT OF ORIGINALITY

To the best of my knowledge and belief, this thesis contains no material previously published by any other person except where due acknowledgement has been made.

This thesis contains no material which has been accepted for the award of any other degree or diploma in any university.

Signature : 

(JAMESON MALANG)

Date : 29 November 2017

ACKNOWLEDGEMENTS

First of all, I would like to express my very great appreciation to my supervisors, Professor Moses Oludayo Tadé, Associate Professor Perumal Kumar and Dr. Agus Saptoro for their constructive and valuable feedbacks, patient guidance and enthusiastic encouragement throughout my Master's studies. I really appreciate their prompt responses and constant availability for advice and supervision. I have learnt much from their wisdom and experience. They deserve my respect and gratitude for being exceptional supervisors and mentors. I am also very grateful for any necessary help they gave me when I was at crossroads and did not know which way to look for.

To my family members (Mr. and Mrs. Robert Malang; Mr. and Mrs. Richard Bayom; Mr. and Mrs. Johnson Malang; Mr. and Mrs. Nixon Malang and Mr. Johnstone Malang), they deserve my thanks for continuously supporting me and motivating me crossing to the finishing line. Their patience and understanding have made this possible. A special gratitude is also conveyed to my colleagues who have gone through the ups and downs in the research field, Chan Hiang Bin, Nong Nurnie, Nor Hashimah and Angnes Tiong. To my former superior, Kamaroizan and my current superior, Foad, thanks for your understanding. Your support in reducing my teaching workload is highly appreciated. To my friends, Larry Asu, Dr. Anita Jimmie, Angelina Laing and Florence Singa and former student, Henry Ngu, who provided support and prayers in time of need.

Last but not least, my utmost gratitude also goes to Professor Marcus Lee, the former Dean of Graduate School and Dr. Lenin Gopal, the chairperson of my thesis who provided support and guidance.

May God bless all of you.

ABSTRACT

The rate of transfer processes in a packed bed is governed by the hydrodynamics of the bed and the knowledge of fluid dynamics in the column is very essential in order to efficiently design and operate packed bed columns. Therefore, the study of the fluid flow within the bed using suitable turbulence model is of paramount importance to obtain detailed descriptions of the flow behaviour and transport mechanisms. To date, however, studies on the above areas are mostly for non-supercritical conditions and reports on comparative turbulence models study on hydrodynamic of supercritical fluid flow are not available in the literature. In this work, turbulent flow of a supercritical fluid through a bed of spherical solids was investigated. The results of the velocity profiles, pressure drop, drag coefficient and turbulent intensity were presented in detail.

Comparison of four RANS turbulence models (standard k-ε, RNG k-ε, realizable k-ε and SST k-ω) was performed for subcritical and supercritical fluid regimes in this study. The simulation study was first carried out for flow around single sphere. For RNG k-ε and SST k-ω turbulence models, the results indicate that the predicted velocity profiles from the simulations are agreeable with the literature data of Dixon et al. (2011) with 10% and 6.77% average error respectively. Meanwhile, the comparison of standard k-ε and realizable k-ε with Clift et al. (1978) for drag coefficients are found to be in good agreement with the average errors of 39.2% and 36.7% respectively. It is revealed that SST k-ω can better capture the recirculation region and the near-wake of the sphere more clearly in subcritical and supercritical conditions. Modelling and simulation works were then extended to model packed beds consisting of 6 layers having a total of 56 spheres and 8 layers with 128 spheres for Reynolds numbers (2000 and 20,000), pressures (65 and 80 bar) and temperatures (283.15 and 308.15K). Qualitatively, the results were found to be in good agreement for drag coefficients and pressure drop when they were compared to the literature data of Reddy and Joshi (2008) and Ergun's equation (1952).

Finally, it can be concluded that SST k-ω turbulence model is recommended for single sphere simulation due to its ability to better capture the flow pattern especially for near wake of the sphere. However, in the case of packed bed of spherical

particles, all the RANS turbulence models had shown similar predictive performances.

PUBLICATIONS ARISING FROM THE THESIS

Journal publications

1. Malang, J., P. Kumar, A. Saptoro and M. O. Tade (2017). "Comparison of Turbulence Models for Single Sphere Simulation Study under Supercritical Fluid Condition." Chemical Product and Process Modeling. (Scopus)
2. Malang, J., P. Kumar and A. Saptoro (2015). "Computational Fluid Dynamics-Based Hydrodynamics Studies in Packed Bed Columns: Current Status and Future Directions." International Journal of Chemical Reactor Engineering. 13(3): 289-303. (ISI: 0.623)

Conference publication

1. Malang, J., P. Kumar, A. Saptoro and M. O. Tade (2016). "Comparison of Turbulence Models for Single Sphere Simulation Study under Supercritical Fluid Condition." 29th Symposium of Malaysian Chemical Engineers.

TABLE OF CONTENTS

List of Tables

List of Figures

Nomenclatures

C_d	Drag coefficient
d_p	Particle diameter (m)
D	Column diameter (m)
k	Turbulence kinetic energy (J kg^{-1})
k_r	Effective radial conductivity (W m^{-1} K^{-1})
k_f	Fluid molecular conductivity (W m^{-1} K^{-1})
N	Channel-to-particle diameter ratio (m m^{-1})
y^+	Dimensionless distance from the wall

Greek Symbols

ε	Turbulence dissipation rate (J kg^{-1} s^{-1})
ω	Specific dissipation rate (s^{-1})

Subscripts

f	Fluid
p	Particle
r	Radial
w	Wall

Dimensionless Groups

Nu_w	Wall Nusselt number ($h_w d_p/k_f$)
Re	Reynolds number ($\rho v d_p/\mu$)

Abbreviations

AKN	Turbulence model of Abe, Kondoh and Nagano
BR	Turbulence model of Bellmore and Reid
BSL	Baseline k-ω models
CFD	Computational fluid dynamics
CH	Turbulence model of Chien
CK	Turbulence model of Cotton and Kirwin
DEM	Discrete element method
EVM	Eddy viscosity models
EVM	Eddy viscosity transport
JL	Turbulence model of Jones and Launder
KTA	Nuclear Safety Standard Commission
LES	Large eddy simulation
LRN	Low Reynolds number
LS	Turbulence model of Launder and Sharma
MK	Turbulence model of Myong and Kasagi
RLM	Radially layered composite packing
RNG	Renormalization Group
RSM	Reynolds stress modelling
RTT	Residence time technique
SCPBR	S-CO_2 cooled pebble bed reactor
SST	Shear-stress transport
TBR	Trickle-bed reactors

CHAPTER 1 INTRODUCTION

1.1 Background

Packed bed columns have become a preferable choice over tray columns due to their advantages such as low pressure drop and high separation efficiency (Subramanian et al. 2009). Some examples of the use of packed bed columns in industrial applications include packed bed reactors and supercritical fluid extraction columns. These columns are also used in many other industrial applications, primarily in the chemical and biochemical industry involving reactive separation, absorption, adsorption, distillation and heterogeneous catalysis in chemical reactors (Rahimi and Mohseni 2008). Meanwhile, trickle-bed reactors are mostly applied in oxidation and hydrogenation reactions, hydrocracking, hydrodenitrogenation and wastewater treatment (Al-Dahhan et al. 1997; Lopes and Quinta-Ferreira 2009). Nevertheless, the presence of channelling (Atmakidis and Kenig 2009) and poor temperature control in packed bed columns has led to the development of new correlations in the literature for the improvement of these drawbacks.

The operation of this reactor is subject to the fluid properties, flow rates and the characteristics of the reactor (Robbins et al. 2012). There are three very important transport phenomena involved in fixed and fluidized bed columns which are momentum, mass and heat transfer (Rahimi and Mohseni 2008). These transport phenomena have been the subject of primary interest for many investigators nowadays since heat and mass transfer rate in a packed bed is governed by the fluid flow pattern in the bed. Therefore, it is of paramount importance to study the flow pattern in packed beds and it is always challenging to provide accurate modelling especially when dealing with turbulent flows in which the flow is more complicated. For instance in Choong et al. (2018) for the study of biogas production of palm oil mill effluent (POME), they were dealing with the complex mechanisms of anaerobic digestion system in packed bed reactor. Also in the work of Mâncio et al. (2017), the complicated flow was detected in the catalyst for the thermochemical conversion of palm oil. In addition, a minimal knowledge of the flow pattern can lead to a

limitation in the heat and mass transfer model in packed beds. Studies on the behaviours of packed bed columns mainly with respect to the understanding of physical processes involved have also been subjects of interest for many researchers (Baker and Tabor 2010).

There are numerous researches involving packed beds found in the literature. This literature focuses on the effects of particle-to-tube/column diameter ratio on porosity distribution (Leva and Grummer 1947; Dixon 1988; Theuerkauf et al. 2006; Yang et al. 2016), while other researchers were interested in the pressure drop of the fluids across packed beds (Raynal et al. 2004; Montillet et al. 2007; Said et al. 2011). Due to an extensive study on packed bed porosity, one of the most important correlations, Ergun equation (1952), was proposed. Ergun (1952) developed this widely used correlation for predicting the pressure drop as a function of void fraction. This significant finding has been very useful to many researchers particularly with respect to data validation.

Research related to packed beds can be categorised into two types: (i) Experimental studies and (ii) Computational Fluid Dynamics (CFD) based numerical studies. Due to the high cost of experimental set-up and availability of advanced computing facilities and software, most researchers nowadays prefer to perform their research studies via CFD modelling and simulation. CFD studies are found not only to be affordable but faster as well (Klöker et al. 2005, Chalermsinsuwan et al 2012, Buchmayr et al 2016). This is particularly effective as industries typically encounter lots of challenges in order to maximise plant performance and minimise capital investment. In this regard, process modelling is necessary to assist the optimum design and operation of packed beds (Wen et al. 2007). In the last decade, the use of CFD for detailed analysis of fluid mechanics, heat and mass transfer of various chemical processes and equipment has significantly increased due to its efficiency and highly economical nature compared to experimental studies. One of the main merits of CFD is that it can obtain a deeper insight into underlying physical mechanisms, and it can also provide information on velocity field and phase distribution with high spatial and temporal resolution (Zheng et al, 2007).

There are also mounting interests in research relating to the application of CFD on the modelling and simulation of supercritical fluid (SCF) due to the popular

and promising use of SCF as solvents for extraction, coating or chemical reactions (Fukushima 2000). It is revealed that an in-depth understanding of transport phenomena involving supercritical fluid is vital in a packed bed and CFD is found to be a promising method in capturing detailed views of these transport behaviours. (Guardo 2007). A careful scrutiny of the previous works on packed bed also indicates that the choice of turbulence model is influenced by the type of packing, fluid and the Reynolds number. However, to date, comparative studies on turbulence models for hydrodynamics in packed bed particularly under supercritical fluid condition are limited in the literature.

This work, therefore, aims to carry out CFD simulation on single sphere and packed bed to investigate and predict the velocity profile, pressure drop, drag coefficients and turbulent quantities of supercritical carbon dioxide. Comparative studies of four Reynolds Averaged Navier-Stokes Equations (RANS) turbulence models (Standard, "Renormalization Group" RNG and Realizable k-ε and SST k-ω) were conducted to recommend the most suitable turbulence model for the simulation. A preliminary study on single sphere simulation to compare two RANS turbulence models, RNG k-ε and SST k-ω, was performed to understand the fluid flow phenomena in a single sphere system before further investigations on the complex phenomena inside a packed bed of spherical particles. The single sphere study was compared to and validated against data from Dixon et al. (2011).

1.2 Research Gap and Research Question

To date, it is revealed that research works on comparative study and evaluation of turbulence models for hydrodynamics in packed bed involving supercritical fluid condition are not available in the literature. Most of the existing works focussed only on the use of one or two turbulence models. Investigations on flow pattern at near critical, critical and supercritical conditions are also not extensively researched. Therefore, the following research questions have arisen:

- Which RANS turbulence model is the most suitable for predicting the hydrodynamics in packed bed of supercritical fluid?

- How will the bed porosity affects hydrodynamics in packed bed of supercritical fluid?

Next, the aim and objectives of the research are established based on the research gap and questions.

1.3 Aim and Objectives of this Research

The aim of the research study is to recommend the most suitable RANS turbulence model in investigating the hydrodynamics in packed bed of spherical solids. This study does not involve new model development; rather it employs the existing turbulence models in order to conduct extensive simulations.

This research project has specific objectives as follows:

- To quantify the difference between four widely used Reynolds Averaged Navier-Stokes Equations (RANS) turbulence models (Standard, "Renormalization Group" RNG and Realizable k-ε and SST k-ω) in terms of velocity, pressure drop and drag coefficient profiles as well as turbulent intensity and pressure coefficient around single sphere and within a packed bed of spherical solids under supercritical fluid condition.
- To quantify the difference between flow patterns inside the packed beds having different porosities using CFD simulation for ordinary and supercritical fluids in terms of velocity, pressure drop and drag coefficient profiles.
- To apply sensitivity analysis on the turbulence models parameters to determine a better turbulence model in the validation studies.

1.4 Significance

The significance of this research has been divided into two aspects as below:

<u>Theoretical Contributions</u>

- To date, comparative studies of turbulence models on single sphere simulation under supercritical conditions are limited in the literature. This study can serve as a platform to further investigate the hydrodynamic studies of more layers of solids inside a packed bed column for supercritical fluid flow.

- A comparative study on turbulence models can arrive at the recommendation on "the most suitable turbulence model" for the prediction of complex fluid flow of both supercritical and non-supercritical fluids.
- These studies can also be used as a basis for heat and mass transfer studies in supercritical columns since the heat and mass transfer in packed beds are governed by the hydrodynamics of the bed.

Practical Implementations

- The successful modelling of the present packed bed column could serve as a platform for the development of similar models to predict heat and mass transfer that can improve the design, operation and optimisation of packed bed columns under supercritical condition. This is because this technology is of interest to the food, cosmetics and pharmaceuticals industry and as far as we are concerned, it is in line with the National Key Economic Areas (NKEA) as announced in the tenth Malaysia Plan particularly in the area of palm oil industry. Therefore, research projects related to the enhancement of this technology will receive prioritised government support and attention.
- Recommendation on "the most suitable turbulence model" for the prediction of complex fluid flow can provide higher efficiency and time saving for researchers in their research work especially in dealing with the complex fluid flow in packed bed columns.

1.5 Scopes of Study

The scopes of this research are outlined below:

- Reynolds numbers of 2,000 and 20,000 are selected for this research to represent the transition and turbulent flow regimes. This is also a good representation of the operation range (Bai et al. 2009).
- Packed beds consisting 56 spheres and 128 spheres arranged in 6 and 8 layers respectively were taken as computational geometrical models. These two models were used in the investigating of the effect of different porosities on flow pattern.
- Four Reynolds Averaged Navier-Stokes Equations (RANS) turbulence models (Standard, "Renormalization Group" RNG and Realizable k-ε and SST k-ω) were

adopted as they are the turbulence models most widely employed in the modelling and simulation of packed bed columns. Furthermore, these models are simple and faster to run.

- Temperatures of 298.15 and 308.15 K and pressures of 65 and 80 bar were chosen to cover the three phases of carbon dioxide: liquid, vapour and supercritical. These selected temperatures and pressures also include the sub-critical and supercritical regions of carbon dioxide to examine the phase behaviour of carbon dioxide in different regions.
- Supercritical carbon dioxide was chosen as a simulation fluid due to its increasing popularity as a greener solvent for supercritical extractions (Bingjie et al. (2002); Eisenmenger (2005); Zaidul et al. (2006); Zaidul et al. (2007); Fernandes et al. (2008); Fernandes et al. (2009); Stamenić and Zizovic (2013)). In addition, it is often promoted as a sustainable solvent due to its non-inflammable properties, low toxicity and abundance.
- The packed bed column in this study is intended for liquid-liquid extraction.

1.6 Thesis Overview

This thesis is structured in six chapters outlined below where Figure 1.1 shows the links between these chapters.

Chapter 1 introduces a brief background of packed bed columns, the aim and objectives of this research, significance or motivation, contributions of this study, the scope of study and thesis overview.

Chapter 2 presents a critical review of the existing literatures and highlights studies related to the study of packed columns in various areas of research. The background of packed bed column is thoroughly reviewed. Past works by other researchers with regard to CFD as well as supercritical fluid are also discussed and summarised.

Chapter 3 describes the methodology of this research covering the geometry creation, meshing details, operating conditions as well as the physical setup of the simulations.

Chapter 4 reports a single sphere study as the preliminary study of CFD simulation to determine the velocity profiles, pressure drop, drag coefficient, turbulent intensity and pressure coefficent values. In this chapter, the work of Dixon et al. (2011), Clift et al. (1978) and Constantinescu and Squires (2004) were used as primary sources for model validation.

In Chapter 5, results and discussion pertinent to the investigation of the effects of porosity on the velocity, pressure drop and drag coefficient of packed bed were presented.

Chapter 6 concludes this research work. This chapter also presents the recommendations and future directions of the research. In the appendix, the graphs and contour plots for data generated by using CFD simulation which were not included in Chapter 4 are also presented. This is to provide a clearer view of the results obtained via CFD simulations since some graphs have shown similar patterns and were already presented in Chapter 4.

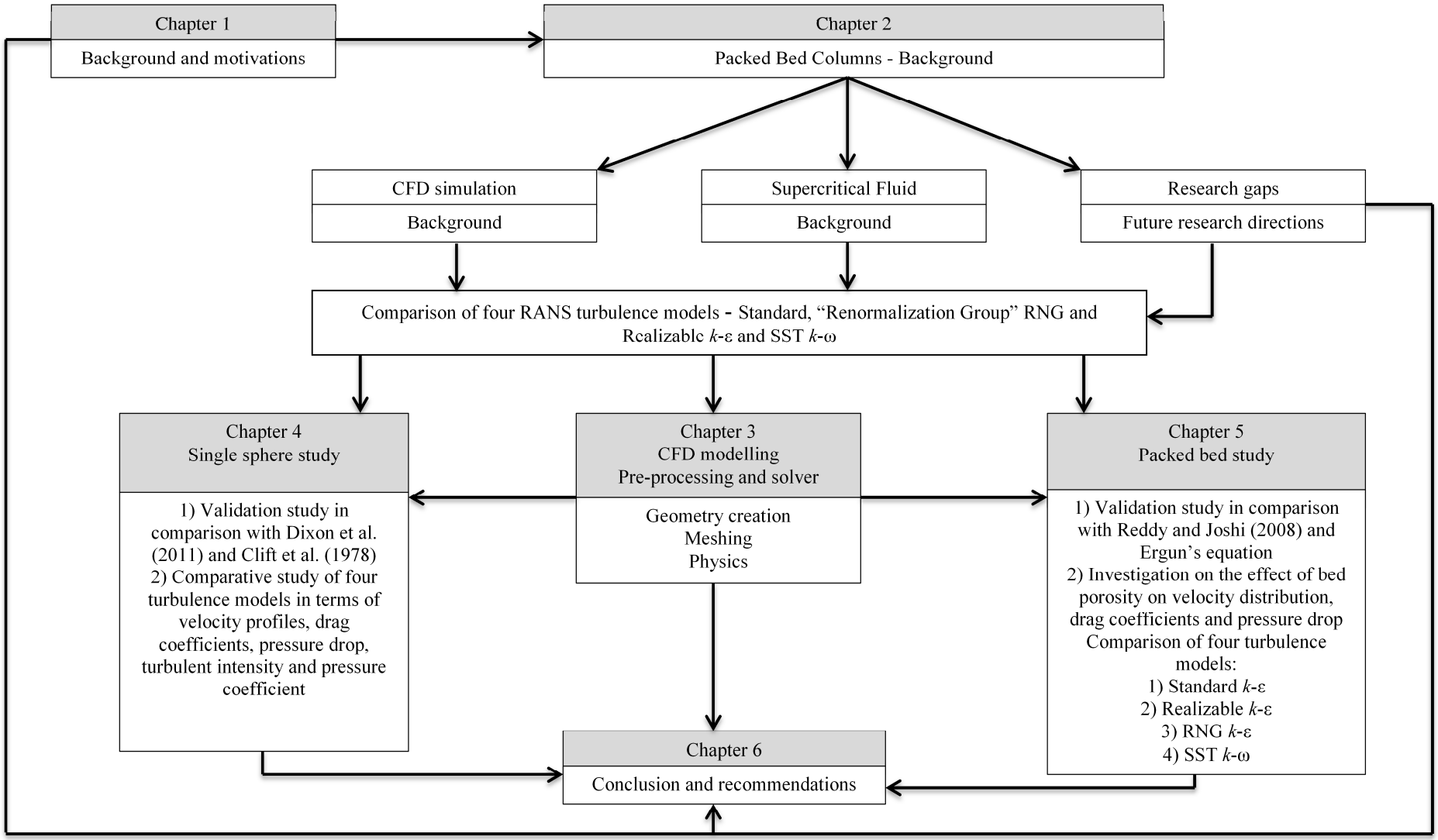

Figure 1.1 Schematic diagram of thesis layout

CHAPTER 2 LITERATURE REVIEW

This chapter introduces the state of the art knowledge for packed bed columns, single sphere simulation works, supercritical fluid and computational fluid dynamics modelling. It also conveys the application of packed bed columns, supercritical fluid and computational fluid dynamics modelling in the chemical engineering fields.

2.1 Packed Bed Column

A packed bed is a cylindrical vessel filled with packing materials. These materials may be gravel, charcoal, catalyst, powdered size component of plants and other types of solids. The size and shape of the packing material is generally random. The shape may range from identical geometric shapes such as spheres, or cylinders to small objects like Raschig rings (Baker and Tabor 2010). The schematic diagrams of typical packed beds are as shown in Figures 2.1 – 2.3.

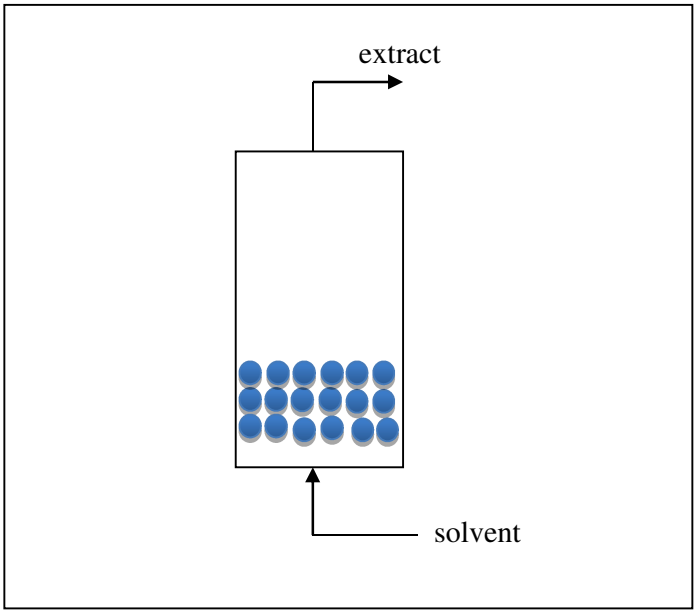

Figure 2.1 Schematic diagram of a typical packed bed of solid-liquid extraction column.

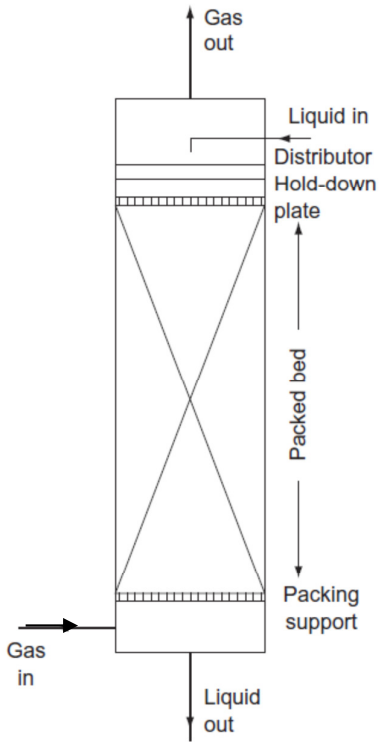

Figure 2.2 Schematic diagram of a typical packed bed absorption column. (Towler and Sinnott 2013)

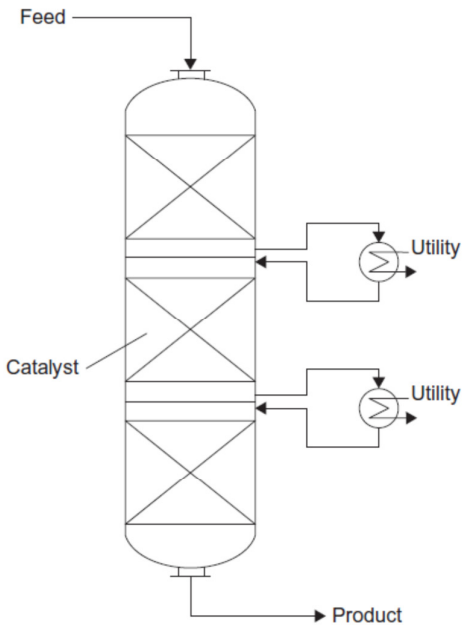

Figure 2.3 Schematic diagram of a typical packed bed reactor. (Towler and Sinnott 2013)

Two types of packings are often used in packed bed columns: structured and unstructured packings. Structured packings have widespread application in a lot of separation processes such as distillation and absorption. Worldwide, structured packing has equipped approximately 25% of all the refinery vacuum towers (Brunazzi and Paglianti 1997). Various materials such as metal, ceramic or plastic can be used to make structured packing depending on its application (Haghshenas Fard et al. 2007). Structured packing proves popular compared to the traditional trays and random packings as they feature moderately high surface area and void fraction that leads to the improvement of mass transfer performance and capacity of the columns with relatively low pressure drop (Hosseini et al. 2012). Other advantages of structured packings compared with the conventional dumped packings are higher separation efficiency, better radial mixing, lower pressure drop and higher capacity. In addition, they also demonstrate strong preferential flow directions for both liquid and gas flow because of crossing channels (Mahr and Mewes 2007).

However, structured packings also have disadvantages such as high cost, and low capacity and efficiency at high flow rates. Due to the aforementioned disadvantages of structured packings, it is necessary to increase the separation efficiency and decrease capital cost in order to obtain a suitable design for these columns (Hosseini et al. 2012). Hence, various studies to increase the columns efficiency have been done. For example, Koh and Guiochon (1998) investigated the impact of column length on the characteristic of packed bed column namely with regards to the packing density, bed porosity, the permeability and the column efficiency. It is found that the columns made with spherical particles were more homogeneous, had a higher external porosity and specific permeability as well as higher efficiency compared to those made with the irregular particles.

For the study of randomly packed distillation column, it is revealed that three main parameters need to be considered in the designing of the column. These three parameters are capacity or flood point, pressure drop and height equivalent to a theoretical plate (HETP) (Senol 2001). There are several works that have employed these three parameters in their studies. Stichlmair et al. (1989) developed a model that covers all flow regimes in packed columns to predict pressure drop and flooding in which gas and liquid flow counter currently. This model has been developed by considering two constraints: (1) They minimised the number of correlating constants and (2) They found out that the basic geometric properties of the packings, such as

surface area and void fraction are needed to describe the differences in packing behaviour. By employing these constraints, the prediction of hydrodynamic pattern in packed bed is more relevant and rigorous. Wagner et al. (1997) established a new model for the prediction and correlation of mass transfer rates in distillation columns containing newer high-efficiency random packings namely IMTP, CMR, Fleximax and Nutter. The model fitted the experimental values of height equivalent to a theoretical plate (HETP).

In packed column, depending on the hydrodynamic condition and physico-chemical properties of the flow, mass transfer effectiveness can be influenced by the flow patterns of both dispersed and continuous phases. In order to design packed columns efficiently, the knowledge of mass transfer coefficients and appropriate fluid dynamics in the columns is very vital (Rahbar-Kelishami and Bahmanyar 2012). Hosseini et al. (2012) emphasised on the important design parameter in packed bed that is liquid holdup which has an impact on the mass transfer performance and pressure drop in the bed. They also highlighted that the main parameters in determining liquid holdup are the thickness and width of a liquid rivulet flowing on the packing surface. Thus, heat and mass transfer rate in a packed bed is highly governed by the fluid flow pattern in the bed.

2.2 Previous Works on Single Sphere

It is of fundamental importance to study transport phenomena inside a packed bed in order to gain better understanding of the interactions between fluid flow, heat transfer, diffusion and reaction (Dixon et al. 2011). In view of this, a CFD simulation has been widely employed throughout the investigations of transport phenomena inside packed bed (Logtenberg and Dixon 1998; Coussirat et al. 2007; Fernandes et al. 2008). Nevertheless, due to the complex transport phenomena involved in a bed of particles, several researchers have carried out single particle simulations to study the fundamental flow behaviours inside a packed bed (Van Der Merwe and Gauvin (1971); Dixon et al. (2011)).

The characteristics of flow past a sphere at various Reynolds numbers have been investigated by many researchers. At low Reynolds numbers ranging from 0.01 to 400, Le Clair et al. (1970) accurately predicted drag on a sphere. They compared their numerical findings to the theoretical results reported by Stokes (1851), Oseen (1927), Goldstein and Burgers (1931), Proudman and Pearson (1957), Jenson (1959),

Rimon and Cheng (1969), and Carrier (1953). The results were also validated with the experimental data provided by Maxworthy (1965) and Steinberger et al. (1968). In another study, Natarajan and Acrivos (1993) applied a finite-element method to examine the stability of the axisymmetric flow past a sphere. Instability of flow was found at Reynolds number 200 and this was attributed to the transition from the steady axisymmetric wake to the steady, non-axisymmetric, double-thread wake. This finding was comparable to that of Tomboulides (1993) who found out that the flow instability occurred at Reynolds number = 212. Johnson and Patel (1999) numerically and experimentally investigated steady and unsteady flow up to Reynolds number 300 for an incompressible viscous fluid past a sphere. They observed that for Reynolds number up to 200, flow was axisymmetric and steady. Flow was found to be non-axisymmetric steady for Reynolds numbers between 210 and 270 and became unsteady at Reynolds numbers greater than 270. At Reynolds number equal to 300, the results exhibited a highly organised periodic flow dominated by vortex shedding. Campregher et al. (2006) utilised an in-house immersed boundary (IB) method called Virtual Physical Model to numerically simulate flow around a sphere for Reynolds numbers ranging from 100 to 1000. Using this method, they were able to simulate two-phase flows and fluid-structure interactions with no requirements of remeshing the fluid grid. Their results for flow pattern and drag coefficients were consistent with the literature data.

Studies of flow around a sphere at high Reynolds numbers were also available in the literature. Breuer (1998) studied numerical and modelling aspect on the quality of LES solutions for turbulent flow past a circular cylinder at a subcritical Reynolds number of Re = 3900. In this work, the recirculation region was found to exist behind the cylinder and the numerical scheme has strong impact on the structure and the length of the recirculation bubbles behind the cylinder. Another previous study on subcritical and supercritical conditions was done by Constantinescu and Squires (2004). In their research, they numerically analysed subcritical and supercritical conditions around a sphere in a uniform flow by using detached-eddy simulation (DES). Pressure distribution, skin friction and drag were predicted for Reynolds numbers between 10^4 and 10^6. For both subcritical and supercritical conditions, reasonable predictions were reported in terms of mean drag and pressure distribution. However, poor predictions of skin friction were detected due to the simplified boundary layers. The wake structure in the subcritical regime

was assumed a helical-like form whereas in the supercritical regime was characterized by "regular" shedding of hairpin-like vortices.

A study by Bakic et al. (2006) utilised Laser Doppler Anemometry (LDA) to investigate the turbulent flow around a sphere. This sphere was attached to a sting at the rear stagnation point in wind tunnels. They also conducted visualisation experiments to investigate the wake structure, separation and laminar-turbulent transition behind the sphere in a wind tunnel ($22{,}000 < Re < 400{,}000$) and water channel ($50{,}000 < Re < 300{,}000$). They compared experimental data with simulation results obtained from LES and the agreement was relatively good. The wake structure of a sphere and the vortex configuration were found to be more complex compared to the simple helical or double helical vortex structure.

A more recent study by Dixon et al. (2011) used a wide range of low to high Reynolds numbers ($400 < Re < 20{,}000$) and focussed on typical high flow rates in industrial steam reformers. Drag coefficient (C_d) and heat transfer Nusselt number (Nu) results were also estimated. For the above range of Reynolds numbers, they obtained good predictions of C_d using a large eddy simulation (LES). The study revealed that Nu was accurately predicted using a combined Reynolds-averaged Navier-Stokes (RANS) method and shear-stress transport (SST) k-ω. Besides that, this study also focussed on the meshing development for single sphere CFD simulation. The meshing details as well as the grid and domain independence studies were being stated clearly and systematically by the authors. Therefore, it has been employed in the present study for the application of supercritical fluid and the results of the single sphere study are used to validate the application of supercritical fluid in packed bed.

It has been acknowledged that the choice of turbulence model has a great impact on the accuracy of CFD simulations (Karimi et al. 2011). To date, however, there is limited literature in the area of comparative studies and evaluation of the turbulence models for a single sphere simulation especially involving supercritical fluid. Most of the existing works focussed only on the use of one or two turbulence models (Constantinescu and Squires (2004); Dixon et al. (2011)). Investigations on flow past a sphere at near critical, critical and supercritical conditions are also not extensively researched.

2.3 CFD Modelling of Packed Columns

The use of Computational Fluid Dynamics (CFD) for detailed analysis of fluid mechanics and heat and mass transfer of chemical processes and equipment has substantially increased in the last decade. This is due to its efficiency and cost effectiveness compared to experimental studies. CFD enables a feasible insight into fundamental physical mechanisms by providing velocity field and phase distribution with high spatial and temporal resolution (Zheng et al. 2007). CFD is proven to be a promising tool in evaluating the phenomenon inside packed bed columns (Logtenberg and Dixon 1998; Guardo et al. 2007; Fernandes et al. 2008). Furthermore, in the design and optimisation of structured packings, the use of CFD simulation is proven to be both quick and cheap (Haghshenas Fard et al. 2007; Mahr and Mewes 2007; Raynal and Royon-Lebeaud 2007; Wen et al. 2007).

In the modelling of packed beds, an adequate qualitative knowledge and a correct quantitative explanation of the heat transfer and fluid flow are very vital to the researchers particularly when dealing with strong exothermic and endothermic processes (Nijemeisland and Dixon 2004). In fact, studies on the simulation of packed beds have been widely presented in the literature. Detailed CFD for packed beds has been reviewed and a great number of CFD models have been developed. The previous works reported by several authors on CFD modelling of packed beds can be grouped into two categories namely unstructured and structured packings. A summary of previous works on CFD modelling of hydrodynamics studies in packed beds is presented in Table 2.1.

Table 2.1 Summary of previous work on CFD modelling of hydrodynamics studies in packed beds

A. CFD modelling of hydrodynamics studies in packed beds with unstructured packings						
Reference	Type of System	Findings	Limitation/Future Study	Turbulence Model Used	Types of Fluid/Flow	*Re* range
Jafari et al. (2008)	Packed bed reactors (non-overlapping spheres)	LES model shows better agreement with results of other researchers in predicting pressure drop	They need to further analyse on the details of the mechanism of turbulent generation	LES and RSM	Non supercritical fluid (Continuous phase)	More than 0.003
Atmakidis and Kenig (2009)	Irregular packed bed of spheres	Channelling was observed near the wall but also partly existed in the inner regions of the packing	Further improvement can be made to the models by developing better empirical correlations	–	Non supercritical fluid	< 100
Bai et al. (2009)	Packed bed reactors of 135 spherical particles	There are variations between pressure drop values predicted via CFD with the experimental measurements depending on the porosity deviation	The modelling of the entire bed was unmanageable due to the limitation of the available computational resources. Therefore, only a segment of the entire bed was included in CFD simulation	Standard k-ε, RNG k-ε, Realizable k-ε, Spalart-Allmaras, RSM and DEM	Air (Non supercritical fluid – continuous phase)	2000 to 20000
Lopes and Quinta-Ferreira (2009)	Fixed bed reactors (trickle-bed) of 200 spheres with 13 layers	There is no strong dependency of CFD code and y^+ values	Problem to account properly the boundary layer	Standard k-ε, RNG k-ε, Realizable k-ε and RSM	Multiphase flow (Non supercritical fluid – continuous and disperse phase)	Wide range of *Re*
Magnico (2009)	Tubular fixed beds of 236 and 620 spheres	They used another approach to describe the heat transfer mechanism which consists of calculating the velocity and temperature profiles at the pore level as well as applying direct numerical simulation and resolution of the heat balance equation	To improve this work, the resolution around the contact points should be increased by applying a grid adaptation. Also, to better define the solid surface, the use of immersed boundary method can be considered	–	Air (Non supercritical fluid – continuous phase)	80 to 160
Augier et al. (2010)	Packed bed of spherical particles	CFD can predict hydrodynamics and transfer at the scale of particles inside granular media	This work can be extended to more complicated packings of non-spherical particles with no empirical correlations	DEM	Fuel oil (Non supercritical fluid – dispersed phase)	1 to 100
Baker et al. (2011)	Packed bed	Image based meshing using 3D MRI was revealed to be accurate in reconstructing packed beds with complex geometries and boundaries	With the development in computational power and resolution of non-invasive methods, more research on much larger beds of particles can be done	SST k-ω	Air (Non supercritical fluid)	1431 to 5074

Eppinger et al. (2011)	Fixed beds of monodisperse spherical particles	New method for meshing spherical fixed beds which is able to calculate accurately pressure drop as well as the local and global porosity within a shorter time	To generate the mesh of around 800 spheres or 6 million volume cells, it can be overcome by dividing fixed bed into smaller parts. After that, each part is being mesh separately and at the end they will be combined together	Realizable k-ε	Non supercritical fluid	10, 100 and 1000
Dixon et al. (2012)	Fixed bed of spheres	Useful validation of CFD works can be obtained from this study for fixed bed heat transfer at high *Re*	Due to computational limitations, only the simulation of tubes containing two largest sizes of spherical packing were done	Realizable k-ε	Air (Non supercritical fluid)	2000 to 27000 for N = 5.45 and 1600 to 5600 for N = 7.44
Riefler et al. (2012)	Packed bed of spheres	Their model has considered the curved fluid flow of the packing together with the combination of the porosity of the geometry and the tortuosity of the fluid flow	The number of cells were limited by enlarging cell volumes	–	Non supercritical fluid	0.00275 to 177
Zobel et al. (2012)	Packed bed reactor	3D structures on the bed walls can be imposed in order to modify the void fraction distribution	Optimal wall structures should be determined to maximise the lateral mixing under various process conditions	Realizable k-ε	Air (Non supercritical fluid)	–
Dixon et al. (2013)	Fixed beds of spheres	To obtain more reliable results for drag coefficient, local method where spherical caps are removed or bridges are inserted only at the points of contact are performed	Any considerations of practicality with regards to implementation were not examined	SST k-ω	Air (Non supercritical fluid – dispersed phase)	500 to 10,000
Yang et al. (2016)	Packed bed of spheres	The RLM can reduce the flow resistance and improve the heat transfer in the bed	The construction of a stable composite random bed with designed or optimal packing structure for practical industry was not easy	RNG k-ε, DEM	Air (Non supercritical fluid)	Less than 2000
Burström et al. (2017)	Packed bed of spheres	The discrete model can be used for non-Stokian flow	Simulations for a continuous model is difficult to perform due to the large quantities of pores in the domains of the porous media	k-ε	Non supercritical fluid (dispersed phase)	Less than 1000

Dorn et al. (2017)	Packed bed chromatographic columns	It is found out that the hybrid packing method evaluated the best results for the hydrodynamics stability of the chromatographic column	Future work will extend towards the measurement and numerical simulation of component diffusion	DEM	Non supercritical fluid	–
Dolamore et al. (2018)	Packed bed of spheres	CFD methods based on LBM were used to describe the chromatography behaviour of ordered configurations of particles	The results can be extended beyond ordered lattices of monodisperse spheres	–	Non supercritical fluid	–

B. CFD modelling of hydrodynamics studies in packed beds with structured packings						
Reference	Type of System	Findings	Limitation/Future Study	Turbulence Model Used	Types of Fluid/Flow	*Re* range
Logtenberg and Dixon (1998)	Fixed bed of 8 spheres	CFD is an useful aid in evaluating heat transfer behaviour in fixed bed reactor	Limitation of the model geometry – the spheres did not touch each other and the wall due to the problem near the contact points for the stability of the numerical solution and the mesh generation	*k-ε*	Air (Non supercritical fluid – dispersed phase)	9 to 1450
Logtenberg et al. (1999)	Fixed-bed reactor (10 spheres in 4 layers)	They have extended the use of CFD by including particle-particle and wall - particle contact points for more realistic and larger models of fixed bed	They were unsure of the suitable turbulence model to be used for specific geometry	*k-ε*	Air (Non supercritical fluid – dispersed phase)	42 to 3344
Calis et al. (2001)	Packed bed of 8 – 16 spheres	The CFD code is proven to be able to predict pressure drop of packed bed of spheres for $1<N<2$	Computational constraint – The size of the grid cell is so small	*k-ε*, RSM & zero equation model	Non supercritical fluid in single phase flow	1.0×10^{-2} to 5.0×10^{4}
Romkes et al. (2003)	Composite Structured Packing (CSP)	The model was able to predict the characteristic of packed bed	Computational constraint – The required number of the grid cells is limited	*k-ε*, RNG *k-ε* & RSM	Non supercritical fluid (dispersed phase)	127 to 1.27×10^{5}
Nijemeisland and Dixon (2004)	Fixed bed of 72 spheres in 6 layers	They were able to identify the parameters which affect the design of catalyst particles that are more effective for heat transfer in fixed bed	Memory restriction - They were unable to create fine graded mesh for the full-bed model	RNG *k-ε*	Non supercritical fluid (dispersed phase)	1000
Guardo et al. (2005)	Fixed bed of 44 spheres	CFD proves to be useful for the calculation of pressure drop in fixed bed reactors	The models do not appropriately estimate the transition regime	Spalart-Allmaras, Standard *k-ε*, RNG *k-ε*, Realizable *k-ε* and Standard *k-ω*	Air (Non supercritical fluid)	less than 1000

Coussirat et al. (2007)	Packed bed reactors of 44 spheres	Data from much simpler flows were incorporated with the EVM turbulence model to predict complicated flow	No strong curvature was found in flow streamline	EVM (Spalart-Allmaras & Standard k-ε) and RSM (Daly Harlow model)	Air (Non supercritical fluid – dispersed phase)	100 to 850
Fernandes et al. (2007)	SULZER EX (Supercritical fluid extraction column)	Differential energy balance was incorporated to the packed column	The model always predicts a steady state temperature since the fluctuations were not fed to the model	–	Supercritical CO_2 (dispersed phase)	–
Haghshenas Fard et al. (2007)	MELLADUR 450Y (Packed distillation column)	CFD is a promising tool in evaluating the performance of structured packed column	They neglected the effect of flow channelling, flow distribution issues and liquid back mixing in the model	k-ε	Air & water – for pressure drop, methanol/ isopropanol – for mass transfer (dispersed phase)	–
Mahr and Mewes (2007)	Sulzer Mellapak 250Y	Prediction of dynamic flow fields was possible even for extreme maldistribution of the phases	–	–	Water and air (Non supercritical fluid – continuous phase)	–
Fernandes et al. (2008)	SULZER EX (Supercritical fluid extraction column)	In the design of SCF extraction column, they found out that dry pressure drop is an important parameter	The study of simultaneous heat and mass transfer need to be done in order to determine the entire hydrodynamics of the column since the study of pressure drop solely is not enough	Realizable k-ε	Supercritical CO_2 and air (dispersed phase)	Wide range of Re
Khosravi Nikou and Ehsani (2008)	Flexipac 1Y	Flow distribution as well as heat and mass transfer can be predicted by using k-ω and BSL	Since they assumed laminar flow in liquid phase, so they were unable to predict the results of heat and mass transfer via different turbulence model	k-ε, RNG k-ε, k-ω and BSL k-ω	2 phase flow (Non supercritical fluid)	Wide range of Re
Reddy and Joshi (2008)	Fixed bed (151 particles) and expanded beds (105 particles and 55 particles)	The model was unable to capture the curvature effects and the boundary layer separation at high Re	The model can be used in chromatographic and biological separation	k-ε	Water in single phase flow (Non supercritical fluid)	0.1 to 10,000
Atmakidis and Kenig (2009)	Regular packed bed of spheres	Strong channelling was observed throughout the bed near the wall particularly with high local void fraction	Further improvement can be made to the models by developing better empirical correlations	–	Non supercritical fluid (dispersed phase)	< 100

Fernandes et al. (2009)	SULZER EX (Supercritical fluid extraction column)	Pseudo-single phase modelling approach is efficient in predicting the wet pressure drop in complex packing geometry	Computational constraint – Only one-third of the packing height was simulated	Realizable k-ε	Supercritical CO_2, water and soya bean oil (dispersed phase)	–
Haghshenas Fard et al. (2009)	Montzpak 250Y & 250X, KATAPAK-S, Flexipac 1Y, 2Y & 3Y	The pressure drop in the structured packings was able to be decreased by using their model	–	LRN k-ε	Non supercritical fluid	Wide range of *Re*
Said et al. (2011)	Montzpak & Flexipac 1Y	The pressure drop and aerodynamic behaviour of the structured packings were able to be predicted	The pressure drop in the structured packings were affected by the change in direction of gas flow and the presence of liquid	RNG k-ε, realizable k-ε & SST k-ω	Non supercritical fluid	–
Hosseini et al. (2012)	Sulzer BX & Gempak 2A	The model may be useful for packed columns that are operating in the range of 80% capacity in terms of design and optimization	Their predicted pressure drop results had some deviations from the experimental data due to the simplifying assumption	k-ε, RNG k-ε & k-ω	Air/water (Non supercritical fluid – dispersed phase)	250 to 2250
Robbins et al. (2012)	Packed bed reactor (Trickle bed)	Developed and validated CFD codes for the prediction of one phase flow by using experimental data from MRI	The validation of single phase flow can be extended to investigate two phase flow at low Mach numbers. The study of the effect of numerical parameters and the mesh on solution stability and accuracy can be considered as well	–	Water (Non supercritical fluid – dispersed phase)	27, 55, 111 and 216
Yu et al. (2015)	Pebble bed reactor	Body-centred cuboid (BCCa) arrangement is adopted for the pebbles, contact points are closer to the rear of the pebble. So, promoted less flow detachment, as a result decrease the temperature in the rear region of the pebble	KTA correlation is claimed to be conservative in the SCPBR core design	EVT	Carbon Dioxide (supercritical fluid)	–

A close look at the tables reveals that the hydrodynamic studies in fixed beds containing spherical particles were subject to extensive investigations compared to other types of packing. In earlier studies of fixed bed of spheres, it is observed that the authors focussed on less than 50 spheres in a bed by means of CFD simulation. For instance, Logtenberg and Dixon (1998) evaluated the radial effective thermal conductivity ratio, k_r/k_f and the dimensionless wall heat transfer coefficient, Nu_w for fixed bed of 8 spheres at different locations in the bed. The values of k_r/k_f and Nu_w were predicted slightly lower than the experimental measurements. This is due to the fact that the spheres were not in contact with each other and the wall. They also investigated the depth, pressure and wall temperature dependence of the effective heat transfer parameters as well as the effect of the temperature profile measurement position above the bed. In the following year, Logtenberg et al. (1999) studied the flow and temperature profile within a bed of 10 spheres. In order for them to obtain a better insight into the flow and heat transfer characteristics in fixed bed reactors, studies on the interaction between flow profile and temperature were discussed. They solved the three-dimensional Navier-Stokes equations to better understand the fluid flow and heat transfer. They also observed the formation of eddy near the wall which had caused a change in the fluid flow behaviour for the predicted Nu_w within $182 < Re < 800$.

In another study Calis et al. (2001) examined the pressure drop and velocity profile in a packed bed of 8 to 16 spheres by using commercial CFD code (CFX-5.3). They used k-ε model and RSM for Reynolds number between 1.0×10^{-2} and 5.0×10^{4}. It is established that k-ε turbulence model yielded almost similar results as compared with RSM model and this is appropriate for design purposes although strong curvature was discovered in the geometry of the packed bed of spheres. Robbins et al. (2012) compared experimental data using magnetic resonance imaging (MRI) which is an experimental method to study the flow and conformation of molecules for packed bed with particle-to-column diameter ratio of 2 with the commercially available CFD code. They indicated some interesting flow features such as overestimation of reverse flow in the center of the bed, good prediction of velocity peaks near to the wall, and the existence of two peaks at the center of the geometry. They then found out that the flow showed more concaves and strong curvatures was formed at the base of each of the high-velocity regions as the inlet particle Re increases. Owing to the good agreement between experimental and computational results, it is believed that CFD is a reliable modelling tool in predicting flow behaviours in packed bed with complicated pore spaces at low Re. In a more recent paper by Dixon et al. (2013), four approaches of dealing with contact points was compared using CFD simulations of both heat transfer and fluid flow. The

four methods are “Gaps” and “Overlaps” for global approach which involved the change of size for the whole sphere in a packing as well as “Bridges” and “Caps” for local approach in which changes are to be made only to the contact point and its direct neighbourhood. It is shown that to solve for drag coefficient/pressure drop, local methods are better than global methods. This is because local methods are able to reduce the changes in bed void fraction.

As will be seen further below, a number of computational work have also been performed to study the hydrodynamics of packed bed containing more than 40 spheres. Romkes et al. (2003) described the particle-to-fluid mass and heat transfer characteristics for packed beds of spherical particles with a square channel-to-particle diameter ratio (N) of 1 to 5. In their study, k-ε, RNG k-ε and RSM turbulence models were used. For $1 < N < 2$, it is noted that the available CFD software (CFX-5.3) was able to predict the heat and mass transfer characteristics with a mean error of 15% compared to experimental values. Nijemeisland and Dixon (2004) investigated the correlation between the local wall heat flux and the local flow field in a packed bed of 72 spheres. Nevertheless, they found out that the local properties of the flow field, such as velocity components, velocity gradients and vorticity components do not show statistical relationship with local heat transfer rates. As an alternative, a conceptual analysis was used whereby they focussed more on the flow structures on a larger scale than that used for the local flow field analysis. For a fixed bed of 44 spheres, Guardo et al. (2005) and Coussirat et al. (2007) both studied the fluid flow and heat transfer mechanisms. In Guardo et al. (2005), five distinct RANS turbulence models (Spalart-Allmaras, Standard k-ε, Renormalization Group (RNG) k-ε, Realizable k-ε and Standard k-ω) were used to study the performance in the bed while Coussirat et al. (2007) used RSM and EVM turbulence models to predict the flow and heat transfer rate. The selected RSM models were modified from Daly and Harlow's (1970) version. For EVM models, the chosen models are one-equation model from Spalart and Allmaras (1992) and the two-equation Standard k-ε from Launder and Spalding (1974). They concluded that CFD proves to be a useful simulation tool in estimating heat transfer parameters as well as being reliable in calculating of pressure drop along the bed. The comparison between Standard k-ε and RSM indicated an average error of about 10% from the experimental values.

With the advancements in the computer technology, hydrodynamics parameters in packed bed with more than 100 spheres can be evaluated more accurately. Studies on hydrodynamics of packed bed consisting of more than 100 spheres have been done by Jafari et al. (2008), Reddy and Joshi (2008), Atmakidis and Kenig (2009), Bai et al. (2009), Lopes and Quinta-Ferreira (2009) as well as Magnico (2009). In his study, Jafari et al. (2008)

observed the flow behaviour through random packing of non-overlapping spheres. They studied pressure drop at various Reynolds numbers with regards to interstitial fluid velocity and pore permeability. A model including inertial terms was simulated based on Navier-Stokes equations but without a turbulence model. Reasonable agreement was found for the simulated pressure drop across the bed with available literature data. Reddy and Joshi (2008) modelled a fixed bed of 151 particles arrayed in 8 layers as well as two expanded beds (0.605 voidage bed of 105 particles and 0.783 voidage bed of 55 particles). They used CFD simulation with k-ε model to predict the single-phase pressure drop and drag coefficient for Reynolds number between 0.1 and 10,000. Later, they continued their work to predict drag coefficient and pressure drop in fixed beds with particle diameter ratio (D/d_p) of 3, 5 and 10. It was reported that the influence of wall on drag coefficient values decreases with an increase in the D/d_p ratio and the value approaches Ergun's equation (Reddy and Joshi 2010). A good agreement between CFD simulation and experimental values from the literature was observed.

For regular and irregular packed bed of spheres, Atmakidis and Kenig (2009) investigated the impact of confining walls on pressure drop. For regular packings, it was found that strong channelling throughout the bed, which is near the wall, occurred when the local void fraction is extensively high compared to the irregular one. Their numerical predictions agreed well with the literature data for wall effect on pressure drop. Bai et al. (2009) also carried out both CFD simulations and experiments to predict the flow profiles and pressure drop in a fixed bed reactor. Due to the constraints in computational simulations, they conducted two types of experiments. The first experiment was to accommodate the CFD simulation for packed bed of approximately 150 spheres. Meanwhile, the second experiment was for simulation of up to 1500 sphere particles. Studies were also performed for both structured and random packings. Their work predicted that the pressure drop would drop significantly, having errors of less than 10% compared to the experimental measurements. For multiphase flow, Lopes and Quinta-Ferreira (2009) evaluated the flow profiles in laminar regimes for a high-pressure trickle-bed reactor (TBR) by employing four RANS turbulence models namely realizable, standard and RNG k-ε, as well as Reynolds stress model (RSM). The four RANS models were coupled with Euler-Euler model in order to comprehend the effect of turbulence models. It is found that the Standard k-ε turbulence model gave better agreement for predictions of both pressure drop and liquid holdup. In the optimization and validation of the grid, the effects of time step, convergence criteria as well as mesh size were determined and the hydrodynamics was predicted as a function of liquid flow rate. Riefler et

al. (2012) studied the pressure drop for randomly structured packed bed of 180 to 248 spheres. They used the pressure drop correlation based on Ergun equation for their prediction. However, the results were not promising since it produced significantly large wall shear stress values. Furthermore, this equation has resulted in bounded flow and channelling effects due to inappropriate use of packings with small cylinder to particle diameter radii. Hence, they suggested to consider the curved fluid flow of the packing trough two scaling parameters i.e. tortuosity of the fluid flow and the porosity of the geometry.

Modelling and simulation involving a larger number of spherical particles (236 and 620) was reported by Magnico (2009). They applied the Bennett method in which they added one sphere at a time on a basal horizontal plane to synthesise two different packing systems with a tube-to-sphere-diameter ratio of 5.96 and 7.8, respectively. In this work, they compared several macroscopic models with experimental data by using MRI. They revealed that for small temperature gradients, realistic results and the microscopic mechanism of heat and mass transfer can be obtained by using direct numerical simulation in 3-D artificial packing with no hydrodynamic assumptions. However, since they used structured mesh near wall and sphere surfaces, they were not able to describe accurately the solid surface (wall and spheres) and the contact points between sphere as well as sphere and wall. Eppinger et al. (2011) also presented the simulation results for beds having a number of spheres ranging from 50 to 750 with D/d ratio between 3 and 10. A new method for meshing fixed beds of spheres was proposed and it was able to accurately predict both the local and global porosity as well as the pressure drop. In this method, the minimum distance between two surfaces was taken into account and, once it fell below a predefined value, the particles were then locally flattened in their respective region. This allowed gaps to exist in between particles and at the same time it permitted the generation of fluid cells.

For studies involving more than 1000 spheres, Dixon et al. (2012) modelled two long tubes with 1000 and 1250 spheres inside, respectively. They pointed out that validation of CFD simulations with experimental results is of paramount importance. In their work, the comparisons were carried out to predict radial temperature profiles over a wide range of Reynolds number. They reported that the temperature profiles were reasonably in good agreement with the experimental data near the tube wall but under-estimated in the center of the bed.

Hydrodynamics in packed distillation column was simulated by Haghshenas Fard et al. (2007). The distillation was carried out for methanol/isopropanol system. The dry as well as two-phase flow pressure drop and the mass transfer efficiency were predicted using

commercially available CFD package, CFX version 10. Firstly, it was observed that CFD model was able to estimate the dry pressure drop with an average relative error of 20.3% and 23% average relative error for irrigated pressure drop. Secondly, the mass transfer efficiency was also predicted well with only 9.15% error.

Several researchers have also addressed the CFD modelling of hydrodynamics in fixed beds with structured packings. Mahr and Mewes (2007) modelled and numerically calculated the three-dimensional macroscopic flow field in the whole column. They adapted the elementary cell model by Mewes et al. (1999) to suit anisotropic porous structures such as corrugated structured packings. This model was appropriate to capture the extreme instabilities and misdistribution in the flow field due to the study of hydrodynamics of the whole column. In order to test the numerical results, they used X-ray radiographic measurements on a quasi-two-dimensional segment of structured packing. For two-phase flow simulation, Khosravi Nikou and Ehsani (2008) predicted the values of mass and heat transfer as well as dry and irrigated pressure drop of Flexipac 1Y structured packing by simulating four various turbulence models namely k-ε, RNG k-ε, k-ω and baseline (BSL) k-ω models using CFD commercial code CFX for Re < 10,000. They studied the dry and irrigated pressure drop by considering incompressible isothermal flow of air and air-water respectively. For heat and mass transfer studies, a binary mixture of methanol-isopropanol was used as simulation fluid. It was concluded based on their simulation results that k-ω and BSL turbulence models were able to predict the flow distribution as well as heat and mass transfer very well. However, k-ω model is preferable since it is more robust than BSL model.

Haghshenas Fard et al. (2009) investigated the effects of geometrical characteristics (dimensions and angle of channels, specific surface area as well as porosity) and type of packing on pressure drop in structured packings such as Montzpak 250Y, Montzpak 250X, KATAPAK-S, Flexipac 1Y, 2Y and 3Y. They used low Reynolds k-ε model for the gas phase. Good agreement was obtained when the simulated results were compared with experimental values and Rocha et al. (1993) model with a mean relative error between 3.3% and 16.1%. They determined that the decrement in pressure drop is proportional to the decrement of specific surface area, increment of bed porosity, increment of the channel angle and dimensions. Said et al. (2011) compared SST k-ω, realizable k-ε and RNG k-ε turbulence models for the Montz-Pak and Flexipac 1Y structured packings. SST k-ω was obtained and was found to demonstrate the best agreement with the experimental data in the literature. They evaluated the pressure drop friction component by using a general correlation. The average error between results from CFD simulation and the correlation was about 6% for air.

It is obvious that this correlation may be promising in the applications for other fluid system. Recently, Hosseini et al. (2012) proposed a simple method adopted from Iliuta and Larachi (2001) to estimate the liquid holdup in Sulzer BX and Gempak 2A structured packings. They investigated both single-phase and two-phase flow and compared k-ε, RNG k-ε and k-ω turbulence models. It was shown by them that k-ω was appropriate for analysing the flows in structured packings. In the loading region, two-phase flow computational model was able to predict well the overall pressure drop of the bed. For that reason, this model can be applied for the design and optimization of packed columns particularly when it is being operated in the range of 80% capacity.

Supercritical fluid extraction packed columns have been broadly used in various areas such as industrial and environmental protection processes (Perrut 2000). Therefore, it is of great interest for researchers to examine their behaviour primarily to have a greater understanding of the complicated fluid flow in the bed as well as the heat and mass transfer processes involved. Fernandes et al. (2007) proposed a non-isothermal dynamic simulation model by incorporating momentum and energy balances in a counter current supercritical fluid extraction column. The model was employed for the fractionation of binary mixture squalene + methyl oleate by supercritical carbon dioxide in order to obtain optimal extraction conditions. The comparison between experiment and simulation at several operating conditions of extraction were found to be acceptable. The pressure and temperature of packed column, the gas-to-liquid flow ratio and the packed bed height were considered as optimisation variables. In a similar study on packed column, Fernandes et al. (2008) investigated the dry pressure drop by using laminar model and realizable k-ε turbulence model. They performed the simulation to determine the pressure drops of Sulzer EX at different gas mass flow rates and different conditions of pressure (0.1 – 30 MPa) and temperature (298 – 393 K). The predicted pressure drop was found to agree reasonably well with the experimental data. It was deduced that the important design parameter in packed bed is dry pressure drop. In a similar vein, a study done by Fernandes et al. (2009) extended a pseudo single-phase CFD model for estimating wet pressure drops in Sulzer EX structured gauze packing. The simulation was carried out for different gas and liquid mass flow rates and different conditions of pressure (8.0 – 26.0 MPa) and temperature (313 – 393 K). The values estimated for pressure drops agreed well with the experimental data.

k-ε turbulence model has been used in most of the packing systems mentioned in the table above. Although k-ε turbulence model is the most used turbulence model for predicting the hydrodynamics in packed beds, it is revealed that k-ω turbulence model can predict the

pressure drop, flow distribution, heat and mass transfer very well (Khosravi Nikou and Ehsani 2008) especially in dealing with more complex flow.

Flow pattern in packed beds has also been comprehensively studied in the literature mainly in terms of pressure drop variation, effects of the Reynolds number and bed geometry ratio. With the recent development of computer technology and the availability of CFD techniques, it is possible that the study of transport phenomena in the complex geometry such as packed beds can be determined more accurately and relatively in a shorter time. As a result, it is possible to reduce the amount of experiment. Moreover, as the experiments are expensive and time consuming, many researchers used CFD methods to study the hydrodynamics behaviour inside packed bed columns. It is also an effective approach to measure parameters such as dry and wet pressure drop in packed bed columns since it is difficult to measure those parameters in a complex geometry by experiment.

2.4 Supercritical Fluid

Supercritical fluid (SCF) is termed as substances in which distinctive liquid and gas phases are not present at a temperature and pressure over its critical point. In recent years, supercritical fluids are frequently and commercially used in various areas such as industrial and environmental protection processes (Perrut 1991). The development of processes and equipment related to supercritical techniques over the last three decades have led to increased used of this technology in certain areas. Table 2.2 shows some commercial applications of the supercritical fluid technology.

Table 2.2 The commercial supercritical fluid application processes and the literature related.

Process	References
Removal of pesticides from foods	Lehotay (1997) Quan et al. (2004)
Production of nanoparticles for medical use	Byrappa et al. (2008) Mayo et al. (2010)
Extraction of chemical compounds from solutions	Ghafoor et al. (2010)
Separation of oil	Reverchon and Marrone (1997) Perakis et al. (2005) Mezzomo et al. (2009) Sovová et al. (2010) Ibrahim et al. (2011)

In chemical engineering, supercritical fluids have become an interesting and efficient solvent because of two properties i.e. its adaptable thermodynamic properties (liquid-like density and high solvation capacity) and favourable transport properties (gas-like viscosity and diffusivity). Due to its adaptable thermodynamic properties, a moderate change in the pressure or temperature or both will cause the solubility parameter of the fluid to accurately match to the solubility of the solute. As a result, the capability and selectivity of a fluid as a solvent can be identified through these properties. Besides, supercritical fluid solvents are also attractive due to favourable transport properties that contribute to a large dissolution rate. This is because better transport properties have resulted in large Schmidt and Grashof numbers as well as large Sherwood numbers (Puiggené, Larrayoz and Recasens 1996). The phase diagram for carbon dioxide is shown in Figure 2.4.

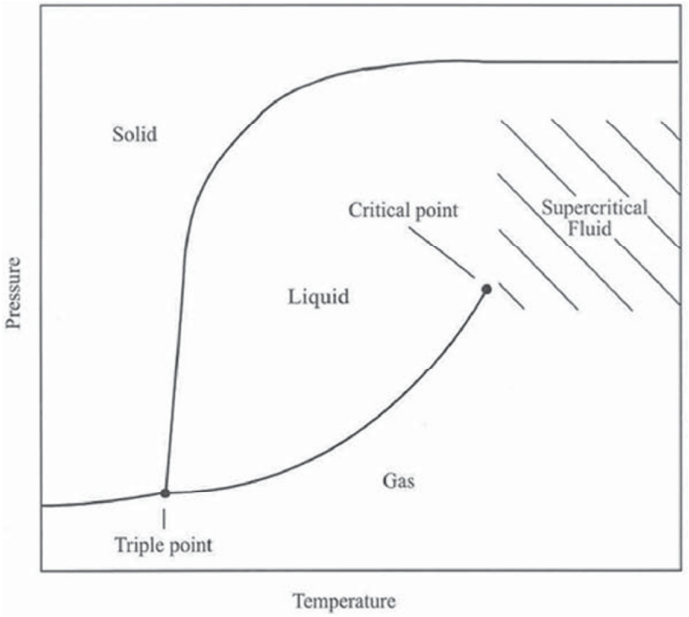

Figure 2.4 The phase diagram of a single substance (Clifford 2002)

The demand for supercritical fluids as solvent compared to conventional organic solvents is due to several advantages. These include achieving higher purity extracts, producing no residual solvent, allowing single step processing, reducing operating costs, permitting selective fractionation, faster separation and being environmentally friendly and physiologically compatible (Herrero et al. 2010, Akanda et al. 2012). The examples of critical properties of some commonly used supercritical fluid solvents are presented in Table 2.3 (Akanda et al. 2012).

Table 2.3 Examples of critical properties of supercritical fluid solvents adapted from Akanda et al. (2012).

Fluid	Critical Temperature (K)	Critical Pressure (bar)
Carbon dioxide	304.1	73.8
Ethane	305.4	48.8
Ethylene	282.4	50.4
Propane	369.8	42.5

Propylene	364.9	46.0
Methane	190.5	45.9
Trifluoromethane (Fluoroform)	299.3	48.6
Nitrous oxide	309.1	72.8
Ammonia	405.5	113.5
Acetylene	308.7	62.4
Water	647.3	221.2
Hydrogen	33.3	12.9
Nitrogen	126.2	33.9
Oxygen	154.5	50.4
Neon	44.4	26.5
Argon	150.6	48.6
Xenon	289.7	58.7
Cyclohexane	553.5	40.7

Supercritical fluid technique is commonly utilised in the supercritical extraction, fractionation and chromatography technology. Nevertheless, the most popular industrial application of supercritical fluid techniques is in the extraction field commonly known as supercritical fluid extraction (SFE). Bingjie et al. (2002) proposed a new model to describe the hydrodynamics and mass transfer performance in supercritical fluid extraction packed column, spray column and sieve tray column based on two theories namely hydrodynamic theory and two-film resistance theory. They discovered that their predicted values exhibited a good agreement with the experimental data. With the new proposed model, they were able to reduce the number of experiments in order to predict the performances of columns. In separate studies Fernandes et al. (2008) and Fernandes et al. (2009) investigated the effects of

shape and geometry on the hydrodynamics inside the complicated Sulzer EX structured gauze packing.

In supercritical fluid technology, numerous numbers of compounds are used as solvent fluid and thus far it is found that carbon dioxide is the most used solvent in this technique. It is always chosen as a solvent due to several advantages such as non-toxicity, non-flammability, affordability, low critical temperature and pressure as well as ease of removal from the product. Many researchers have used carbon dioxide as supercritical fluid solvent (Bingjie et al. 2002; Eisenmenger 2005; Zaidul et al. 2006; Zaidul et al. 2007; Fernandes et al. 2008; Fernandes et al. 2009; Stamenić and Zizovic 2013). Figure 2.5 depicts the popular real-life application of supercritical fluid techniques.

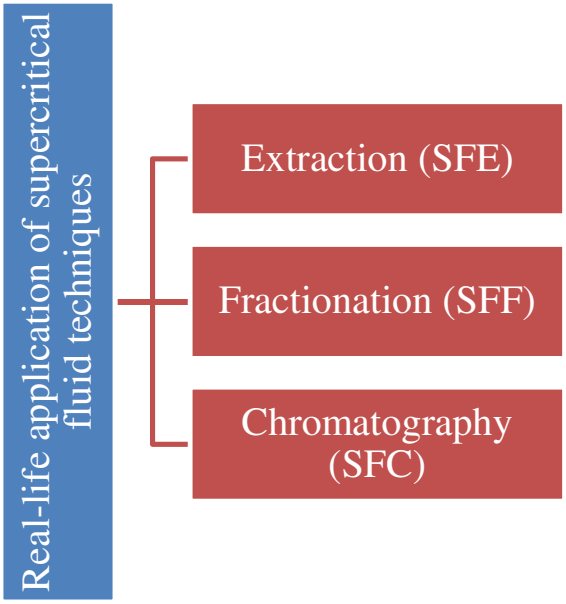

Figure 2.5 Diagram showing the popular real-life application of supercritical fluid techniques in industries.

Stamenić and Zizovic (2013) simulated for the extraction of essential oils from glandular trichomes (secretory structures of Lamiaceae plant family). Their model is found to be more reliable than other models available in the literature since the cracking time distribution of the trichomes which was untouched by the grinding was included in the model. This has allowed trichomes to crack due to the SC CO_2 dissolving. Meanwhile Berna et al. (2000) studied the effects of particle bed height on the kinetics of supercritical fluid extraction of essential oil from orange peel. They did experiments with extraction volumes of

0.5 and 51 and used Sovová's model to analyse the results. They discovered that the height of the bed has little impact when the flow is homogeneous. Another literature also applying Sovová's model is by Ferreira and Meireles (2002). Their black pepper essential oil extraction was modelled using the extended Lack's plug flow model which was developed by Sovová. The extraction processes were conducted using temperatures of 30, 40 and 50 °C with the pressures of 150, 200 and 300 bar. The kinetic aspects of the black pepper essential oil extraction were determined. The experimental data was well described by the model.

The use of supercritical technology in palm oil industry is becoming more popular over conventional methods due to its advantages. Zaidul et al. (2006) applied supercritical carbon dioxide for the extraction of palm kernel oil from dehulled ground palm kernel. The operating conditions were 313.2 K and 353.2 K and pressures between 20.7 to 48.3 MPa. They were able to reduce the short and medium chain as well as decrease the concentrate fatty acid constituents. In another work, Zaidul et al. (2007) developed a simple correlation based on kinetic mass transfer model and it can be used to estimate the minimum amount of carbon dioxide used for a given yield.

The use of supercritical fluid technology in food processing industries has also increased due to its clean and "green" processing technique. Eisenmenger (2005) examined the viability of supercritical fluid technology for the extraction and fractionation of wheat germ oil in packed column. It was the first study to report the supercritical fluid fractionation of wheat germ oil. For the supercritical carbon dioxide extraction of hazelnut oil, Özkal et al. (2005) determined the solubility and mass transfer behaviour of hazelnut oil at pressure 15 – 60 MPa and temperature of 40 – 60 °C. The Adachi-Lu equation was used to represent the solubility behaviour. It was found that the crossover pressure was between 15 – 30 MPa. For the extraction below the crossover pressure, the solubility of hazelnut oil increased with pressure but decreased with temperature. However, for above the crossover pressure, the solubility of hazelnut oil increased with pressure but increased with temperature.

The latest application of supercritical fluid extraction is in the area of nanoparticle formation and supercritical drying which was popularised in the late 90s. Some examples of nanoparticle formation are the synthesis of gold nanoparticles by using supercritical carbon dioxide that was presented by Wong et al. (2007), the synthesis of poly (methyl methacrylate) (PMMA)-TiO_2 nanoparticles composites and poly (styrene) (PS)- TiO_2 nanoparticles composites in supercritical carbon dioxide that were studied by Matsuyama and Mishima

(2009), supercritical continuous extraction (SCE) to acetone and acetone/ethanol mixtures removal from water based nanoparticle suspensions that was done by Campardelli et al. (2012) to name a few. For supercritical drying, several authors have conducted investigations related to silica aerogels (García-González et al. 2012; Błaszczyński et al. 2013; Iwai et al. 2013; Rueda et al. 2014; Sanz-Moral et al. 2014), and also studies on silica alcogel (Griffin et al. 2014; Özbakır and Erkey 2014).

The review above shows that supercritical fluid technology is gaining popularity. Furthermore, this technique has been widely applied in the industries all over the world and is proven to be a fast, clean and cheap technology. It is also revealed that supercritical carbon dioxide is a promising solvent as an alternative for traditional solvents as it is more environmental friendly.

2.5 Pressure Drop and Drag Coefficient

Flow rate and pressure drop are two of the most important parameters in the design of packed bed and they are dependent on each other (Reddy and Joshi 2008). Haghshenas Fard et al. (2009) applied CFD approach to study specific surface area, channel dimensions and angle as well as porosity and the type of packing that affects pressure drop.

The dry pressure drop has been established as an important design parameter since the computation of dry pressure drop may lead to the calculation of the total wet pressure drop through correlations. In structured packings, dry pressure drop is considered to consist of two components. The first one is drag force, which occurs when there is change in direction near the column walls and in the transition region between two packing layers rotated to each other by 90^{o}. The second component is the friction force between the packing solid walls and the different gas flows inside the structured packing channels (Said et al. 2011).

Prediction of pressure drop in packed bed columns was a subject of many studies. For instance, Raynal et al. (2004) revealed that the prediction of wet pressure drop was possible by associating data from dry pressure drop and liquid holdup. In their work, commercially available CFD codes were used and they compared k-ε, realizable k-ε and RNG k-ε turbulence models for $10 < Re < 100{,}000$. They also determined that RNG turbulence model was the preferred choice in calculating the dry pressure drop. Experimental work on predicting pressure drops through packed beds of spheres has been done by Montillet et al. (2007). They proposed a correlation for the pressure drop prediction for large ranges of

Reynolds numbers (10 – 2500) and of geometric aspect ratio of 3.5 to 40-50 which is more reliable for the prediction of experimental data particularly for narrow beds. In a more recent work by Said et al. (2011), dry pressure drop friction component was modelled for Montz-Pak and Flexipac 1Y. In their work, SST k-ω model is found to have the best agreement with the experimental values in the literature. These researchers have also investigated the influence of packing geometry such as channel opening angle, channel height dimension and corrugation angle on dry pressure drop.

It is well understood that to study the hydrodynamics behaviour inside the packings, the influence of drag force cannot be omitted since it is correlated with the fluid flow rate and pressure drop. A few studies are available in the published literature on prediction of drag coefficient (C_d) in packed beds. In earlier works by Wentz and Thodos (1963), they made measurements to resolve the form and shear drag contributions to the total drag for packed and distended beds of spheres. The authors measured the parameters in turbulent flow of air in the Reynolds number of 1500 to 8000. As discussed earlier, Reddy and Joshi (2008) simulated pressure drop and drag coefficient in fixed and expanded beds for Reynolds numbers 0.1 – 10,000. They simulated drag coefficient and pressure drop in creeping, transition and turbulent flow regimes. For creeping flow, the simulated results of drag coefficient were in good agreement with the experimental data whereas in turbulent flow the difference was approximately 10 – 25%. For multiphase flow, Subramanian et al. (2009) investigated the hydrodynamics behaviour of counter current flow by means of three dimensional CFD model. They examined the parameters i.e. contact angle, surface tension and drag force between the phases. The simulation results showed that the local film thickness was proportional to the gas flow rate for a constant liquid. However, it was also found that an increasing gas flow rate results in lower local velocity due to the drag force from the counter current gas flow.

Drag coefficients (C_d) for single sphere has also been a subject of constant interest by many researchers. For supercritical flow regime, Clamen and Gauvin (1969) performed experiments to obtain the drag coefficients of single spherical particles moving in a turbulent air stream. They observed the shape of drag curves in the range of Reynolds numbers and found that the flow structure changes around the sphere with increasing Reynolds number. For non-supercritical flow, Le Clair et al. (1970) studied the hydrodynamic drag on a rigid sphere by solving the steady-state Navier-Stokes equations of motion for Reynolds number in between 0.01 to 400. The importance of obtaining more reliable information on the drag coefficient of spheres in turbulent flow has been emphasized by Neve and Shansonga (1989).

They reported a drag coefficient for $2\times10^3 < Re < 2\times10^5$ and modelled the spheres with diameter 37.7mm for the wind tunnel jet based on the work of Neve (1986). Lloyd and Boehm (1994) presented the average Nusselt numbers and drag coefficients data for a linear array of eight spheres as well as a single sphere with periodic boundary conditions. Brucato et al. (1998) introduced a new experimental technique for measuring average particle drag coefficients in turbulent media that is called "residence time technique" (RTT). Particle drag coefficients were found to be higher under the free stream turbulence conditions. The authors also proposed a new correlation in predicting the effect of free stream turbulence on drag coefficients.

CHAPTER 3 METHODOLOGY

In this chapter, details of the geometry, boundary conditions, operating conditions as well as mesh design for both single sphere and packed bed of spherical particles are explained comprehensively. The general CFD methodology is shown in Figure 3.1.

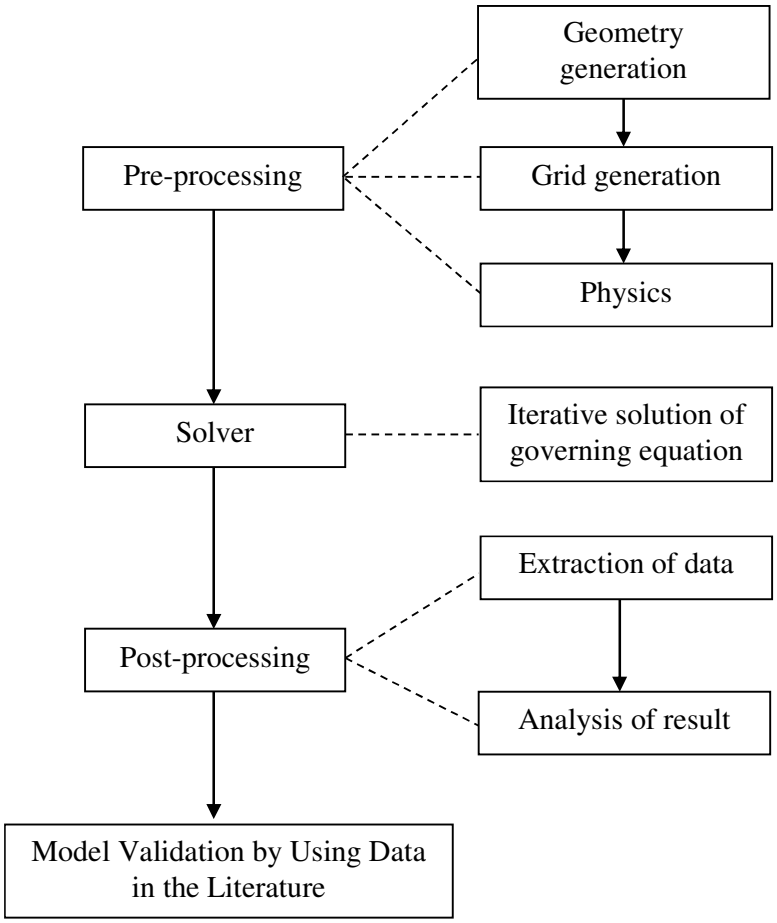

Figure 3.1 Schematic diagram of the CFD methodology

3.1 Numerical Procedure for Single Sphere

3.1.1 Geometry Details

The physical problem considered in the present work is a single sphere, as depicted in Figure 3.2.

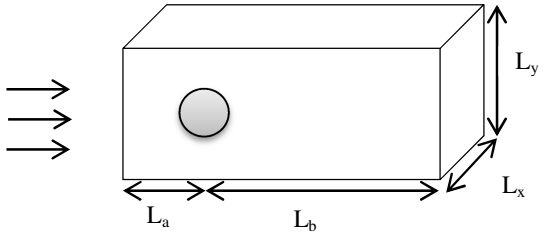

Figure 3.2 Schematic diagram of a single sphere inside a rectangular vessel

The geometry of a single spherical inside a rectangular vessel was built. The solid single sphere was assumed to be stationary and it was placed closer to the inlet based on the geometry created by Dixon et al. (2011). Dixon et al.'s (2011) model for non-supercritical fluid is employed as benchmark to validate the current simulation results. This validation is important due to no literature available for the evaluation of turbulence models involving supercritical fluid. This geometry was built as if it was horizontally placed on the ground. The details of the geometry creation for single sphere inside a rectangular vessel are listed below:

Table 3.1 The dimensions used in geometry creation (Dixon et al. (2011))

Geometry details	**Value**
Diameter of the sphere	0.0254 m
L_a	0.127 m
L_b	0.381 m
L_x	0.508 m
L_y	0.508 m

3.1.2 Mesh Design

Proper mesh design is of paramount importance in order to capture the detailed hydrodynamics around the spherical particle. For comparison purposes, meshing design used by Dixon et al. (2011) is adopted in this study. In the generation of the mesh, special attention was paid to the area closer to the surface of sphere. The mesh density was made finer close to

the wall of the sphere to enable clear observations of the flow behaviour. The meshing details are summarised in Table 3.2 and 3.3.

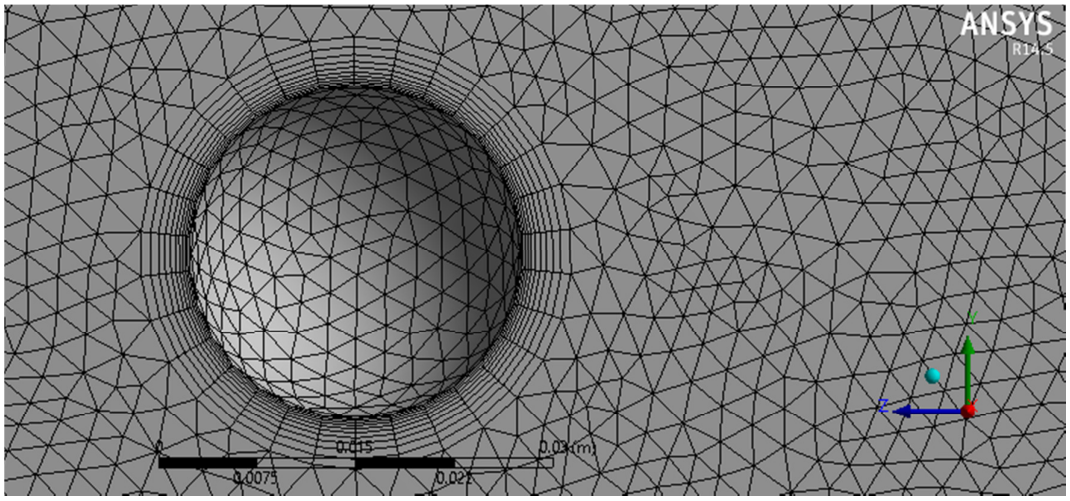

Figure 3.3 Detail of mesh over a particle surface

A. Sizing

Table 3.2 Sizing details in meshing

Sizing	Value
Minimum Size	2.66×10^{-5} m
Maximum Face Size	2.66×10^{-3} m
Maximum Size	5.31×10^{-3} m
Growth Rate	1.135

B. Inflation

The chosen meshing values have resulted in 2.87 M number of cells with an average aspect ratio of 4.1352 and a standard deviation of 4.7815. The average skewness for this meshing is 0.2055 while its standard deviation is 0.1155.

Table 3.3 The details of inflation in meshing

Inflation	Value
Transition Ratio	0.272
Maximum Layers	10
Growth Rate	1.14

In this study, it is noted that special attention was paid to the area closer to the surface of the sphere, therefore, the characteristic of y^+ parameter is being determined in order to verify a good meshing particularly simulation under turbulent flow. This is because mesh density is dependent on the near-wall modelling approach which can be determined by the characteristic of y^+ parameter (Guardo 2007). In addition, it is crucial to determine the y^+ parameter particularly involving the k-ε models due to the fact that these models do not work well in the near-wall region (Guardo et al. 2005; Guardo 2007). For the proposed geometry, it is important that the mesh is able properly defined a minimum cell size in order to capture the hydrodynamics near the sphere surface. Therefore, in this work standard wall functions were applied as the near-wall treatment for k-ε models. An example of the above-mentioned y^+ parameter can be observed in Figure 3.4.

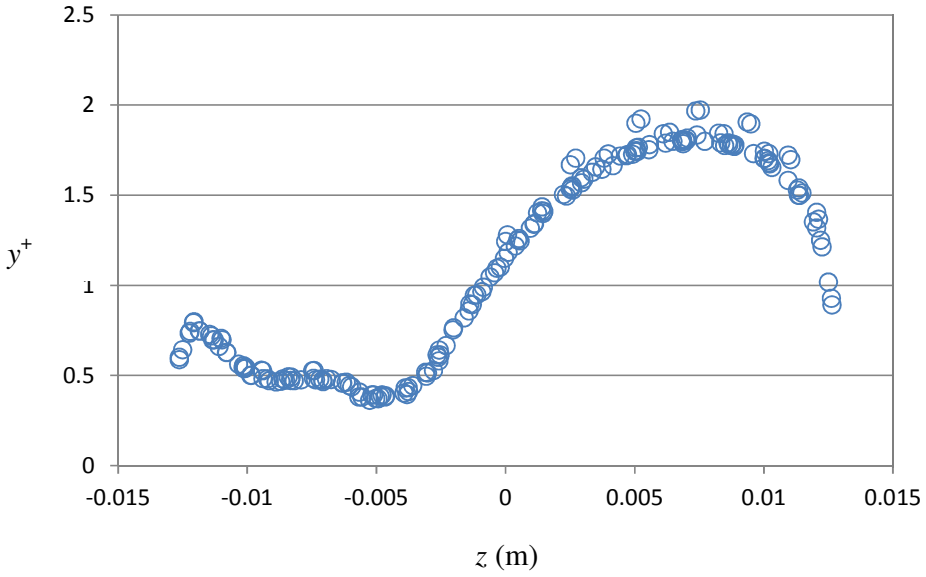

Figure 3.4 y^+ for Re = 2,000 applying realizable k-ε model in single sphere simulation

Table 3.4 Values for y^+ parameter around the single sphere surface for the different Reynolds numbers and turbulence models tested

Re		2000	20000
Standard *k-ε*	y^+_{max}	2.01	9.83
	y^+_{min}	0.32	2.20
RNG *k-ε*	y^+_{max}	2.03	9.95
	y^+_{min}	0.28	1.71
Realizable *k-ε*	y^+_{max}	1.97	9.67
	y^+_{min}	0.36	2.24
SST *k-ω*	y^+_{max}	1.79	10.11
	y^+_{min}	0.20	2.04

As a result, the y^+ parameter indicated values of $0.20 < y^+ < 2.03$. As can be seen in Table 3.4, the used of Realizable *k-ε* has resulted in the lowest range of y^+ values.

3.1.3 Boundary Conditions

The boundary conditions used in the single sphere simulations are shown in Table 3.5. Dixon et al. (2011) employed a user-defined fluid with properties typical of steam reforming gas mixtures. For the packed bed simulation, carbon dioxide was employed as the simulating fluid and its operating conditions are listed in Table 3.6.

Table 3.5 Boundary conditions used in single sphere simulation work (Dixon et al. 2011)

Boundary condition	**Value**
Temperature at the inlet, K	824.15
Total pressure, bar	21.6
Reynolds number	5000
Flow inlet	Velocity-inlet
Exit boundary	Pressure-outlet
Sphere and repeating boundaries	Sphere, symmetry

Table 3.6 Operating conditions used in single sphere and packed bed simulations

Operating conditions	**Values**	
Reynolds number	2000	20,000
Temperature	298.15 and 308.15 K	298.15 and 308.15 K
Pressure	65 and 80 bar	65 and 80 bar

The operating conditions for supercritical regime were chosen based on the typical operating conditions of supercritical fluid extraction reported in the literature (del Valle et al. 2005). For subcritical simulations, three different regimes were chosen i.e. (i) T = 298.15 K and P = 65 bar for liquid phase, (ii) T = 298.15 K and P = 80 bar for liquid phase, (iii) T = 308.15 K and P = 65 bar for vapour phase. For supercritical simulation, (iv) T = 308.15 K and P = 80 bar was selected. The selection of these operating conditions is to represent the subcritical and supercritical regimes. Reynolds numbers 2000 for laminar flow and 20,000 for turbulent flow were chosen in order to investigate the effects of different flow regimes on the hydrodynamics.

In this work, the flow was assumed to be in steady state and incompressible. No slip boundary condition was imposed on the solid walls as well as on the particle surface. In this model, velocity-inlet and pressure-outlet were used for the flow inlet and exit boundary respectively.

The velocity has been calculated as:

$$V = \frac{\mathrm{Re}\,\mu}{D\rho} \tag{3.1}$$

Where V is the velocity of the fluid (m/s), μ is the viscosity (kg/m/s), D is the diameter of the particle and ρ is the density of the fluid (kg/m^3).

3.1.4 Solution Procedure

In the current study, the commercial CFD code of Ansys Fluent 14.5 was used to solve the governing equations. The velocity and pressure coupling was resolved using the SIMPLE algorithm. The second order upwind differencing scheme was used for spatial discretization of all terms of the governing equations for steady state. For all the under-relaxation factors, default values were used.

Four different turbulence models namely standard k-ε, RNG k-ε, realizable k-ε and SST k-ω models were employed to simulate the hydrodynamics around the single sphere. All the simulations were performed using a DELL Latitude E5440 Notebook, a 64-bit server with an Intel i7-4600U Processor at 1600 MHz with total of 8 GB RAM. The RNG, standard and realizable k-ε model simulations took approximately 3 to 4 hours per simulation to complete while the SST k-ω model simulation took longer time to complete which is around 6 to 7 hours.

3.1.5 Density and Viscosity of SC CO_2

The correlations proposed by Bahadori et al. (2009) and Heidaryan et al. (2011) were used for the calculation of viscosity and density of supercritical carbon dioxide respectively. Density and viscosity of supercritical carbon dioxide are both functions of temperature and pressure. Bahadori et al.'s model (2009) can be utilised to predict the viscosity of carbon dioxide for pressure between 25 and 700 bar and temperatures in the range of 293 to 433 K. Meanwhile, Heidaryan et al.'s model for density (2011) is valid for pressure ranging from 75 to 1014 bar and temperature between 310 and 900 K. Heidaryan et al.'s density model (2011) is described as:

$$\rho = \alpha + \beta T + \gamma T^2 + \theta T^3 \tag{3.2}$$

where

$$\alpha = A_1 + B_1 P + C_1 P^2 + D_1 P^3 \tag{3.3}$$
$$\beta = A_2 + B_2 P + C_2 P^2 + D_2 P^3 \tag{3.4}$$
$$\gamma = A_3 + B_3 P + C_3 P^2 + D_3 P^3 \tag{3.5}$$
$$\theta = A_4 + B_4 P + C_4 P^2 + D_4 P^3 \tag{3.6}$$

Equation (3.7) is the viscosity correlation proposed by Bahadori et al. (2009).

$$\mu = \frac{A_1 + A_2 p + A_3 p^2 + A_4 \ln(T) + A_5 (\ln(T))^2 + A_6 (\ln(T))^3}{1 + A_7 p + A_8 \ln(T) + A_9 (\ln(T))^2} \tag{3.7}$$

In equation (3.7), the unit of viscosity is Centipoise (cp). The tuned coefficients for the above-mentioned correlations can be found in Bahadori et al. (2009) and will not be discussed here.

3.2 Numerical Procedure for Packed Bed of Spherical Particles

3.2.1 Geometry Details

For data validation, the geometry of packed bed with six layers of 56 spheres was adopted from Reddy and Joshi's model (2008). For validation purpose, simulation was also done with non-supercritical fluid and comparison was done with Reddy and Joshi (2008). The spheres were made without contact points in order to avoid problems for the mesh generation as well as to ensure reliable numerical solutions (Logtenberg and Dixon 1998). In the present study, a packed bed of 56 particles of 6 layers was then extended to a packed bed of 128 particles of 8 layers in order to represent a fully developed bed (Reddy and Joshi 2008). The top view of both geometries is shown in Figures 3.5 and 3.6.

Table 3.7 Boundary conditions used in packed bed simulation work (adopted from Reddy and Joshi (2008))

Parameters	**Bed porosity = 0.8454**	**Bed porosity = 0.6467**
Diameter of the column	127 mm	127 mm
Diameter of particle	25.4 mm	25.4 mm
Diameter of inlet and outlet	127 mm	127 mm
Number of particles	56 particles arranged in 6 layers	128 particles arranged in 8 layers
Fluid	(i) Water (ii) Supercritical CO_2	(i) Water (ii) Supercritical CO_2
Height of the bed	175.4 mm	186.9 mm

Distance between the inlet and the starting point of the particle bed	35 mm	28.1 mm
Distance between the outlet and the ending point of the particle bed	35 mm	30.4 mm
Total height of the geometry	245.4 mm	245.4 mm
Ratio of surface area of wall to the particles (S_w/S_p)	0.6165	0.6569

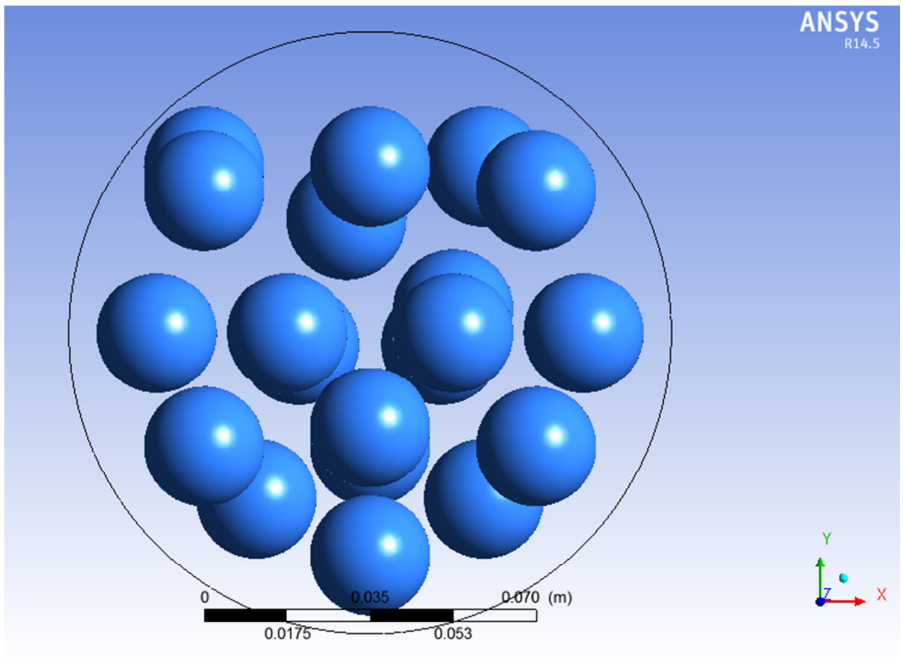

Figure 3.5 Top view of the geometry for packed bed of 56 spheres

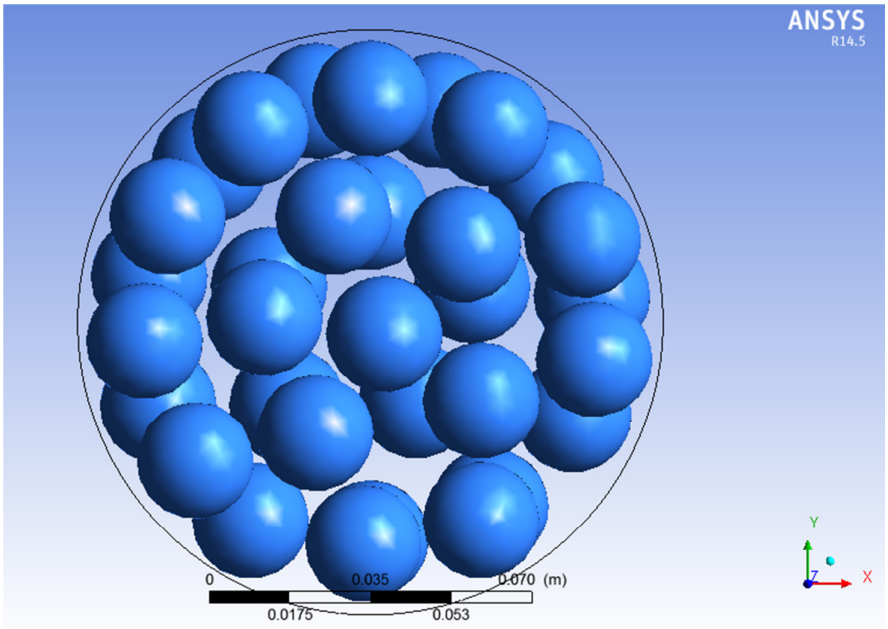

Figure 3.6 Top view of the geometry for packed bed of 128 spheres

3.2.2 Mesh Design and Grid Independence Study

The next vital stage after the geometry creation is the mesh generation. Unstructured tetrahedral mesh was used in this study due to the complicated geometry of the flow domain in packed bed. It is very important to carry out the grid refinement and grid independence study in order to obtain more reliable results for pressure drop and drag coefficients (Dixon et al. 2013). The detail of mesh for packed bed of 128 spheres is shown in Figure 3.7.

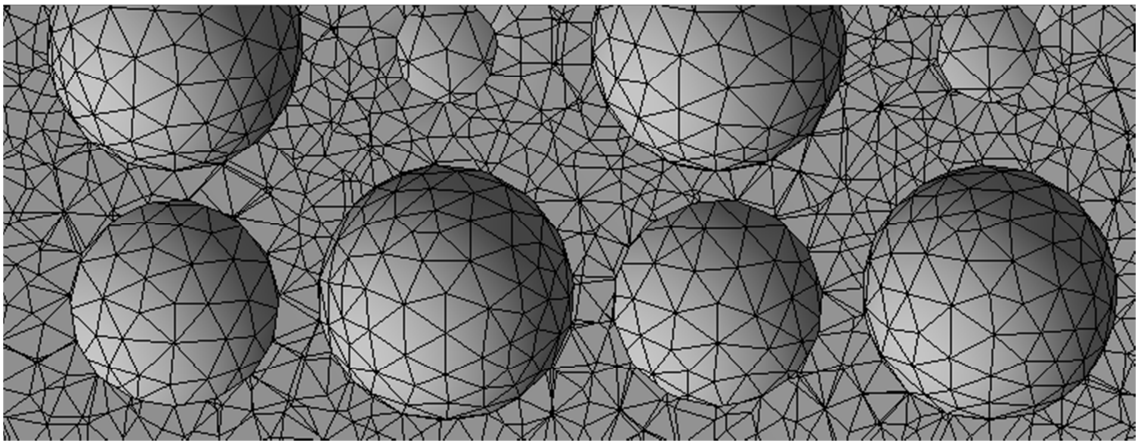

Figure 3.7 Detail of mesh for packed bed of 128 spheres

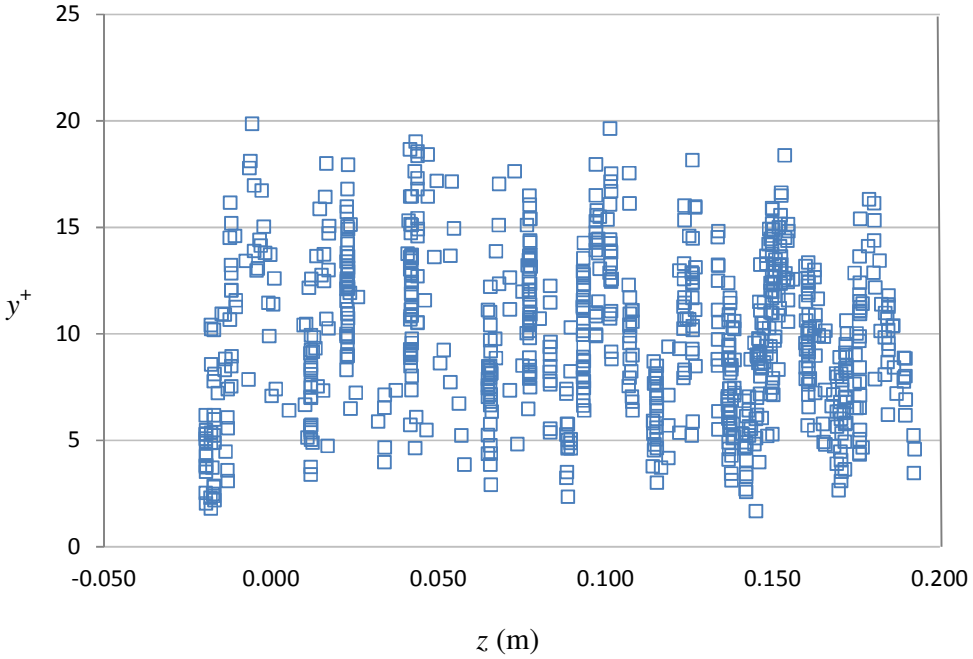

Figure 3.8 y^+ for Re = 2,000 applying realizable k-ε model in 128 spheres simulation

Table 3.8 Values for y^+ parameter around the particle surface for the different turbulence models tested

Re		2000
Standard k-ε	y^+_{max}	22.10
	y^+_{min}	1.99
RNG k-ε	y^+_{max}	21.07
	y^+_{min}	1.93
Realizable k-ε	y^+_{max}	22.10
	y^+_{min}	1.67
SST k-ω	y^+_{max}	22.43
	y^+_{min}	1.81

From Table 3.8 and Figure 3.8, the y^+ parameter indicated values ranging from 1.67 to 22.43 due to the use of standard wall functions. It is also noted that the y^+ parameter for each turbulence model has low values because of the finer mesh applied in this model (Guardo 2007). It is of paramount importance to observe the y^+ parameter in the selection of the suitable turbulence model (Guardo 2007).

For the grid independence study of 128 spheres, the graph of pressure drop result displays the % of deviation from the chosen case against number of generated elements is shown in Figure 3.9. The marked data point (♦) designates the selected mesh density for subsequent simulations. For each case, larger number of cell elements was used progressively in the grid independence study. It can be noted that there is practically no change in the pressure drop as the number of grid is increased.

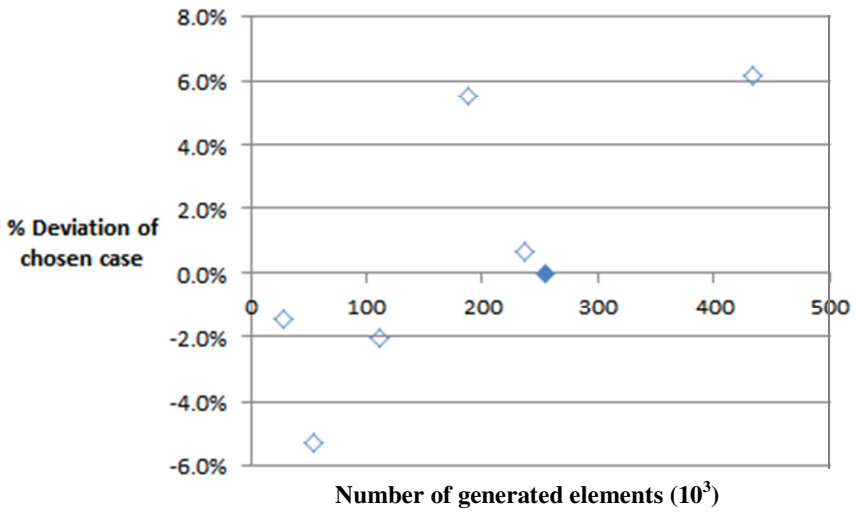

Figure 3.9 Grid independence study for 128 spheres

3.2.3 Boundary Conditions

The following assumptions were considered in this study:

- The fluid is Newtonian.
- The flow is steady and fully developed.
- Slip on the wall and spheres surfaces are zero.
- No heat transfers to be modelled.
- No reaction involved.

The overall process including the packing generation, meshing and running of the simulations were done with the same operating conditions used in single sphere study. All the operating conditions were discussed in detail in Table 3.6.

In this study, upflow mode was considered for the fluid motion direction since the fluid was flowing in the opposite direction to gravity.

3.2.4 Solution Procedure

All simulations have been obtained using the commercially available CFD code of Ansys FLUENT version 14.5. All CFD simulations were performed in two computers powered by DELL Latitude E5440 Notebook, a 64-bit server with an Intel i7-4600U Processor running at 1600 MHz with total of 8 GB RAM as well as HP Pavilion Notebook with an Intel i7-5500U Processor running at 2.4 GHz with total of 1 TB RAM, respectively.

3.2.5 Numerical Approach

Once the boundary conditions have been defined, the governing conservation of mass and momentum equations were solved by an iteration process in FLUENT version 14.5 which is based on the finite volume method. The finite volume method was employed for flow solutions which enable the local conservation equations to be solved more accurately although the grid creation was relatively coarse (Teaters 2012). Carbon dioxide was chosen to be the simulation fluid. The physical properties of the fluid in the simulations and the turbulence models used are shown in Table 3.9.

General equations were applied for the conservation of mass (the continuity equation), conservation of momentum, and conservation of energy as well as the finite volume method used to discretize them (Patankar 1980; Nijemeisland and Dixon 2004). In this present work, particular emphasis was given to the choice of turbulence model, and to the wake region near the solid particles.

Table 3.9 Physical properties of the fluid in the simulations and the turbulence models used.

Simulation	Turbulence Model	Reynolds Number	Phase	Temperature, T (K)	Pressure, P (Pa)	Density, ρ (kg/m^3)	Viscosity, ν (m^2/s)
A1	SST k-ω	2000	Liquid	298.15	6.5×10^6	715.50	5.7721×10^{-5}
A2			Liquid	298.15	8.0×10^6	776.64	6.6785×10^{-5}
A3			Vapour	308.15	6.5×10^6	185.38	1.8637×10^{-5}
A4			Supercritical	308.15	8.0×10^6	419.09	2.9843×10^{-5}
B1		20,000	Liquid	298.15	6.5×10^6	715.50	5.7721×10^{-5}
B2			Liquid	298.15	8.0×10^6	776.64	6.6785×10^{-5}
B3			Vapour	308.15	6.5×10^6	185.38	1.8637×10^{-5}
B4			Supercritical	308.15	8.0×10^6	419.09	2.9843×10^{-5}
C1	Realizable k-ε	2000	Liquid	298.15	6.5×10^6	715.50	5.7721×10^{-5}
C2			Liquid	298.15	8.0×10^6	776.64	6.6785×10^{-5}
C3			Vapour	308.15	6.5×10^6	185.38	1.8637×10^{-5}
C4			Supercritical	308.15	8.0×10^6	419.09	2.9843×10^{-5}
D1		20,000	Liquid	298.15	6.5×10^6	715.50	5.7721×10^{-5}
D2			Liquid	298.15	8.0×10^6	776.64	6.6785×10^{-5}
D3			Vapour	308.15	6.5×10^6	185.38	1.8637×10^{-5}
D4			Supercritical	308.15	8.0×10^6	419.09	2.9843×10^{-5}

E1	RNG *k*-ε	2000	Liquid	298.15	6.5×10^6	715.50	5.7721×10^{-5}
E2			Liquid	298.15	8.0×10^6	776.64	6.6785×10^{-5}
E3			Vapour	308.15	6.5×10^6	185.38	1.8637×10^{-5}
E4			Supercritical	308.15	8.0×10^6	419.09	2.9843×10^{-5}
F1		20,000	Liquid	298.15	6.5×10^6	715.50	5.7721×10^{-5}
F2			Liquid	298.15	8.0×10^6	776.64	6.6785×10^{-5}
F3			Vapour	308.15	6.5×10^6	185.38	1.8637×10^{-5}
F4			Supercritical	308.15	8.0×10^6	419.09	2.9843×10^{-5}
G1	Standard *k*-ε	2000	Liquid	298.15	6.5×10^6	715.50	5.7721×10^{-5}
G2			Liquid	298.15	8.0×10^6	776.64	6.6785×10^{-5}
G3			Vapour	308.15	6.5×10^6	185.38	1.8637×10^{-5}
G4			Supercritical	308.15	8.0×10^6	419.09	2.9843×10^{-5}
H1		20,000	Liquid	298.15	6.5×10^6	715.50	5.7721×10^{-5}
H2			Liquid	298.15	8.0×10^6	776.64	6.6785×10^{-5}
H3			Vapour	308.15	6.5×10^6	185.38	1.8637×10^{-5}
H4			Supercritical	308.15	8.0×10^6	419.09	2.9843×10^{-5}

3.2.5.1 Turbulence models

In this thesis, for the investigation of non-supercritical fluid i.e. the validation study with literature data of Dixon et al. (2011) and Clift et al. (1978), two turbulence models namely RNG *k-ε* and SST *k-ω* models were employed. Since the purpose of this validation study is to generate almost similar results as Dixon et al. (2011), it is of vital importance to employ the same models as those used in Dixon et al. (2011). However, for supercritical condition, four Reynolds Averaged Navier-Stokes (RANS) (see Table 3.9) were considered due to their wide use in the modelling of packed bed columns. The turbulence modelling equations and their descriptions are given as follows:

3.2.5.2 Standard k-ε model

The standard *k*-ε turbulence model is the most popular two-equation models and has been widely used in industrial and engineering applications (Hosseini et al. 2012). In this model, the Navier–Stokes equation uses the transport equations of the turbulent kinetic energy *k* and its specific dissipation rate ε.

For turbulence kinetic energy, κ

$$\frac{\partial}{\partial t}(\rho\kappa)+\frac{\partial}{\partial x_i}(\rho\kappa u_i)=\frac{\partial}{\partial x_j}\left[\left(\mu+\frac{\mu_t}{(\mathrm{Pr}_t)_\kappa}\right)\frac{\partial\kappa}{\partial x_j}\right]+G_\kappa-\rho\varepsilon+S_\kappa \tag{3.8}$$

For dissipation, ε

$$\frac{\partial}{\partial t}(\rho\varepsilon)+\frac{\partial}{\partial x_i}(\rho\varepsilon u_i)=\frac{\partial}{\partial x_j}\left[\left(\mu+\frac{\mu_t}{(\mathrm{Pr}_t)_\varepsilon}\right)\frac{\partial\varepsilon}{\partial x_j}\right]+C_{1\varepsilon}\frac{\varepsilon}{\kappa}(G_k+C_{3\varepsilon}G_b)-C_{2\varepsilon}\rho\frac{\varepsilon^2}{\kappa}+S_\varepsilon \tag{3.9}$$

where S_k and S_ε are source terms.

Turbulent viscosity in *k*-ε model is assumed to be linked with the turbulence kinetic energy and dissipation and is modelled as:

$$\mu_t=\rho C_\mu\frac{\kappa^2}{\varepsilon} \tag{3.10}$$

where C_μ is a constant.

The values of *k* and ε comes directly from differential transport for the turbulence kinetic energy and turbulence dissipation rate (Khosravi Nikou and Ehsani 2008).

3.2.5.3 Realizable k-ε model

Under turbulent flow conditions, standard *k*-ε model was modified to accommodate the standard wall functions. The difference between the modified turbulence model and the standard one is that it comprises of a new formulation for the turbulent viscosity and a new equation for the dissipation rate. Due to certain mathematical constraints on the Reynolds stresses which are consistent with the physics of turbulent flows, this modified turbulence model is sometimes known as the "realizable" *k*-ε model (Fernandes et al. 2008).

For turbulence kinetic energy, κ

$$\frac{\partial}{\partial t}(\rho\kappa)+\frac{\partial}{\partial x_j}(\rho\kappa u_j)=\frac{\partial}{\partial x_j}\left[\left(\mu+\frac{\mu_t}{(\mathrm{Pr}_t)_\kappa}\right)\frac{\partial\kappa}{\partial x_j}\right]+G_\kappa+G_b-\rho\varepsilon-Y_M+S_\kappa \tag{3.11}$$

For dissipation, ε

$$\frac{\partial}{\partial t}(\rho\varepsilon)+\frac{\partial}{\partial x_j}(\rho\varepsilon u_j)=\frac{\partial}{\partial x_j}\left[\left(\mu+\frac{\mu_t}{(\mathrm{Pr}_t)_\varepsilon}\right)\frac{\partial\varepsilon}{\partial x_j}\right]+\rho C_1 V_\varepsilon-\rho C_2\frac{\varepsilon^2}{\kappa+\sqrt{v\varepsilon}}+C_{1\varepsilon}\frac{\varepsilon}{\kappa}C_{3\varepsilon}G_b+S_\varepsilon \tag{3.12}$$

where

$$C_1=\max\left[0.43,\frac{\eta}{\eta+5}\right];\quad \eta=V\frac{\kappa}{\varepsilon};\quad V=\sqrt{2V_{ij}V_{ij}} \tag{3.13}$$

Turbulent viscosity is modelled as:

$$\mu_t=\rho C_\mu\frac{\kappa^2}{\varepsilon} \tag{3.14}$$

where $C_\mu=\dfrac{1}{A_o+A_s\dfrac{\kappa U^*}{\varepsilon}}$ (3.15)

In the realizable model *k*-ε, C_μ is a function of the mean strain rate tensor and the mean rate of rotation tensor (Said et al. 2011).

Model constants:

$$C_{1\varepsilon}=1.44;\quad C_{2\varepsilon}=1.9;\quad (\mathrm{Pr}_t)_\kappa=1.0;\quad (\mathrm{Pr}_t)_\varepsilon=1.2 \tag{3.16}$$

G_k represents the generation of turbulence kinetic energy due to the mean velocity gradients, G_b is the generation of turbulence kinetic energy due to buoyancy, $(\mathrm{Pr}_t)_k$ and $(\mathrm{Pr}_t)_\varepsilon$ are the turbulent Prandtl numbers for k and ε and V_{ij} is the mean strain rate tensor. From these equations, it can be observed that $C\mu$ is not a constant; it differs with mean strain and rotation rates. To ensure the good performance of the model for certain canonical flows, the model constants are assigned to the values in Eq. (3.16) Shih et al. (1995).

3.2.5.4 RNG k-ε model

The RNG k-ε model was developed based on renormalization group analysis of the Navier–Stokes equations. The transport equations for turbulence generation and dissipation are similar to those in the standard k-ε model. Nevertheless, the model parameter is exchanged with a function (Khosravi Nikou and Ehsani 2008).

For turbulence kinetic energy, κ

$$\frac{\partial}{\partial t}(\rho\kappa)+\frac{\partial}{\partial x_i}(\rho\kappa u_i)=\frac{\partial}{\partial x_j}\left(\alpha_\kappa\mu_{eff}\frac{\partial\kappa}{\partial x_j}\right)+G_\kappa+G_b-\rho\varepsilon-Y_M+S_\kappa \tag{3.17}$$

For dissipation, ε

$$\frac{\partial}{\partial t}(\rho\varepsilon)+\frac{\partial}{\partial x_i}(\rho\varepsilon u_i)=\frac{\partial}{\partial x_j}\left(\alpha_\varepsilon\mu_{eff}\frac{\partial\varepsilon}{\partial x_j}\right)+C_{1\varepsilon}\frac{\varepsilon}{\kappa}(G_k+C_{3\varepsilon}G_b)-C_{2\varepsilon}\rho\frac{\varepsilon^2}{\kappa}-R_\varepsilon+S_\varepsilon \tag{3.18}$$

Turbulent viscosity is modelled as:

$$\mu_t=\rho C_\mu\frac{\kappa^2}{\varepsilon} \tag{3.19}$$

where $C_\mu=0.0845$.

Low-Reynolds-number and near-wall flows in the RNG k-ε model can be better represented when C_μ is given by a differential equation (Said et al. 2011).

Model constants:

$$C_\mu=0.0845;\quad C_{1\varepsilon}=1.42;\quad C_{2\varepsilon}=1.68;\quad (\mathrm{Pr}_t)_\kappa=0.7194;\quad (\mathrm{Pr}_t)_\varepsilon=0.7194;$$
$$\beta=0.012 \tag{3.20}$$

Through modifications of the RNG statistical technique, the forms of the main balances in the RNG *k*-ε model are the same as the balances in the standard *k*-ε model such as the effective viscosity which is found to be similar to the turbulent viscosity defined in the standard *k*-ε model. Furthermore, it is being calculated using the form of a high Reynolds number. The RNG *k*-ε model is different from the standard *k*-ε model in the value of constant, C_μ which is 0.09 in the standard *k*-ε model and 0.0845 in the RNG *k*-ε (Nijemeisland and Dixon 2004).

According to Khosravi Nikou and Ehsani (2008), *k*-ε type model is often assumed to exist in high Reynolds number flow. The turbulent kinetic energy, *k* is identical for all the three *k*-ε turbulence models. For the ε equations, extra term has been added in the RNG model compared to the standard *k*-ε models. However, the ε equation is in a different form from the realizable *k*-ε model which is based on the dynamic equation of the mean-square vorticity fluctuation and with respect to some physical constraints on normal stresses (Said et al. 2011).

3.2.5.5 SST k-ω model

This model is very flexible since it was developed based on the combination of *k*-ω model and *k*-ε model to accommodate the condition in the inner parts of the boundary layer as well as the bulk flow. Hence, this model is suitable for adverse pressure gradient flow and separating flow (Karimi et al. 2011). This model is also known as Menter's Shear Stress Transport turbulence model since it was developed by Menter (1994) and has similar form to standard *k*-ω model:

$$\frac{\partial}{\partial t}(\rho \kappa)+\frac{\partial}{\partial x_i}(\rho \kappa u_i)=\frac{\partial}{\partial x_j}\left(\Gamma_\kappa \frac{\partial \kappa}{\partial x_j}\right)+\tilde{G}_\kappa-Y_\kappa+S_\kappa \tag{3.21}$$

and

$$\frac{\partial}{\partial t}(\rho \omega)+\frac{\partial}{\partial x_i}(\rho \omega u_i)=\frac{\partial}{\partial x_j}\left(\Gamma_\omega \frac{\partial \omega}{\partial x_j}\right)+G_\omega-Y_\omega+D_\omega+S_\omega \tag{3.22}$$

CHAPTER 4 SINGLE SPHERE STUDY

4.1 Introduction

In this chapter, the comparison of turbulence models for fluid flow past single sphere under supercritical conditions is reported. Firstly, Dixon et al.'s models (2011), which were previously proposed under non-supercritical conditions, were used as benchmark to validate the simulated results. The parameters of two turbulence models namely RNG k-ε and SST k-ω models were fine-tuned to obtain comparable results with the ones generated by Dixon et al.'s models (2011). Meanwhile, the fine-tuning for standard k-ε and realizable k-ε were compared with the experimental data of Clift et al. (1978). The simulations were then extended to predict carbon dioxide flow past a sphere at subcritical and supercritical conditions. The second part of this chapter presents a comparative study of the turbulence models: standard k-ε, RNG k-ε, realizable k-ε and SST k-ω models. This study emphasises on the predictions and evaluations of the velocity profiles at different flow regimes namely recirculation, recovery and near-wake. Simulations were carried out to determine the flow profiles at subcritical and supercritical conditions by varying Reynolds numbers (2000 and 20,000), pressures (65 and 80 bar) and temperatures (283.15 and 308.15K). The comparison of turbulent intensity and drag coefficients for all turbulence models were also done.

4.2 Results and Discussion

4.2.1. Model Validation and Fine Tuning

The fine tuning process is very important to be carried out before comparing the actual data with the literature data. All the model parameters for all RANS turbulence models were being fine-tuned. Fine tuning of the turbulence model parameters for non-supercritical fluid was performed in order to obtain the results generated by Dixon et al. (2011) as close as possible so that it can be employed in the comparative studies of turbulence models. Therefore, fine tuning of model parameters was carried out as shown in Tables 4.1 and 4.2. Based on the operating conditions mentioned in Chapter 3, the models were simulated and the percentage average errors were then recorded. The comparison with Dixon et al. (2011) is shown in Figures 4.1 and 4.2.

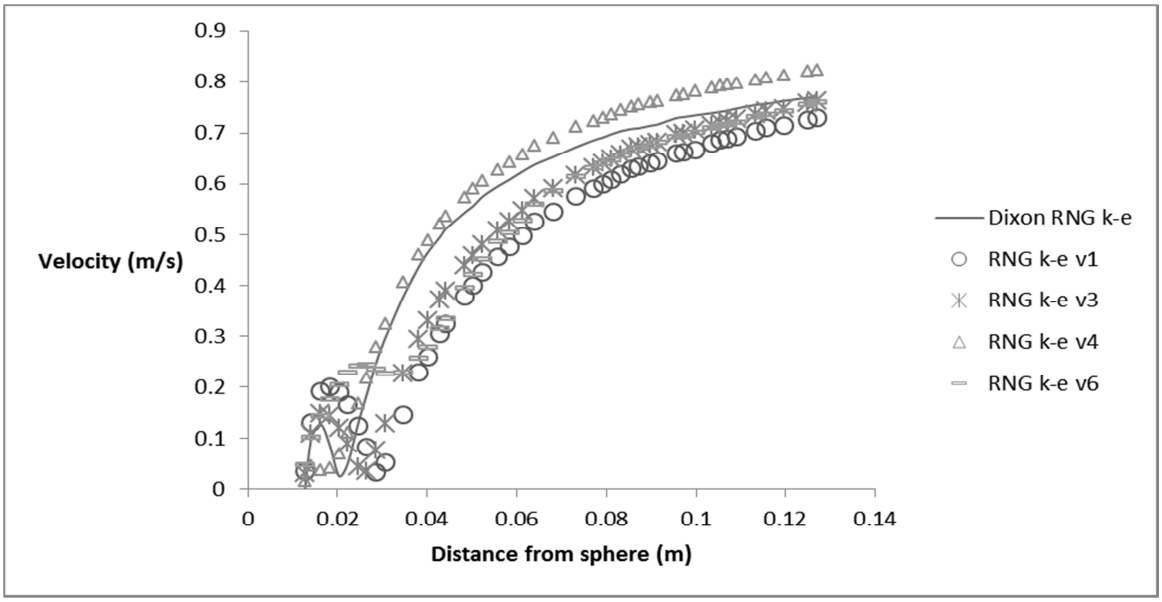

Figure 4.1. Comparison of RNG *k-ε* model predictions with Dixon et al. (2011) for non-supercritical fluid

Table 4.1. Fine-tuning of RNG *k-ε* model parameters.

Model parameters	C_{μ}	$C_{1\varepsilon}$	$C_{2\varepsilon}$	% average error	Number of iterations
Default (v1)	0.0845	1.42	1.68	23.00%	316
v2	0.0950	1.55	1.75	19.80%	316
v3	0.1000	1.60	1.82	16.33%	311
v4	0.1500	1.75	1.95	10.00%	325
v5	0.0750	1.30	1.55	30.54%	331
v6	0.0650	1.20	1.45	15.13%	338
v7	0.0500	1.10	1.35	-	No convergence
v8	0.1000	1.75	1.82	22.29%	315
v9	0.1500	1.20	1.95	27.70%	323
v10	0.1500	1.20	1.45	17.97%	333

From Table 4.1, it can be observed that the values of model parameters for RNG *k-ε* have been increased (fine-tuned) for v2 to v4 and resulted in the decrement of the percentage average error. Then, the values of model parameters for RNG *k-ε* have been decreased (fine-tuned) for v5 to v6 and resulted in the decrement of the percentage average error but further

decrement of the values of the model parameters (v7) has resulted in non-convergence of the simulation. Therefore, it is decided not to further decrease the model parameters. For v10, when it was decided to increase the C_{μ} but decrease the $C_{1\varepsilon}$ and $C_{2\varepsilon}$, it can be observed that, the percentage average errors was still high as compared to v4. Finally, it was decided to choose simulation version 4 (v4) since it has the lowest percentage average error which is 10%. Figure 4.1 also shows the simulation results with the fine-tuned model parameters (i.e. v4) agree very well with the literature data.

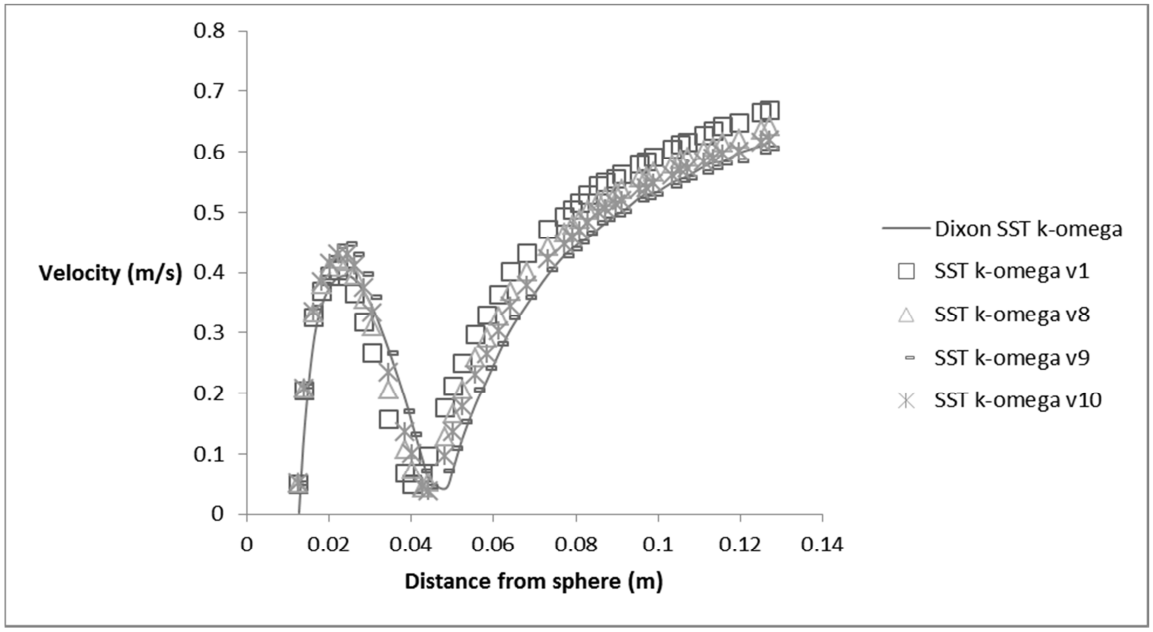

Figure 4.2. Comparison of SST *k-ω* model predictions with Dixon et al. (2011) for non-supercritical fluid

Table 4.2. Fine-tuning of SST *k-ω* model parameters.

Model parameters	α_∞^*	α_∞	β_∞^*	ζ^*	a1	% average error	Number of iterations
Default (v1)	1.00	0.52	0.09	1.50	0.31	25.60%	316
v2	1.00	0.52	0.09	1.50	0.40	-	No convergence
v3	1.10	0.50	0.09	1.50	0.31	29.15%	309
v4	1.00	0.52	0.12	1.70	0.31	41.17%	337
v5	1.20	0.72	0.19	1.90	0.31	-	No convergence
v6	1.50	0.80	0.09	1.50	0.31	45.05%	296
v7	1.00	0.20	0.09	1.50	0.31	25.60%	316
v8	0.80	0.40	0.09	1.50	0.31	16.79%	338
v9	0.60	0.20	0.09	1.50	0.31	6.77%	602
v10	0.70	0.30	0.09	1.50	0.31	11.71%	446

For the SST *k-ω* model parameters, α_∞^* and α_∞ were chosen due to the non-convergence of the other model parameters during the fine tuning process. Table 4.2 depicts that the fine tuning of model parameter a1 as well as β_∞^* and ζ^* have resulted in non-convergence of the simulations (v2 and v5). Therefore, further decrement of the values of the model parameters was not carried out. Next, when the values of α_∞^* and α_∞ were being increased, the percentage average error were also increased as can be seen in v3, v4 and v6. Finally, it was decided to decrease the values of α_∞^* and α_∞ and it is revealed that the results obtained with this fine tuning were promising (v7 to v10). Similar to RNG *k-ε* model, it was found that longer convergence time occurred when lowest values of α_∞^* and α_∞ were used in the simulation.

From Table 4.2, model parameters for simulation version 9 (v9) has the lowest percentage average error which is 6.77% demonstrating excellent agreement with the literature data. The results show that model parameters α_∞^* and α_∞ are very sensitive. Simulation results on local velocities for SST *k-ω* model agree better with the literature compared to RNG *k-ε* model since the percentage average error for SST *k-ω* model was lower than that for RNG *k-ε* model. Figure 4.2 shows a clearer comparison between the literature data, the default model parameters as well as the three model parameters with the lowest percentage error.

Table 4.3. Fine-tuning of standard *k-ε* model parameters.

Model parameters	C_μ	$C_{1\varepsilon}$	$C_{2\varepsilon}$	C_d	% Difference with Clift et al. (1978)	Number of iterations
Default (v1)	0.09	1.44	1.92	0.2284	44.3%	351
v2	0.09	1.00	1.30	0.2303	43.8%	332
v3	0.05	1.00	1.30	0.2284	44.3%	338
v4	0.14	1.00	1.30	0.2324	43.3%	329
v5	0.09	1.40	1.30	0.2303	43.8%	332
v6	0.09	1.00	1.00	-	-	No convergence
v7	0.09	1.80	1.30	-	-	No convergence

The fine-tuning of the other two turbulence models: standard *k-ε* and realizable *k-ε* were also being carried out. The drag coefficients values were predicted for both turbulence models and recorded in Tables 4.3 and 4.4. These predicted values were compared with the available experimental data of Clift et al. (1978) and percentage differences were also tabulated. For standard *k-ε* model, it is found out that the decrement of the values of $C_{1\varepsilon}$ and $C_{2\varepsilon}$ has resulted in higher percentage average error as can be seen in v2, v3 and v5. When it was decided to further decrease the parameters, non-convergence of the simulation (v6) was observed. In addition, non-convergence for v7 was also detected when the values of $C_{1\varepsilon}$ and $C_{2\varepsilon}$ were increased at the same time. Therefore, it was decided to increase C_μ and decrease $C_{1\varepsilon}$ and $C_{2\varepsilon}$ in order to obtain lower percentage average error for the predicted C_d as compared to the literature. As for realizable *k-ε*, the decrement of the model parameter values in v2, v3 and v4 have resulted in non-convergence of the simulation. As a result, the model parameter values were increased in order to obtain low percentage average error for this model as can be seen for v5 to v9.

For both standard *k-ε* and realizable *k-ε*, there is only a small difference in the drag coefficients values generated for all the fine-tuning simulations. However, in comparison with Clift et al. (1978), the lowest percentage difference is found to be for simulation version 4 (v4) which is 43.3% and simulation version 9 (v9) which is 39.8% for standard *k-ε* and realizable *k-ε* respectively. This has shown that the changes made to the model parameters for both turbulence models are not very sensitive to drag coefficients.

Table 4.4. Fine-tuning of realizable k-ε model parameters.

Model parameters	$C_{2\varepsilon}$	C_d	% Difference with Clift et al. (1978)	Number of iterations
Default (v1)	1.9	0.2132	48.0%	342
v2	1.5	-	-	No convergence
v3	1.3	-	-	No convergence
v4	1.0	-	-	No convergence
v5	2.3	0.2191	46.6%	317
v6	2.7	0.2148	47.6%	331
v7	3.2	0.2339	43.0%	300
v8	3.5	0.2389	41.7%	289
v9	4.0	0.2467	39.8%	285

4.2.2 Simulations at Different Flow Regimes

4.2.2.1 Velocity profiles for subcritical and supercritical condition

After the validation, RNG k-ε and SST k-ω turbulence models were used to predict the flow of subcritical and supercritical carbon dioxide. Besides the aforementioned turbulence models, another two RANS turbulence models namely the standard k-ε and realizable k-ε were also used to solve the three-dimensional steady-state flow around a single sphere. The results for velocity profiles and drag coefficients corresponding to the Reynolds number (Re = 2,000 and 20,000) are used to assess the performance of the four different RANS turbulence models. Although it is revealed that SST k-ω turbulence model agreed well with literature data of Dixon et al. (2011) for non-supercritical fluid as mentioned in 4.3.1, the four RANS turbulence models are still being employed in the simulations of subcritical and supercritical carbon dioxide. This is to enable the comparison under supercritical conditions.

In the present study, the boundary conditions were selected in order to focus attention on the flow of subcritical and supercritical carbon dioxide. Reynolds number of 2,000 and 20,000 were selected to represent transition and turbulent regimes. The effects of Reynolds number, temperature and pressure on the velocity profiles were predicted. No slip boundary condition was used on the sphere surface so that flow velocity on the sphere surface be equal to zero.

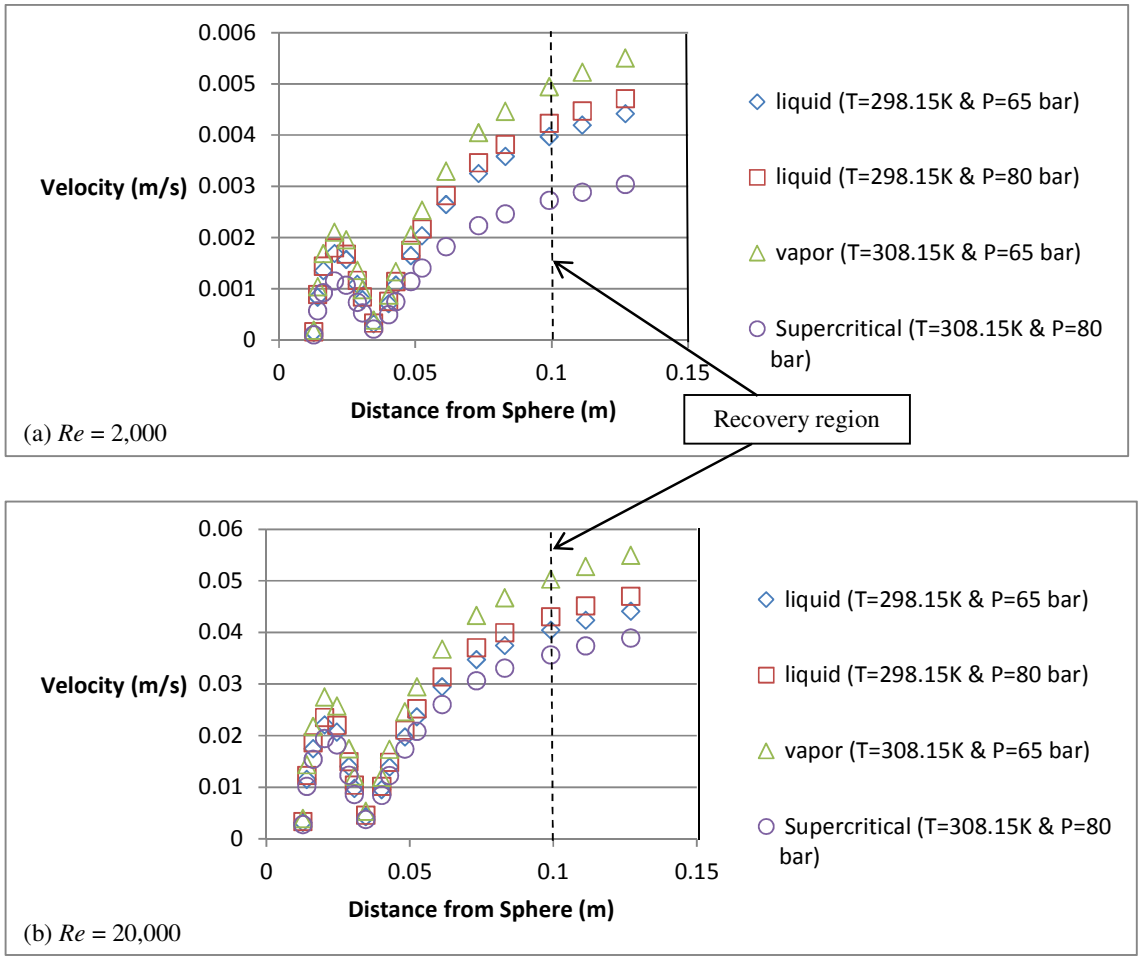

Figure 4.3. The velocity profiles in subcritical and supercritical regimes by using realizable *k-ε* turbulence model.

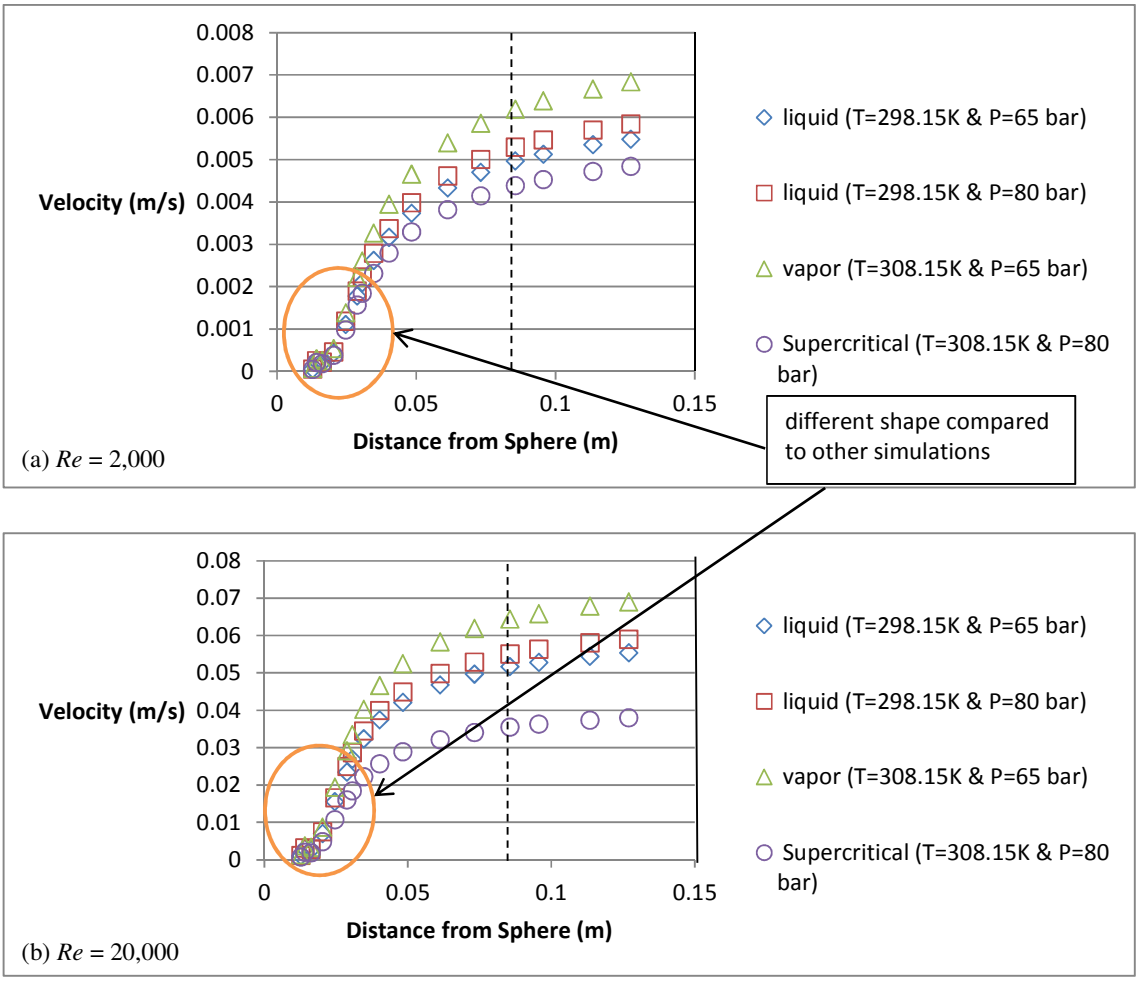

Figure 4.4. The velocity profiles in subcritical and supercritical regimes by using RNG k-ε turbulence model.

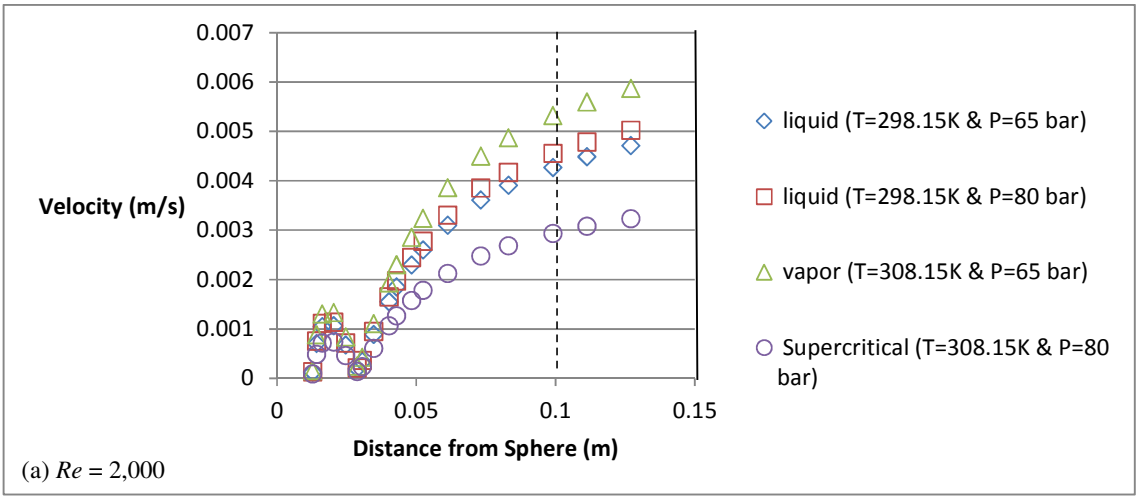

(a) *Re* = 2,000

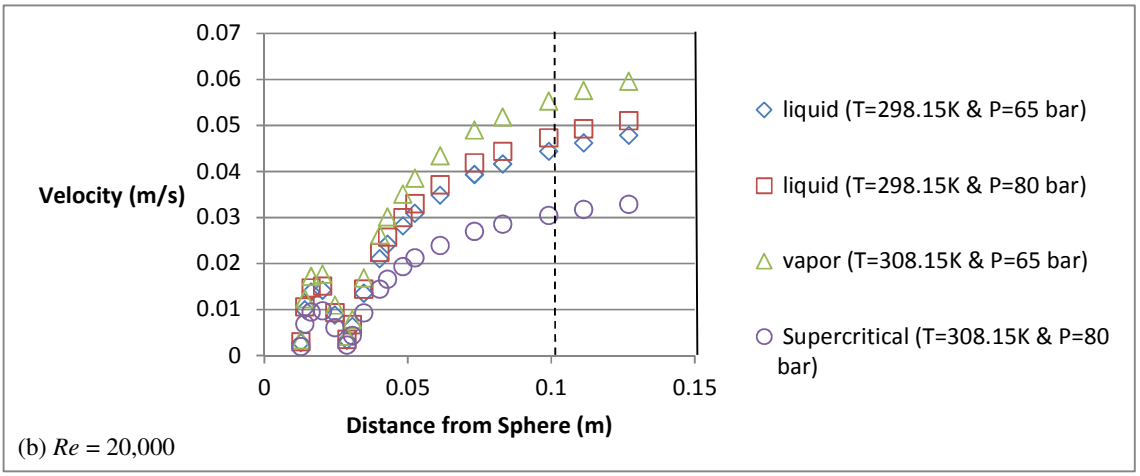

(b) *Re* = 20,000

Figure 4.5. The velocity profiles in subcritical and supercritical regimes by using standard *k-ε* turbulence model.

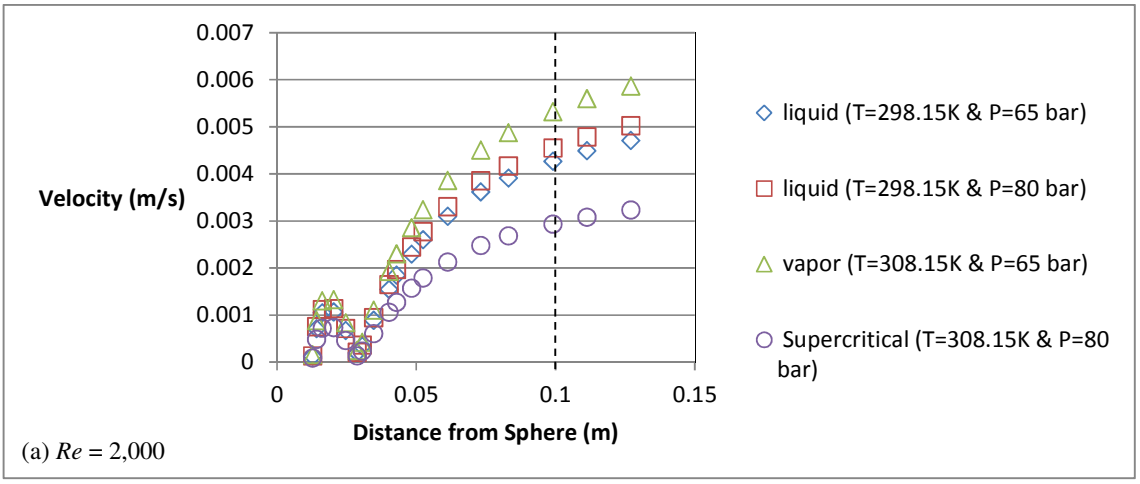

(a) *Re* = 2,000

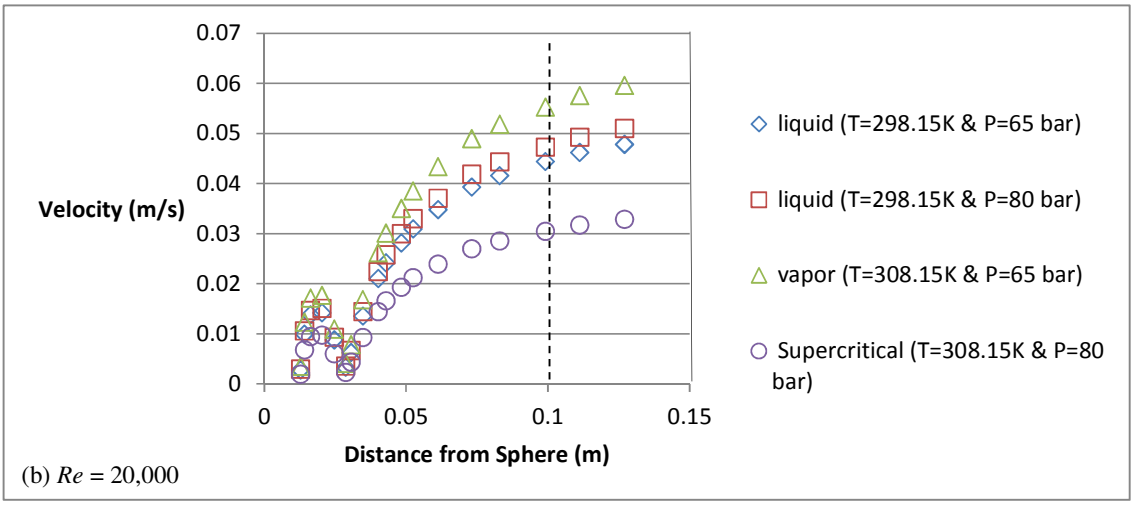

(b) *Re* = 20,000

Figure 4.6. The velocity profiles in subcritical and supercritical regimes by using SST *k-ω* turbulence model.

Figures 4.3 – 4.6 represent the velocity profiles generated by using realizable k-ε, standard k-ε, RNG k-ε and SST k-ω turbulence models. It is noticeable that in all simulations the velocity results for supercritical regimes were found to be the lowest whereas the highest velocity was found in the vapour phase which is twice the velocity in the supercritical region. This may due to the physicochemical properties of supercritical carbon dioxide, for instance density, viscosity, diffusivity and dielectric constant are easily manipulated by the changes in pressure or temperature without crossing phase boundaries (Abbas et al. 2008) and was found to be very dependent on the change in density of the fluid (Sihvonen et al. 1999). The density of supercritical fluid which is close to critical point is also exceptionally sensitive. This is because any small changes in temperature and pressure will affect its density (Abbas et al. 2008). It is also revealed that the maximum velocity occurs approximately 0.125 m away from the sphere. With the aforementioned physicochemical properties of supercritical carbon dioxide has led to the lowest velocity which was found in the supercritical regimes. Another reason is due to the retrograde behaviour of supercritical fluids (Abbas et al. 2008). Retrograde behaviour means an increase in temperature of a solution increases the solubility of the solute over certain ranges of pressure. Thus, the increase in solubility will decrease the velocity of the fluid for supercritical regimes.

By looking at the trend of the graphs in Figures 4.3 to 4.6, it can be concluded that the velocity profiles predicted were comparable with Dixon et al. (2011) since the trend of the graphs obtained were almost similar (see Figures 4.1 and 4.2 in section 4.3.1). Nevertheless, the trend of the graph for the velocity profiles depicted in Figure 4.4 is slightly different as compared to the other profiles generated by using realizable k-ε (Figure 4.3), standard k-ε (Figure 4.5), and SST k-ω (Figure 4.6) turbulence models. It is clearly observed that the shape of the graph for simulations by using RNG k-ε turbulence model at the point of 0.012 m away from the sphere surface to 0.05 m have significant difference compared to other simulations (see Figures 4.4a and b). This may be due to boundary layer separation occurred in the velocity profiles simulated and captured more clearly by realizable k-ε, standard k-ε and SST k-ω. These results are quite comparable to the simulations in Figure 4.1 and 4.2 which were simulated by using non-supercritical fluid. As can be seen in Figure 4.1, for simulations by using RNG k-ε, it is revealed that this turbulence model was unable to capture the boundary separation layer as compared to simulations by using SST k-ω shown in Figure 4.2. It is observed that SST k-ω models can better capture curvature effect on flow as compared to other models. Hence it can accurately predict flow separation under adverse pressure gradient (Bardina et al. 1997). The above mentioned also comparable to the

simulations in supercritical condition since the supercritical profiles are similar to non-supercritical profile except for RNG k-ε.

The graphs in Figures 4.3, 4.5 and 4.6 also show that at the point 0.012 m from the sphere surface, the velocity was minimal and then increased drastically until the point of 0.026 m. After that, the velocity was found to drop rapidly until point 0.048 m. Nearly at the point of 0.05m away from the sphere surface, it is revealed that the velocity started to increase again towards the outlet. Meanwhile, for the graphs in Figure 4.4, the velocity was found to be minimal at the point 0.012m away from the sphere surface and then significant increment of the velocity profiles were observed until 0.0875 m away from the sphere.

4.2.2.2 Pressure coefficient for subcritical and supercritical condition

There is a definite value of fluid pressure at each point on a sphere surface and the distribution of pressure coefficient (C_p) around the sphere versus polar angle plot are plotted in Figures 4.7 – 4.10 for both subcritical and supercritical conditions. The current C_p values predicted via CFD simulation of four RANS turbulence models are being compared with the available literature data of Constantinescu and Squires (2004). Their data were divided into two categories in which the first data were predicted by using DES and the second data were obtained via experiment. For a better comparison, similar Reynolds numbers are being chosen and comparison showed that the predicted C_p for supercritical fluid is in good agreement with the literature. The trend of the graphs for all simulations was found to be consistent with the literature. However, the predictions were underestimated for polar angle in between 80° to 120° but overestimated for polar angle of over 120°. This may due to the difference in the turbulence models and simulating fluid used in the current studies. As depicted in Figure 4.7, the predictions of C_p values for SST k-ω are the closest to the literature data and the pressure distribution curve is also consistent particularly for simulation of supercritical fluid. The fluid pressure distribution in front of the sphere surface is revealed to be the highest as compared to the back surface of the sphere as a result of high velocity at the rear of the sphere surface as can be seen in the trend of the curve in all figures. The value and angular position of the minimum C_p at about 60° to 90° is comparable with the literature data as well. It is also observed that for polar angle around 120° and 150°, the CFD simulation is found to be flat and slightly increased after 150°. It is also revealed that as Reynolds number increases, the value of C_p somewhat decreases (Norberg 2002). Higher Reynolds number has found to deepen the C_p because of the delay in flow detachment

(Constantinescu and Squires 2004). For the current work of subcritical condition, the predicted C_p is found to be quite similar to the supercritical condition. This may due to the temperature and pressure chosen were near to the critical value point. The values of C_p generated were between +1 to −1 only due to the incompressible flow in this study. C_p of zero indicates the pressure is the same as the free stream pressure. C_p of one corresponds to the stagnation pressure and indicates stagnation point. If C_p is negative, the flow is cavitating (Anderson 2007).

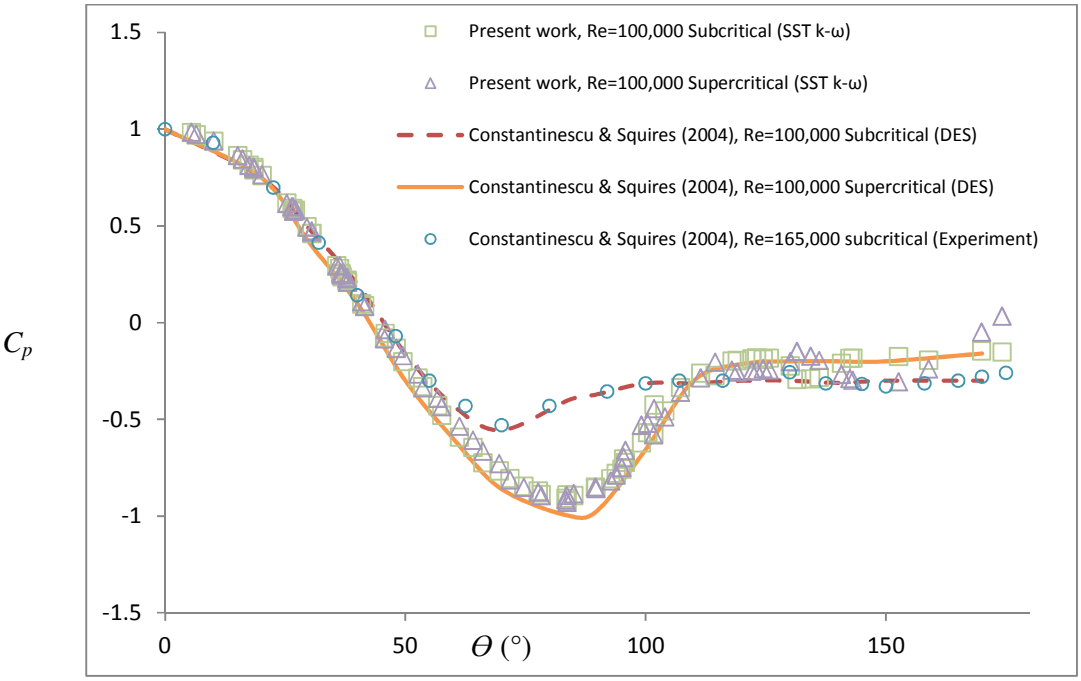

C_p

Figure 4.7. The comparison of C_p for SST k-ω in subcritical and supercritical regimes

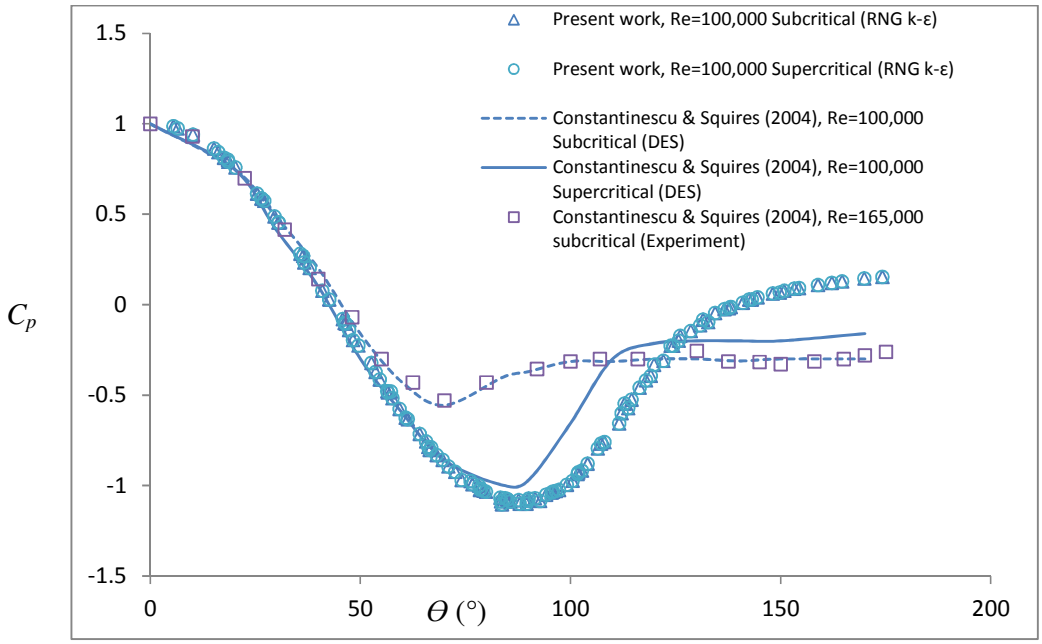

Figure 4.8. The comparison of C_p for RNG k-ε in subcritical and supercritical regimes

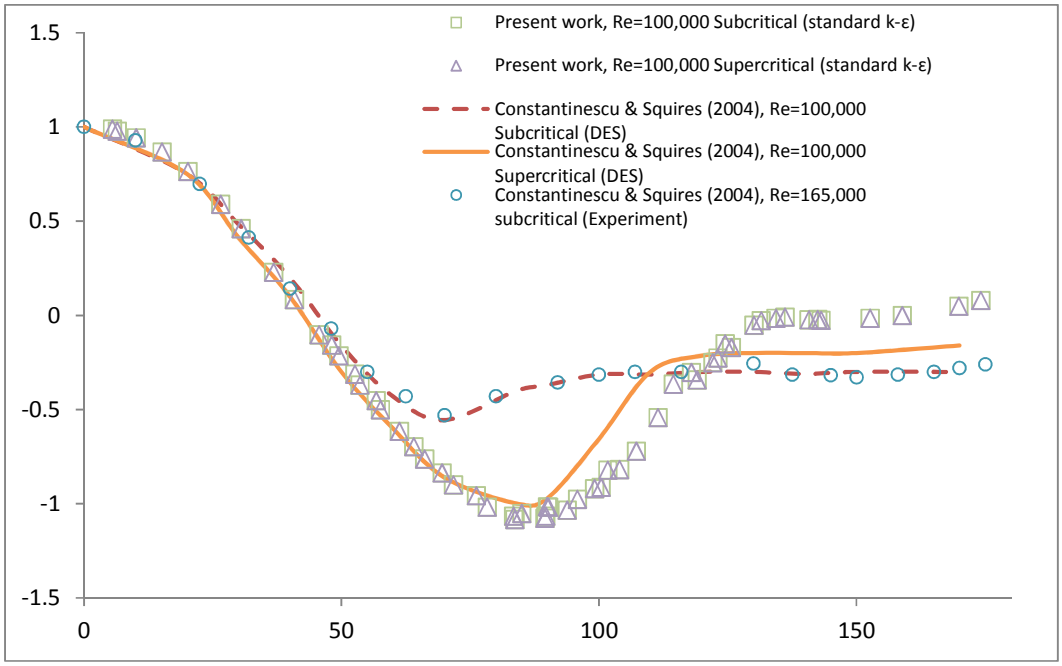

Figure 4.9. The comparison of C_p for standard k-ε in subcritical and supercritical regimes

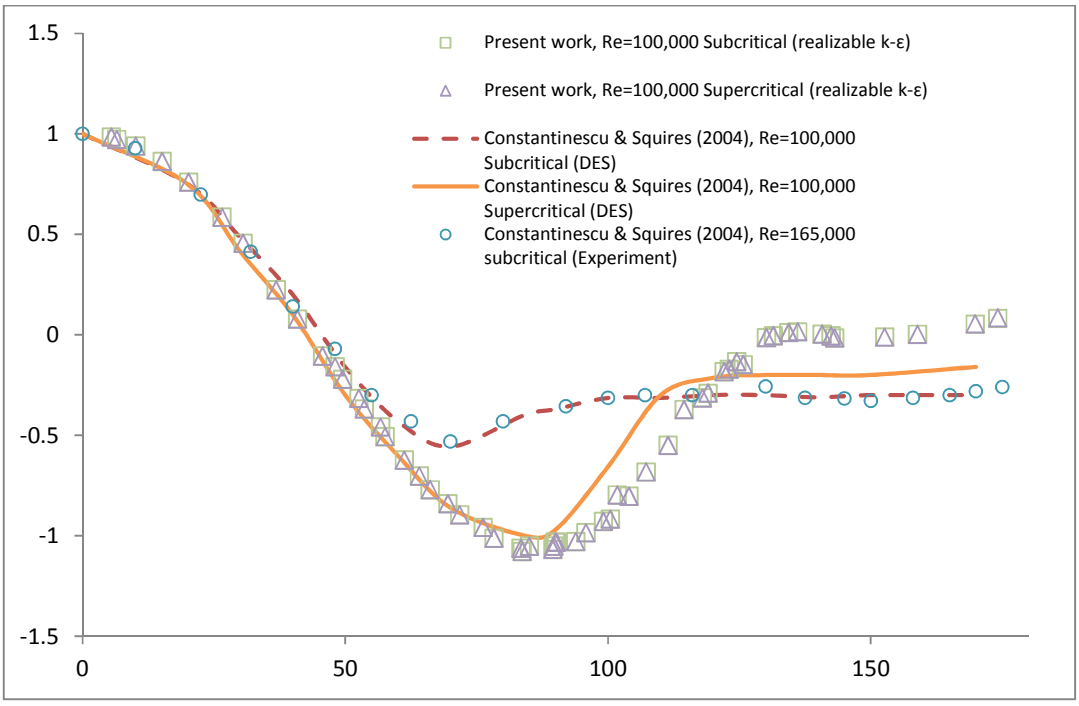

Figure 4.10. The comparison of C_p for realizable k-ε in subcritical and supercritical regimes

4.2.2.3. Flow visualisations for subcritical and supercritical condition

It is also vital to visualise the flow behaviour around a sphere particularly in the wake region. In order to describe in detail the differences in subcritical and supercritical regions for different turbulence models, three main regions at the wake area namely recirculation, recovery and near-wake as proposed by Constantinescu and Squires (2004) will be discussed. Here, streamline plot was used to visualise the wake regions and comparison of the streamlines shows variations of the flow development for all turbulence models used and for both Reynolds numbers of 2000 and 20,000 (Figures 4.11 – 4.18). It is also noted that the flow direction is from left to right for all the streamlines.

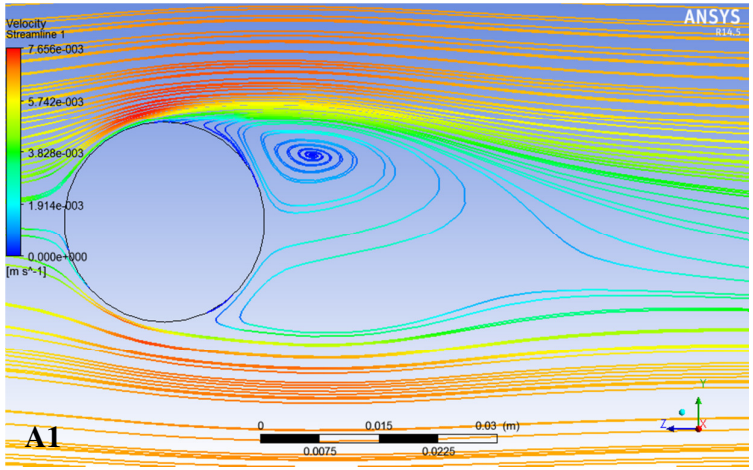

T = 298.15K, P = 65bar

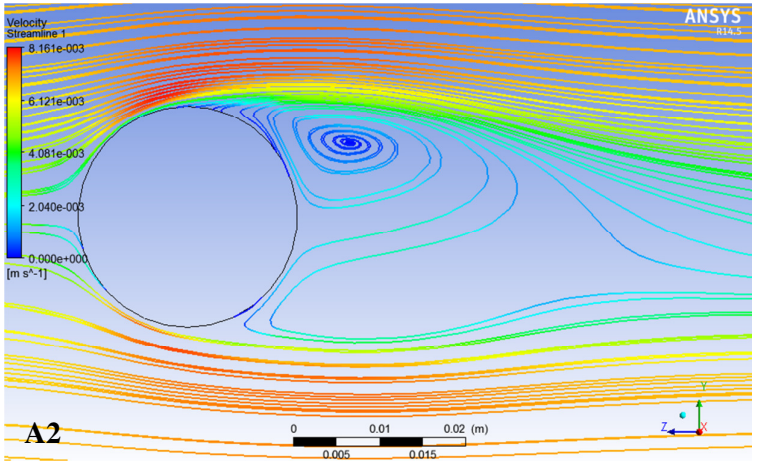

T = 298.15K, P = 80bar

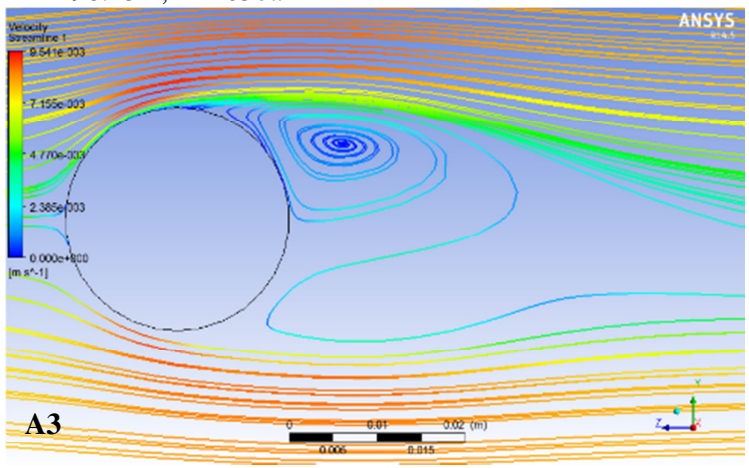

T = 308.15K, P = 65bar

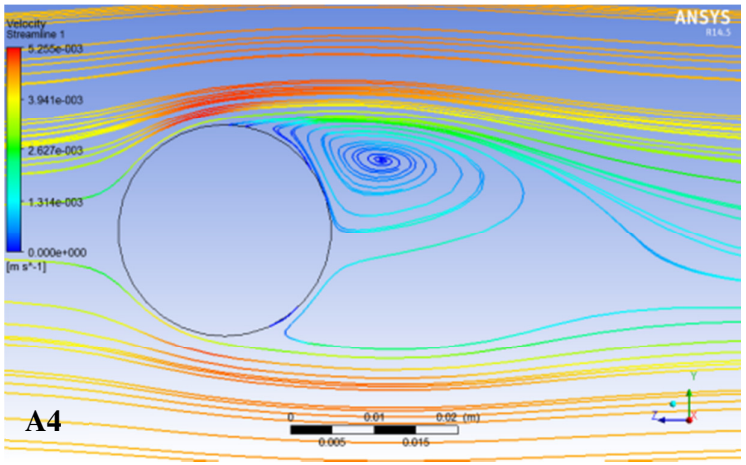

T = 308.15K, P = 80bar

Figure 4.11. Streamline plot of velocity profiles for Re = 2,000 by using SST *k-ω* turbulence model.

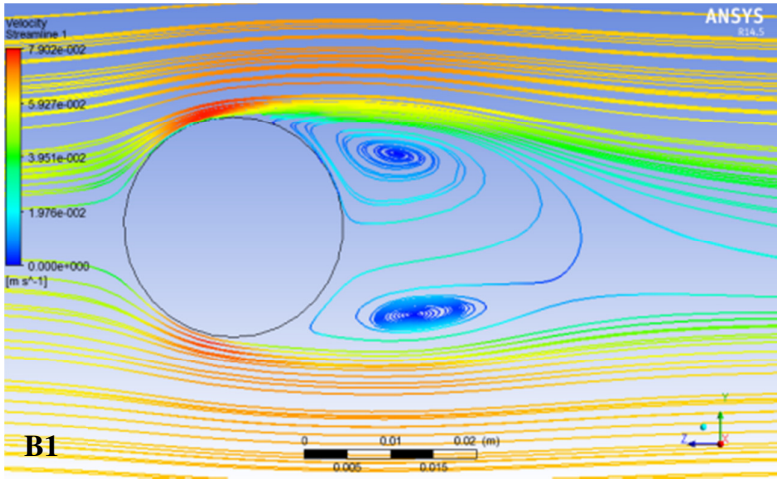

T = 298.15K, P = 65bar

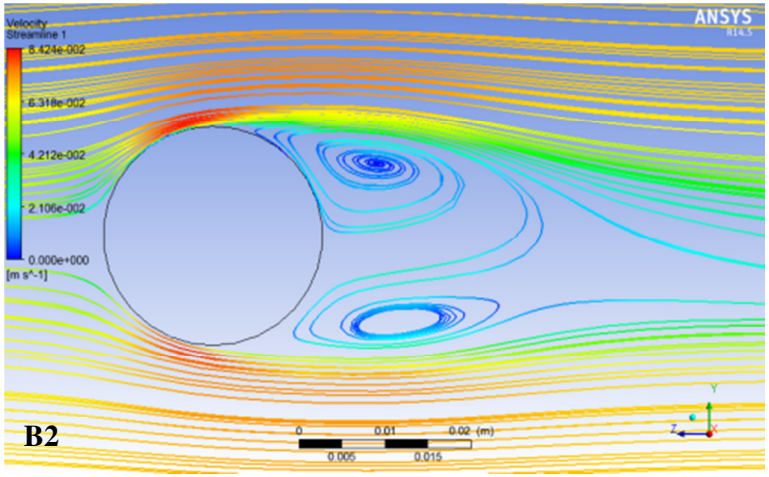

T = 298.15K, P = 80bar

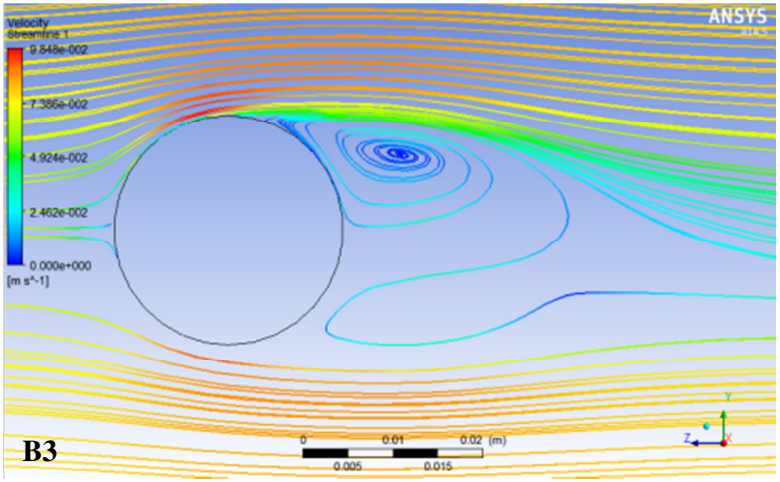

T = 308.15K, P = 65bar

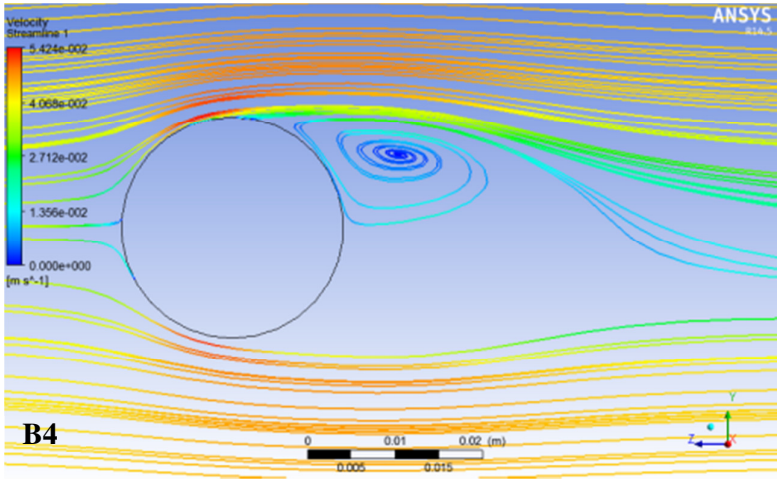

T = 308.15K, P = 80bar

Figure 4.12. Streamline plot of velocity profiles for Re = 20,000 by using SST *k-ω* turbulence model.

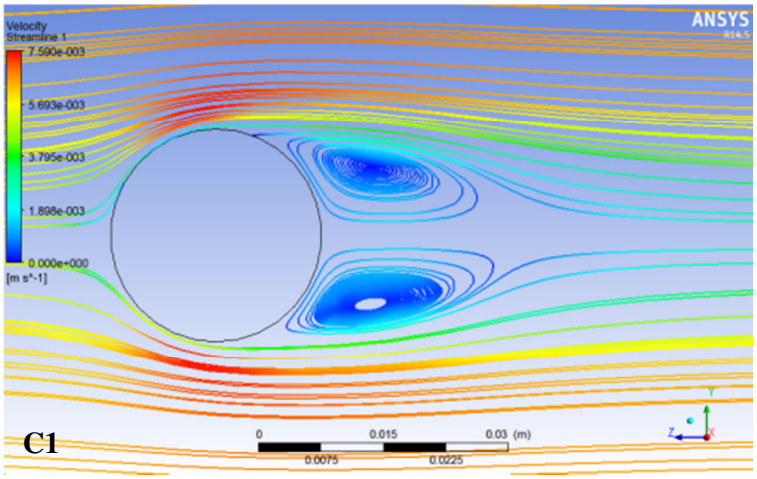

T = 298.15K, P = 65bar

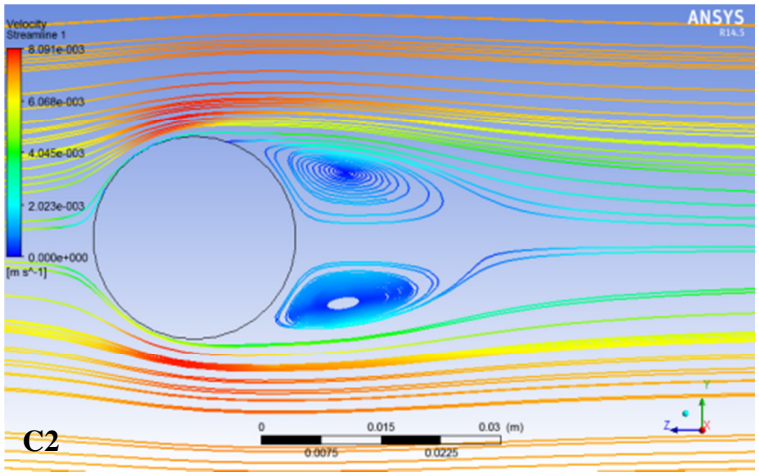

T = 298.15K, P = 80bar

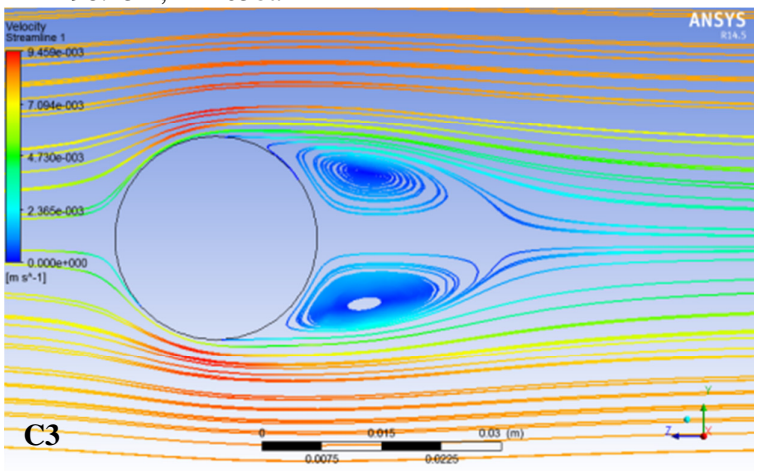

T = 308.15K, P = 65bar

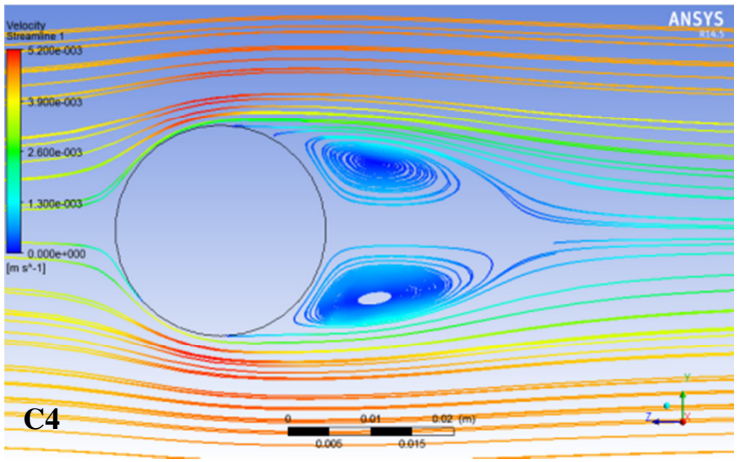

T = 308.15K, P = 80bar

Figure 4.13. Streamline plot of velocity profiles for Re = 2,000 by using realizable *k-ε* turbulence model.

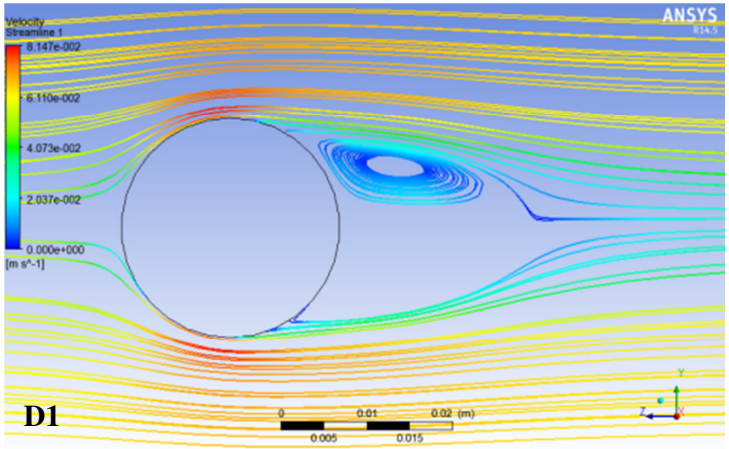

T = 298.15K, P = 65bar

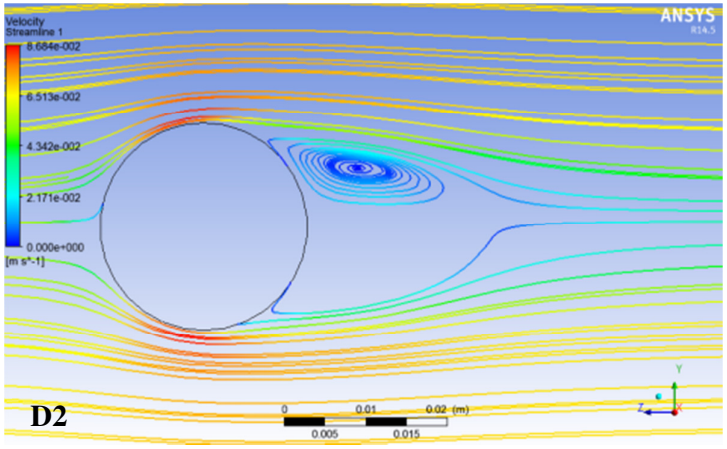

T = 298.15K, P = 80bar

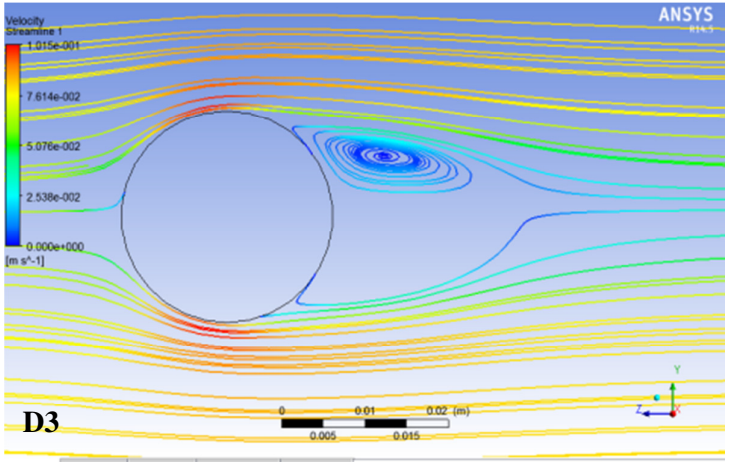

T = 308.15K, P = 65bar

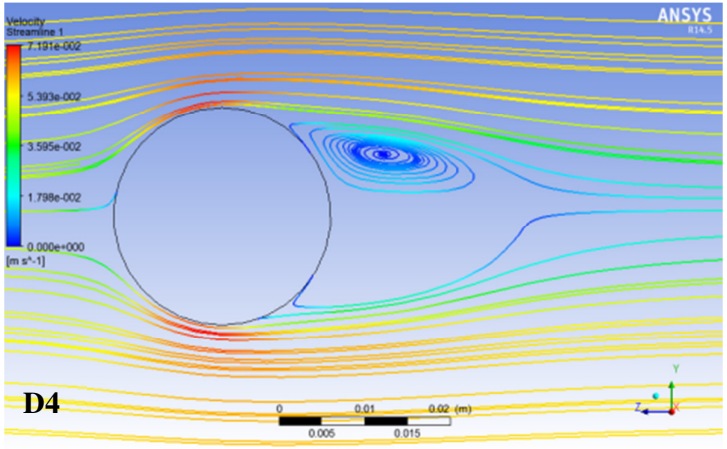

T = 308.15K, P = 80bar

Figure 4.14. Streamline plot of velocity profiles for Re = 20,000 by using realizable *k-ε* turbulence model.

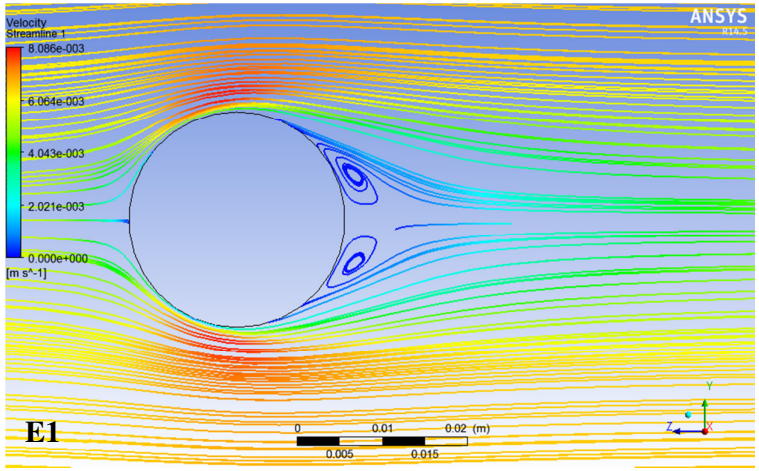

T = 298.15K, P = 65bar

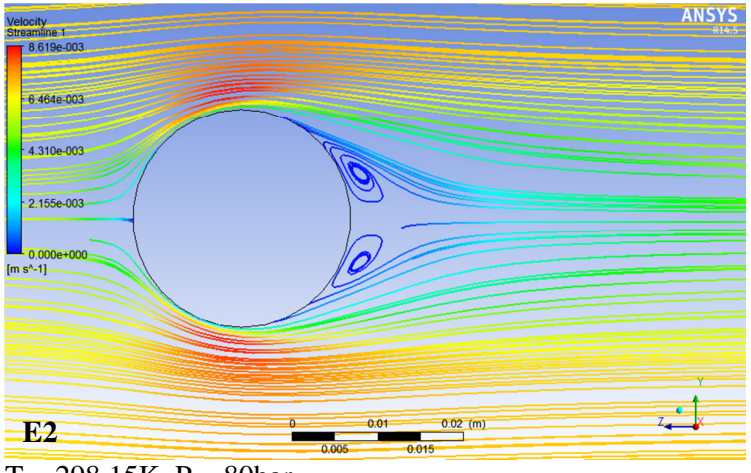

T = 298.15K, P = 80bar

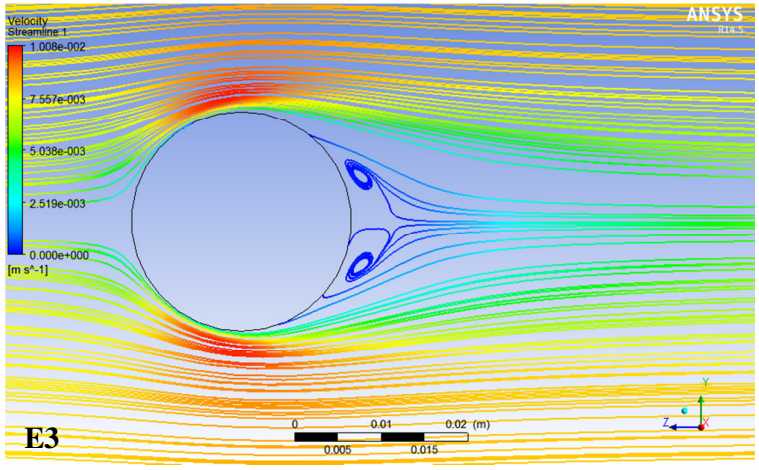

T = 308.15K, P = 65bar

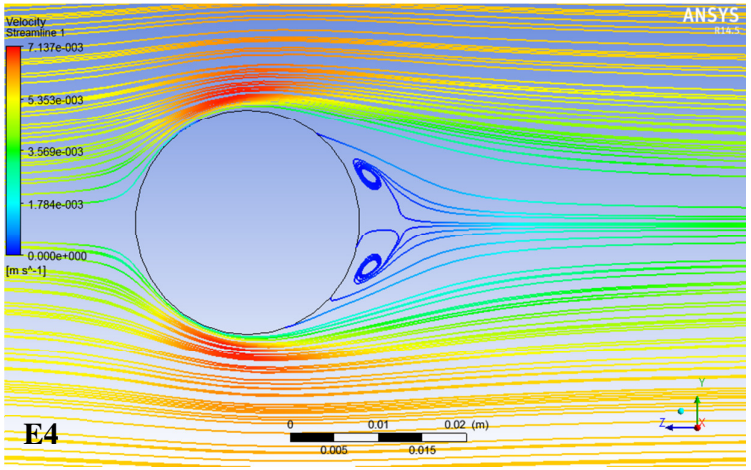

T = 308.15K, P = 80bar

Figure 4.15. Streamline plot of velocity profiles for Re = 2,000 by using RNG *k*-*ε* turbulence model.

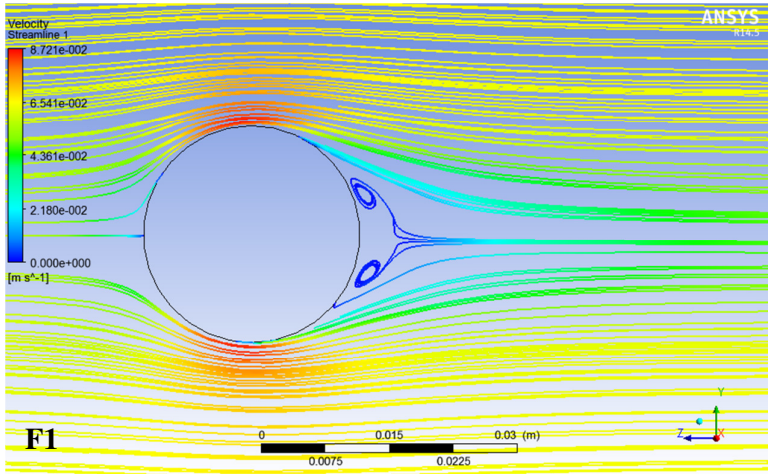

T = 298.15K, P = 65bar

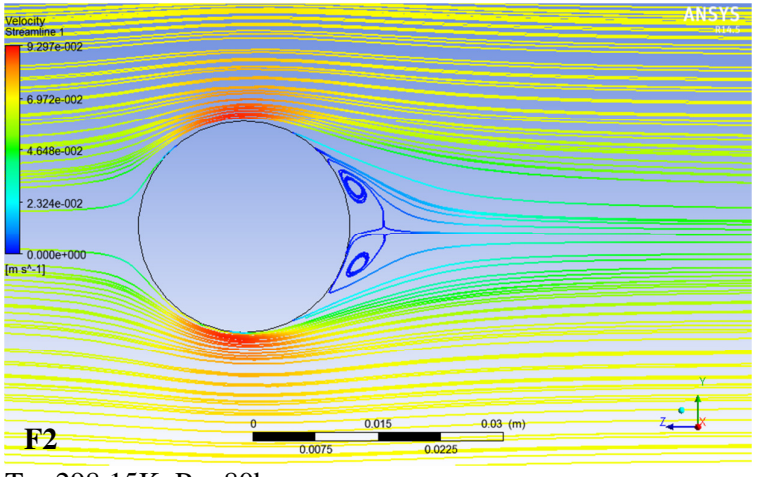

T = 298.15K, P = 80bar

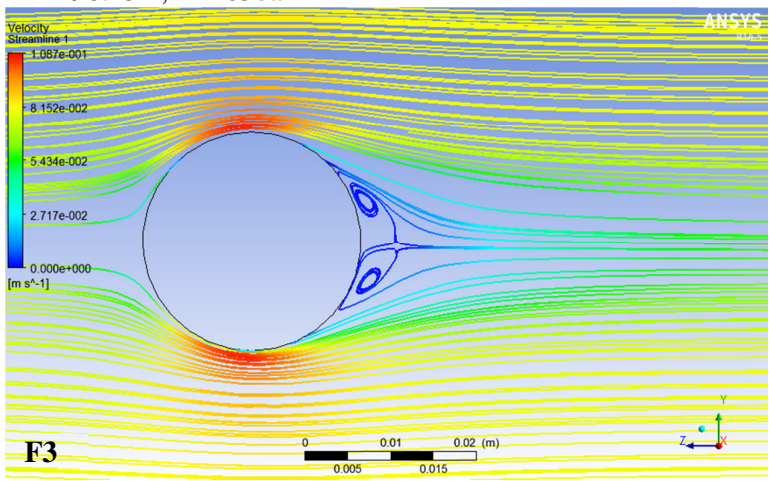

T = 308.15K, P = 65bar

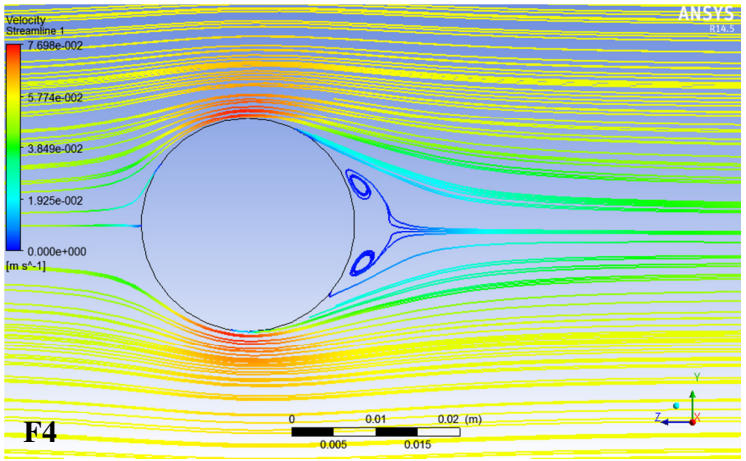

T = 308.15K, P = 80bar

Figure 4.16. Streamline plot of velocity profiles for Re = 20,000 by using RNG *k-ε* turbulence model.

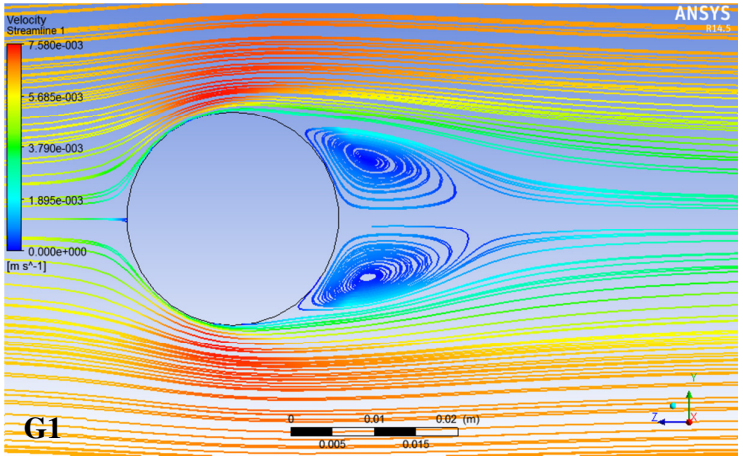

T = 298.15K, P = 65bar

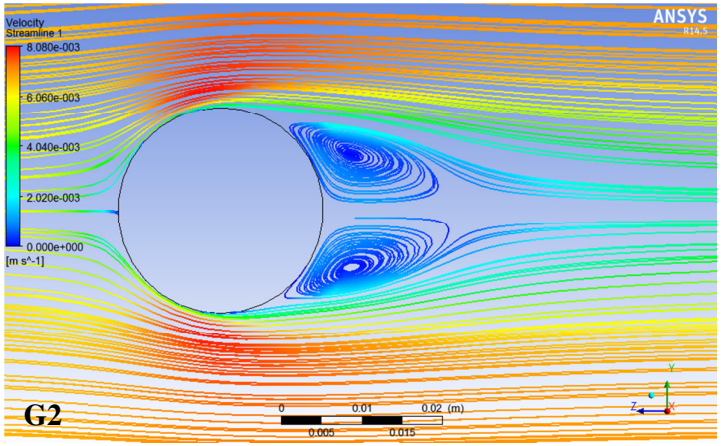

T = 298.15K, P = 80bar

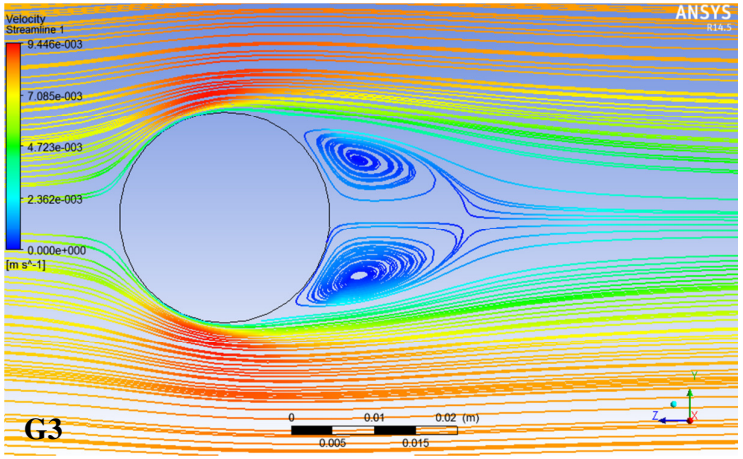

T = 308.15K, P = 65bar

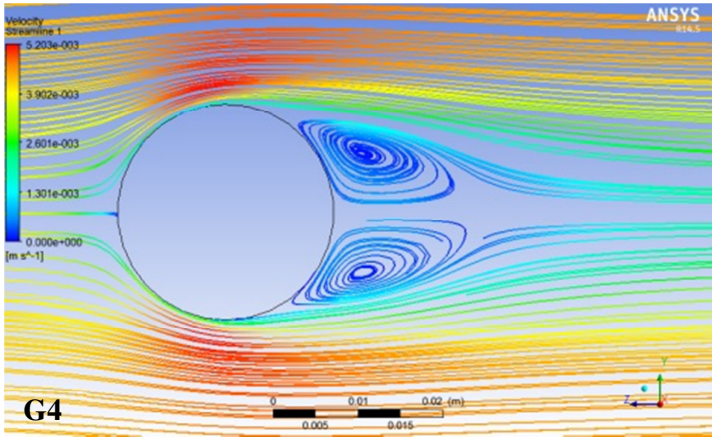

T = 308.15K, P = 80bar

Figure 4.17. Streamline plot of velocity profiles for Re = 2,000 by using standard *k-ε* turbulence model.

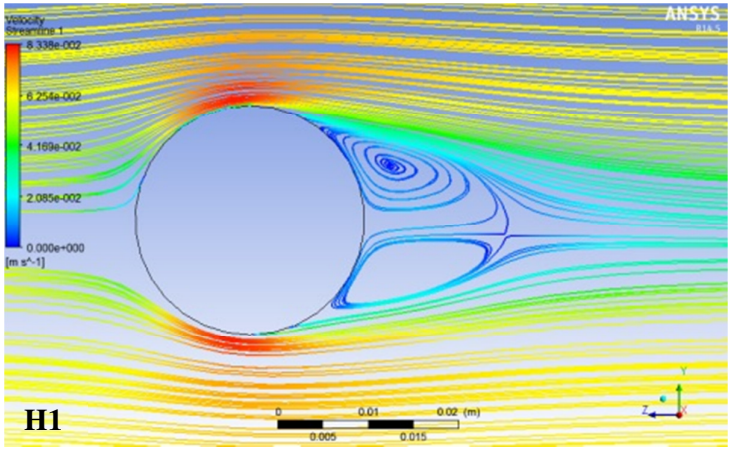

T = 298.15K, P = 65bar

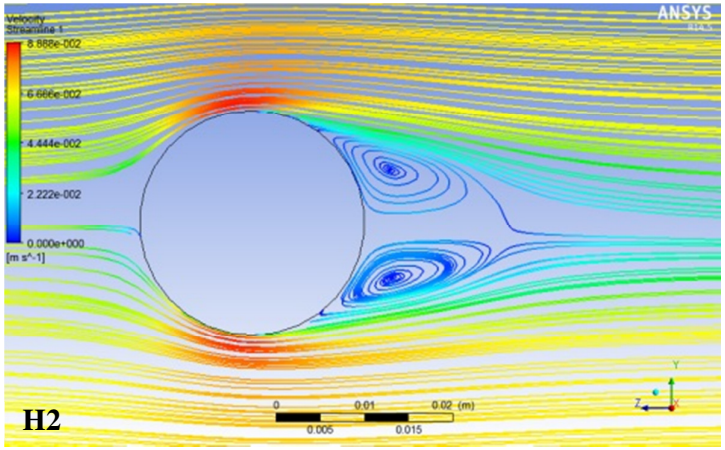

T = 298.15K, P = 80bar

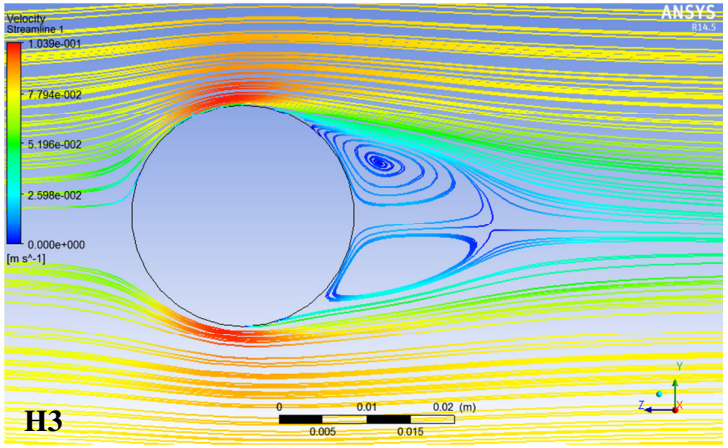

T = 308.15K, P = 65bar

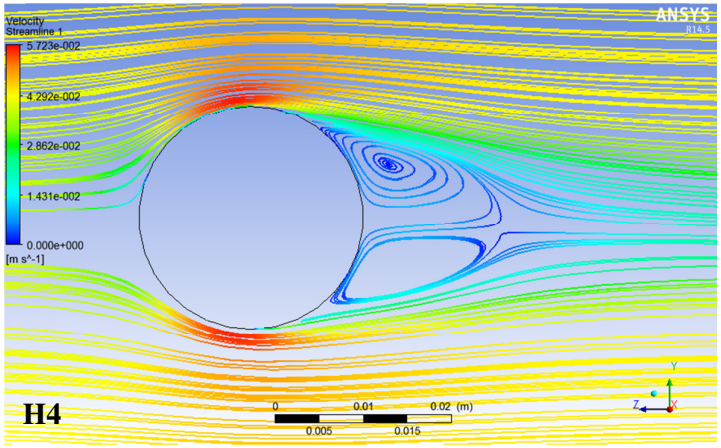

T = 308.15K, P = 80bar

Figure 4.18. Streamline plot of velocity profiles for Re = 20,000 by using standard *k*-*ε* turbulence model.

From the streamline plots, the visualisation of the recirculation region can be done and the qualitative comparison of the prediction by the RANS models can be made. The longest recirculation region was found in streamline plots of A1 – A4 and B1 – B4 for simulations by using SST k-ω turbulence model in both subcritical and supercritical regimes. When a fluid flows over a solid particle, the streamline comes to a stop at the front of the particle (i.e. at azimuthal angle zero). This point is called the stagnation point, where all the dynamic pressure of the fluid is converted to static pressure. The static pressure at this point is the maximum and decreases till a certain distance as the fluid flows towards the rear of the particle. But a certain angle (depending on the Reynolds number) fluid detaches itself from the solid surface because of the forward momentum and as a result of this a region of high pressure forms towards the rear, which promotes recirculation in the rear of the particle. This point where the fluid detaches itself from the solid surface is called separation point. At the separation point, wall shear stress exerted by the fluid is zero (Appendix A). The separation point predicted by the different RANS models is shown in Table 4.5 along with the literature values for non-supercritical fluid. It can be noted that the increase in Reynolds number will decrease the angle of separation of the fluid from the particle surface. Hence, faster detachment of the fluid from the particle surface can be observed for higher Reynolds number. The recirculation in the rear of the particle creates a pressure imbalance between the front and rear of the particle, which contributes to the pressure drag. The size of the recirculation region increases with increase in Reynolds number and hence the pressure increase as well. However, beyond $Re > 10^6$, the separation point is pushed closer to the rear of the particle, which reduces the size of the recirculation region and thus leads to better pressure recovery. This increase in pressure at the rear decreases the pressure imbalance and thus reduces the pressure drag. It is evident from the above discussion that an accurate prediction of the size of the recirculation region is important for a better estimation of the pressure coefficient. It should be noted here that the SST k-ω predicts pressure coefficient in a much better way compared to other RANS models. The streamlines predicted by the four RANS models is shown in Figures 4.11 – 4.18. It is to be noted that the recirculation region shrinks for supercritical fluid flow for both Re = 2,000 (Figure 4.11, A4) and 20,000 (Figure 4.12, B4). This prediction is in agreement with the experimental observation by Taneda (1978). Unlike the SST k-ω models, other RANS models predict similar streamlines for both the Reynolds numbers (i.e. subcritical and supercritical conditions). A close examination of the turbulent intensity contours as can be seen in Appendix C reveals that the turbulent intensity values at the rear of the particle (i.e. at the azimuthal angle of 180°) are bigger for

the SST k-ω model. This prediction qualitatively supports the better pressure coefficient by the SST k-ω at $Re = 10^5$. It can also be observed from Figure 4.8 that the pressure coefficient prediction by the RNG k-ε model is not good, particularly at the rear of the particle due to the weak and small recirculation regions predicted by this model (Figures 4.15 – 4.16). Although the streamline plot is made for Re = 20,000, it can be argued that with increase in Re to 10^5, the separation point will further move towards the rear of the particle and as a result the recirculation is only going to become smaller. This reduction on the size of the recirculation will further increase the pressure coefficient values and the comparison with Constantinescu and Squires (2004) will become poorer at the rear of the particle.

Table 4.5. Comparison of angle of separation for non-supercritical fluid.

Model /experiment	Re = 2,000	Re = 20,000
SST k-ω	83°	78°
Standard k-ε	67.5°	67°
RNG k-ε	60°	56°
Realizable k-ε	78°	67°
Clift et al. (1978)	94.5°	84°

4.2.2.4 Drag coefficient for subcritical and supercritical condition

Based on the good agreement for velocity profiles between the present work and literature data, the simulations were extended in order to predict C_d for subcritical and supercritical of carbon dioxide. Table 4.6 shows the predicted results of C_d for simulation by using carbon dioxide as simulation fluid. The effect of four turbulence models on C_d values were observed and reported for subcritical as well as supercritical regimes. For all the regimes, C_d values were found to be similar. At both Re = 2,000 and 20,000, simulations by using RNG k-ε turbulence model had resulted in the highest value of C_d whereas the lowest C_d was obtained via simulation of SST k-ω. It is also observed that the increase in Re has also resulted in the increase of C_d. This result was also being found in the work of Hoerner (1935) in which the supercritical drag of a sphere is proportional to the increased of Reynolds

number. However, contradiction was found for the C_d values in Dixon et al. (2011) as can be seen in Table 4.7. Their results showed that when Reynolds number increases, the C_d values decreases. This contrary result is due to the different fluid used in both works.

Table 4.6. The simulated results of C_d for carbon dioxide.

Model	C_d			
	(1) Liquid	(2) Liquid	(3) Vapor	(4) SCF
Re = 2000				
Standard k-ε	0.300	0.301	0.300	0.300
RNG k-ε	0.373	0.374	0.373	0.373
Realizable k-ε	0.281	0.280	0.280	0.278
SST k-ω	0.262	0.262	0.262	0.262
Re = 20,000				
Standard k-ε	0.428	0.428	0.428	0.428
RNG k-ε	0.504	0.504	0.503	0.504
Realizable k-ε	0.374	0.374	0.374	0.374
SST k-ω	0.306	0.306	0.306	0.306

Table 4.7. C_d for non-supercritical fluid.

Model/experiment	C_d for Re = 2,000	C_d for Re = 20,000	Reference
Standard k-ε	0.3066	0.1626	-
RNG k-ε	0.2776	0.1206	-
Realizable k-ε	0.2640	0.1394	-
SST k-ω	1.3327	0.1996	-
experimental	0.41	0.425	Clift et al. (1978)
CFD simulation	0.6	0.2	Dixon et al. (2011)

From the comparison of C_d in Table 4.6 and 4.7, the predicted C_d values for Re = 2000 were observed to be lower than the C_d values by Dixon et al. (2011) compared to the predicted C_d values for Re = 20,000 which were found to be higher than the predicted values by Dixon et al. (2011). It can be observed that for Re = 2,000, the C_d values for simulation results of carbon dioxide are found to be lower than the simulated results of Dixon et al. (2011) and Clift et al. (1978) whereas the C_d values for Re = 20,000 are revealed to be higher for all the turbulence models. According to Wadsworth (1958), the movement of the separation circle on a sphere due to the effect of free-stream turbulence may also affect the drag significantly although the displacement is found to be very minimal. This is another reason that may affect the slight change of the supercritical drag values.

It is also observed that the phase behaviours of the fluid did not affect the C_d values. The only effects were caused by the different Re and turbulence models used. Many published literatures also disclosed that the turbulence characteristics of the approaching flow can affect the value of C_d at the Reynolds numbers between 2,000 to 200,000 (Neve and Shansonga 1989).

4.2.2.5 Turbulent intensity for supercritical condition

After the fine-tuning of all four turbulence models, the comparison for these four models on their turbulent intensity has been made. The graph of the comparison is presented in Figure 4.19. This comparison is vital in choosing the suitable turbulence model for single sphere simulation under supercritical fluid condition. From Figure 4.19, the predicted trends of turbulent intensity for all the simulations by using *k-ε* models have shown similarity as compared to SST *k-ω*. The lowest turbulent intensity has been predicted by using SST *k-ω* model although all simulations have predicted quite low turbulent intensity which is less than 1%.

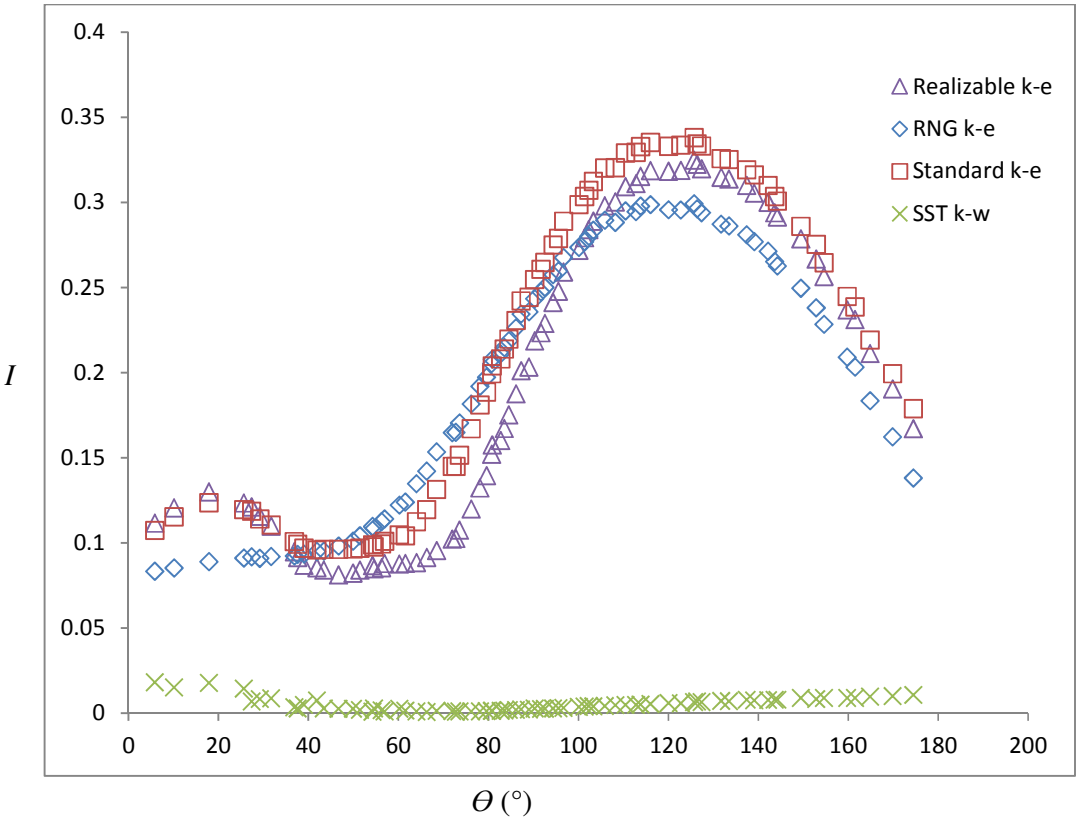

Figure 4.19. Comparison of turbulent intensity for *Re* = 2000

4.3 Conclusion

The predicted results of velocity profiles were presented in detail including the results of velocity profiles given by Dixon et al. (2011) were also reproduced. The predicted results were found to agree well with the literature data of Dixon et al. (2011). Simulations were then carried out to determine the velocity profiles at subcritical and supercritical conditions of Reynolds numbers (2000 and 20,000), pressures (65 and 80 bar) as well as temperatures (283.15 and 308.15K). Interesting flow features were noted for all the simulations. The RANS turbulence models results were found to be satisfactory in the three regions i.e. recirculation, recovery and near-wake. It is found that SST k-ω can better capture the recirculation region and the near-wake of the sphere more clearly in subcritical and supercritical conditions. This has led to a better prediction of pressure coefficient by SST k-ω model as compared to other models. It is also detected that the longest recirculation regions were found in the simulation by using SST k-ω turbulence model. It has been shown that SST k-ω turbulence model method can perform better over a wide range of Reynolds numbers and has been designed to be integrated all the way to the wall without using wall functions (Dixon et al. 2013). SST k-ω models also can better capture curvature effect on flow as compared to other models. Therefore, it can accurately predict flow separation under adverse pressure gradient (Bardina et al. 1997). However, less recirculation regions were predicted in RNG k-ε turbulence model simulations and it has led to the longest recovery regions for these simulations. As for the drag coefficient values, the predicted result by using RNG k-ε turbulence model was found to be the nearest to the literature in the transitional flow regime whereas for the turbulent regime, SST k-ω turbulence model was found to be comparable to the literature data. In addition, SST k-ω turbulence model was also able to capture the value and angular position of C_p quite accurately and has good comparison with the literature data. Therefore, it is recommended to employ SST k-ω turbulence model since it is able to capture the flow pattern more clearly in the subcritical and supercritical regimes.

CHAPTER 5 PACKED BED STUDY

In this chapter, simulations were performed for packed bed of spherical particles. Firstly, the simulations were carried out to investigate the hydrodynamics of packed bed consisting of 6 layers having a total of 56 spheres. The work from Reddy and Joshi (2008) was adopted in this study as indicated in Chapter 3 for validation purposes. The drag coefficient and pressure drop were predicted using water as fluid and results were validated with of Reddy and Joshi (2008) before extending the simulations to supercritical carbon dioxide. Most of the validation works were done by using standard k-ε turbulence model in order to be comparable with the simulation work of Reddy and Joshi (2008) which employed k-ε turbulence model. In addition, the comparative studies of RANS turbulence models were also done to determine the suitable turbulence model for the investigation of hydrodynamics in packed bed of spherical particles.

After the validation of the simulated results for packed bed of 56 spheres of 6 layers, further investigations were then carried out for packed bed of 128 spheres of 8 layers. These further investigations are important in order to study the effect of bed porosity on the flow distribution in packed bed. The simulated results of drag coefficient and pressure drop were presented and reported in this chapter.

5.1 Flow Pattern for Packed Bed of Spherical Particles

Axial and radial cuts were made along the bed in order to produce velocity vector plots. This is to enable the investigation of the velocity distribution along the packed bed. Figures 5.1 and 5.2 show the vector plots generated by using SST k-ω turbulence model. Comparisons of flow pattern were made at different axial positions in the packed bed. In all of the figures, it can be clearly observed that the simulation data are only collected at a certain number of axial positions which is along the z-axis. Although certain locations were chosen, it is still able to show a good overview of the flow pattern inside the bed.

From the vector plots, the arrows depict the velocity of the fluid inside the bed and they have both magnitude and direction. In addition, these magnitude and direction are represented by the arrows in which the head of the arrow points the direction of the fluid and the tail of the arrow signifies the magnitude of the fluid. It is also noted that the direction of the fluid shows the local flow, and the magnitude of the velocity vector is proportional to the

length of the arrow which also implies the speed of the fluid flow (Logtenberg, Nijemeisland et al. 1999). As expected, we can observe that low velocity or almost zero velocity can be detected in between the sphere particles as well as low velocity for packed bed with more spherical particles.

From the vector plots, it can be seen that fluid was flowing and accelerated between the gaps of the spheres particularly for the spheres positioned further from the wall. This is shown by the long arrows (vectors magnitude) (Logtenberg, Nijemeisland et al. 1999). Stagnant zones were clearly detected in all of the cases analysed due to the no slip condition applied near wall and sphere surfaces (see Figures 5.1 and 5.2) in particular for the simulation for packed bed of 128 spheres in which more stagnation points can be observed. Secondary flows were also noticeable in between the spheres (see Figure 5.2). The highest velocity was visible at the central layer area which is in between the first and the second layer of the spheres. The strong vectors through the centre were also detected due to the large open gap in between the spheres in the bed. This observation can also be seen in the simulation studies of Logtenberg and Dixon (1998).

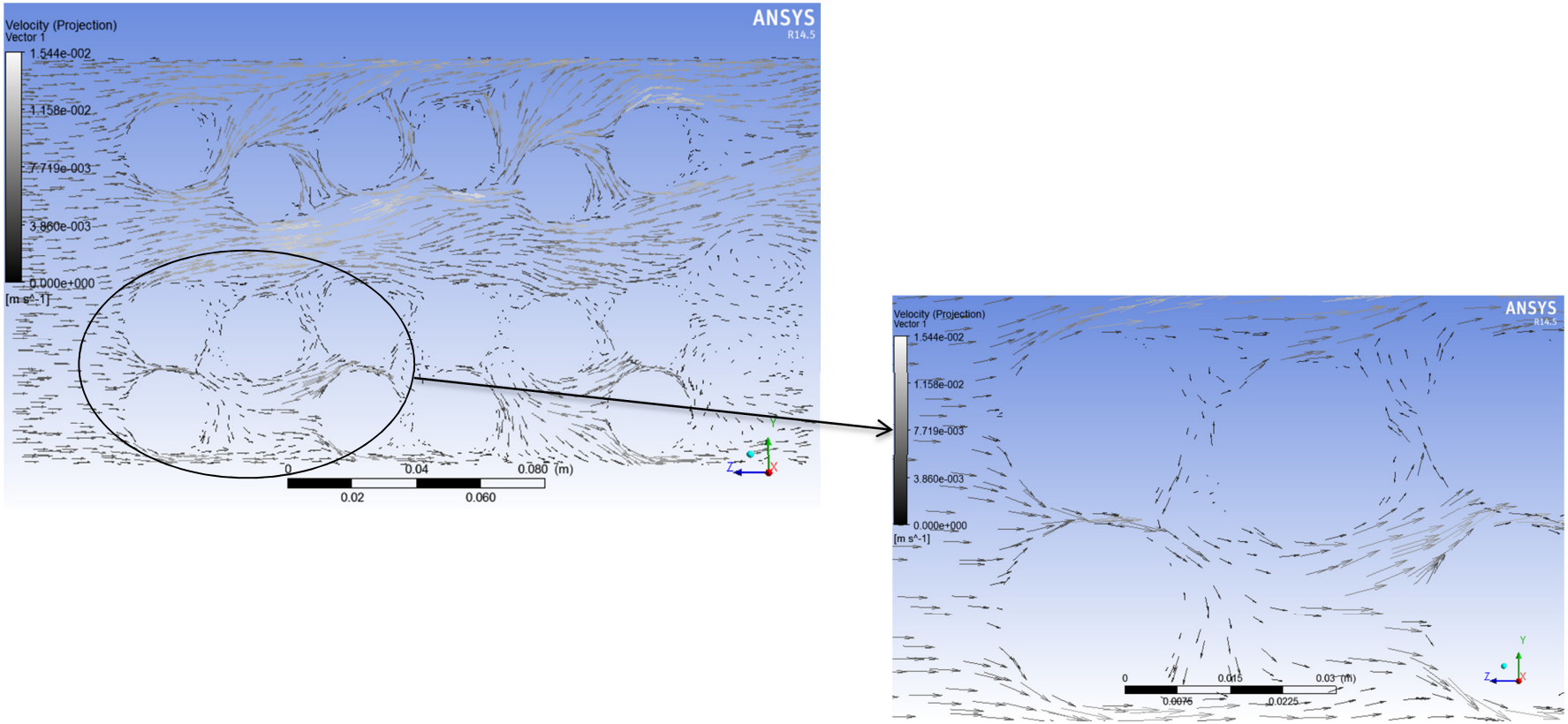

Figure 5.1. Vector plot showing the velocity in a cross section ($x = 0$) for Re = 2,000 by using SST k-ω turbulence model for packed bed of 56 spheres.

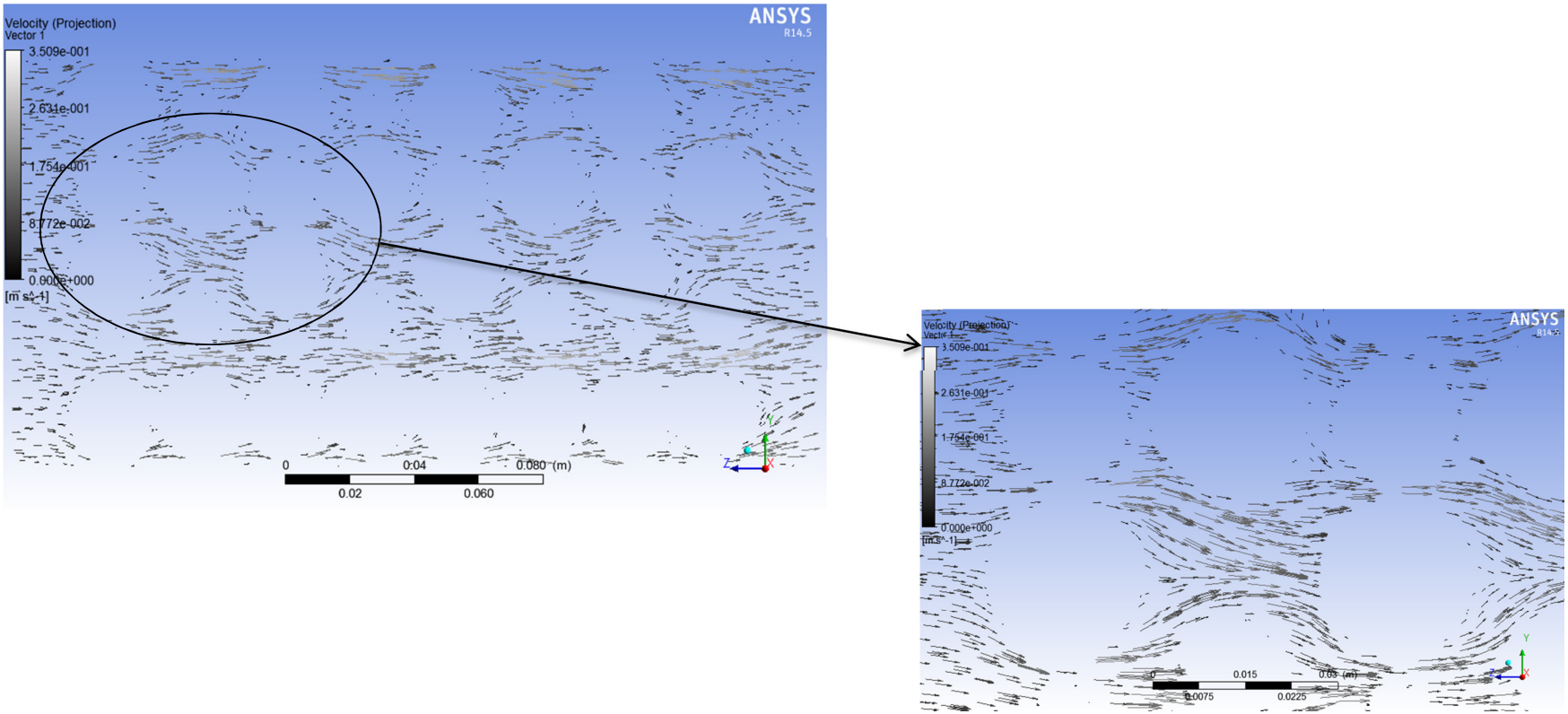

Figure 5.2. Vector plot showing the velocity in a cross section ($x = 0$) for Re = 2,000 by using SST k-ω turbulence model for packed bed of 128 spheres.

5.2 The Effect of Reynolds Number on Drag Coefficients for Packed Bed of 56 Spheres (non supercritical fluid)

The validation for the prediction value of drag coefficient was done by comparing the values with the CFD results reported in the literature as well as with Ergun's equation (1952). The details of the predicted results via CFD simulation in comparison with the literature data are depicted in Figure 5.4. The validation study was done by imitating the model employed in Reddy and Joshi (2008) which was *k-ε* turbulence model. By using Reddy and Joshi's model, almost similar results can be predicted so that it can be employed in the further studies of supercritical fluid condition. It can be observed clearly from the graph that the higher the Reynolds number, the lower the value of drag coefficient obtained. This may due to the premature transition of the boundary layer at the sphere and a narrow wake (Neve et al. 1986). It is also evidence that the present work is found to be in good agreement with the literature data of Reddy and Joshi (2008) as well as Ergun's equation.

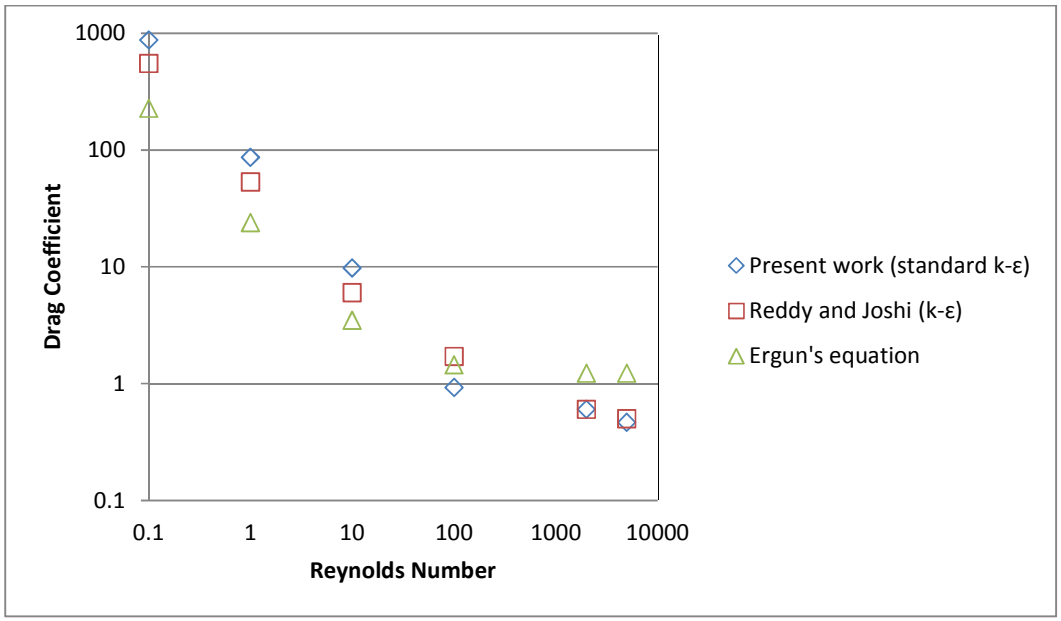

Figure 5.3. Comparison of predicted drag coefficient values with the literature data of Reddy and Joshi (2008) and Ergun's equation.

It is also observed that the predicted results in laminar flow regimes i.e. Reynolds numbers of 0.1, 1 and 10 are in good agreement with the results obtained by Reddy and Joshi (2008). However, the values of drag coefficients were overestimated for the same Reynolds numbers in comparison with Ergun's equation. This may be caused by the countering effects

of wall friction and channeling near the wall as can be found in Reddy and Joshi (2008). Meanwhile in turbulent flow regimes, the predicted results were being underestimated as compared to both Ergun's equation and literature data of Reddy and Joshi (2008). This similar trend can also be detected for the comparison of the literature data of Reddy and Joshi's with Ergun's equation. This is probably due to the effect of channeling overrides the effect of wall friction and resulting in decreasing of drag coefficients values in comparison with Ergun's equation.

5.3 The Effect of Turbulence Models on Drag Coefficients for Packed Bed of 56 Spheres (supercritical fluid)

After a good comparison in the validation work previously for non-supercritical fluid, the simulation work is extended to investigate the effect of turbulence models on drag coefficients.

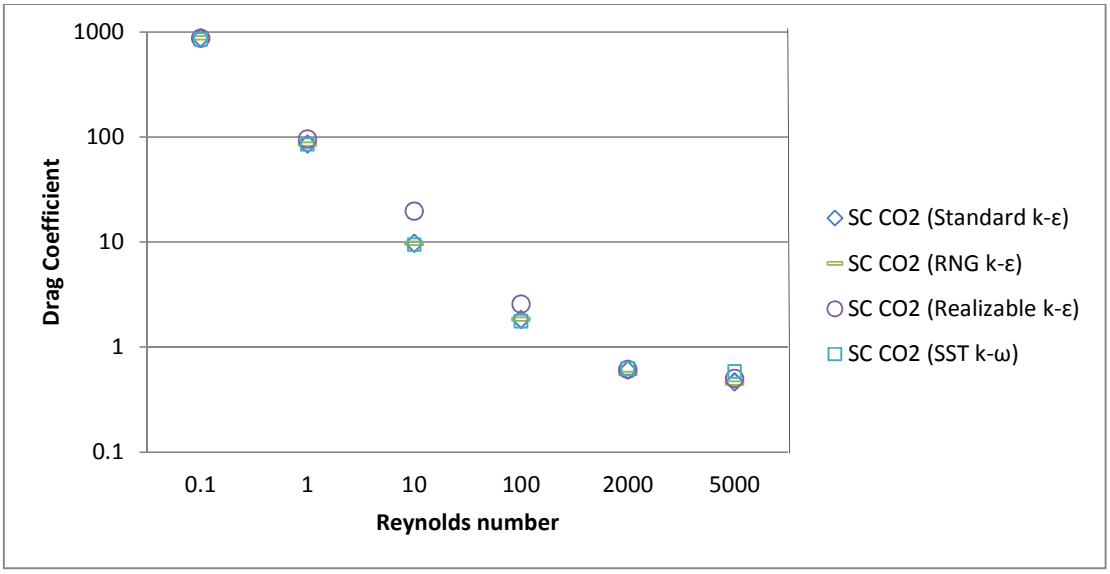

Figure 5.4. Comparison of simulated drag coefficient values for supercritical carbon dioxide.

Figure 5.4 shows the comparison of the drag coefficient values for supercritical carbon dioxide simulated by using four different RANS turbulence models. It is interesting to know that the trend of the graph for drag coefficient values is similar for all the simulations.

A few factors may cause this trend. Firstly, *k-ε* turbulence models are widely used when solving relatively simple flows. In this case, the simulating fluid was supercritical carbon dioxide and simulated in high Reynolds numbers. Therefore, the flow is found to be turbulent. Inaccuracy may be detected for the simulations via *k-ε* turbulence models when dealing with cases where strong gradients exist, for instance at the areas of great curvature with recirculation (Cabezón et al. 2011). Secondly, *k-ε* turbulence models are also known as isotropic model. This type of model cannot capture the separation at the boundary layer as well as curvature effects at high Reynolds number (Reddy and Joshi 2008). As a result, these limitations led to the similar trend of the graph (see Figure 5.5).

5.4 The Effect of Reynolds Number on Pressure Drop for Packed Bed of 56 Spheres (non supercritical fluid)

The validation for the values of pressure drop for the simulation by using supercritical carbon dioxide as simulating fluid was being done and compared with the literature data of Reddy and Joshi (2008) as well as Ergun's equation. The comparison is shown in Figure 5.5.

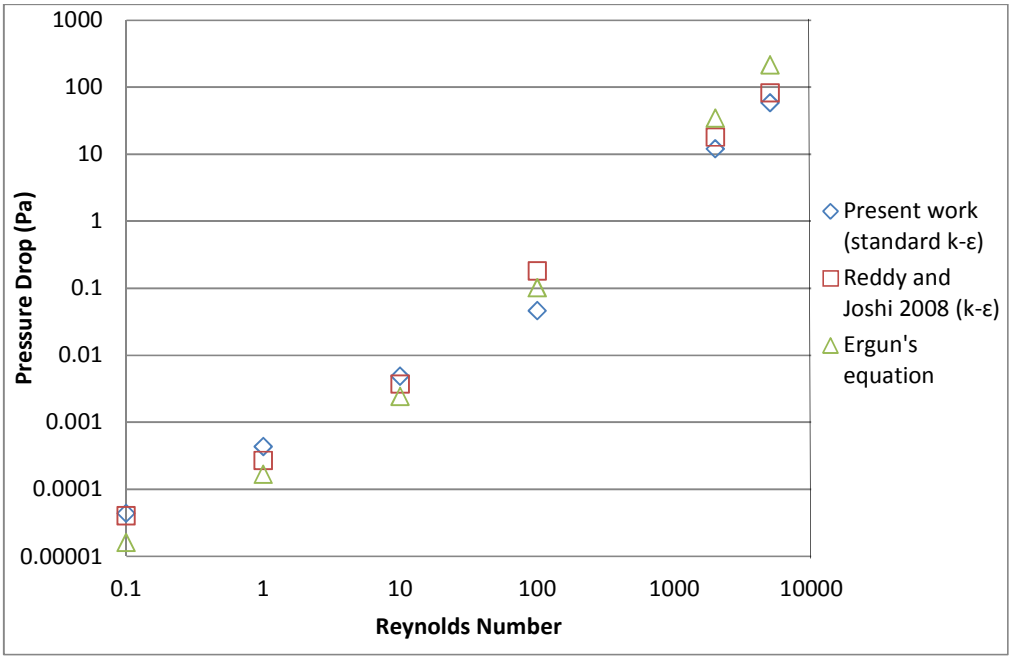

Figure 5.5. Comparison of predicted pressure drop values with the literature data of Reddy and Joshi (2008) and Ergun's equation.

As can be seen in Figure 5.5, there is a noticeable agreement between the simulated results of pressure drop in the current studies and the literature data of Reddy and Joshi (2008) although for the Reynolds numbers ranging from 0.1 to 10 (laminar flow regimes) shows that the simulated values of pressure drop are overestimated as compared to Ergun's equation and underestimated for Reynolds numbers 100 – 10000 (transition to turbulent flow regimes). The predicted pressure drop values have also been compared with Ergun's equation in Figure 5.5. Similar trend has been observed for this comparison for all flow regimes. Good agreement between the simulated pressure drop and Ergun's equation has also been observed. However, smaller deviation has been detected for the comparison between the simulated results and Reddy and Joshi (2008) as compared to Ergun's equation. Therefore, it can be concluded that the simulated pressure drop values are more comparable with Reddy and Joshi (2008).

5.5 The Effect of Turbulence Models on Pressure Drop for Packed Bed of 56 Spheres (supercritical fluid)

The effect of four turbulence models namely SST k-ω, standard k-ε, RNG k-ε and realizable k-ε turbulence models on pressure drop were employed in this study as shown in Figure 5.6. All of the simulations for supercritical carbon dioxide are found to be lower than the pressure drop of simulation by using water as simulating fluid. It is observed that the simulations by using all four RANS turbulence models predicted almost similar results for the Reynolds numbers ranging from 0.1 to 5000.

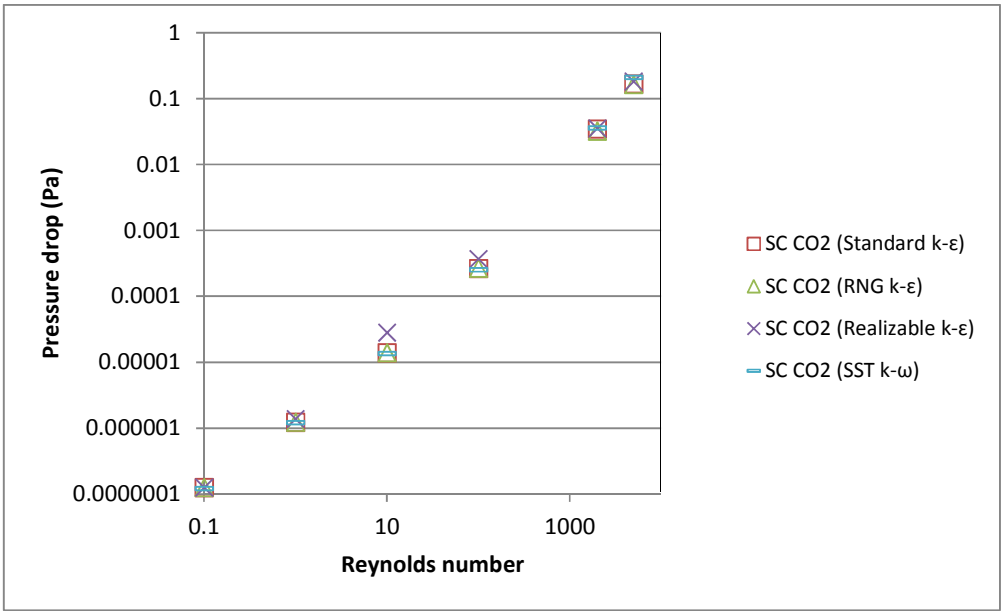

Figure 5.6. Comparison of simulated pressure drop values for supercritical carbon dioxide.

As can be seen in Figure 5.6, the pressure drop values predicted by all turbulence models are consistent with each other. Almost similar results were obtained for all turbulence models with the difference of less than 9% as compared among the four turbulence models themselves. Therefore, it can also be concluded that different turbulence models used has no effect on the pressure drop. As far as the statistics is concerned, the two quantitative variables namely Reynolds number and pressure drop are linearly correlated. This shows that pressure drop is independent to the RANS turbulence models. Thus, other appropriate models should be considered due to this limitation. The best fitted line can be constructed in order to make the prediction of the pressure drop values if the Reynolds number is given. Statistically, these two variables are positively correlated. Hence, as Reynolds number increases, the pressure drop also increases.

5.6 The Effect of Reynolds Number on Drag Coefficients and Pressure Drop for Packed Bed of 128 Spheres

For the simulations of packed bed of 128 spheres, the effect of Reynolds number on drag coefficient and pressure drop is shown in Figure 5.7. The simulations were run by using four widely used Reynolds Averaged Navier-Stokes Equations (RANS) turbulence models (Standard, RNG and realizable *k*-ε as well as SST *k*-ω).

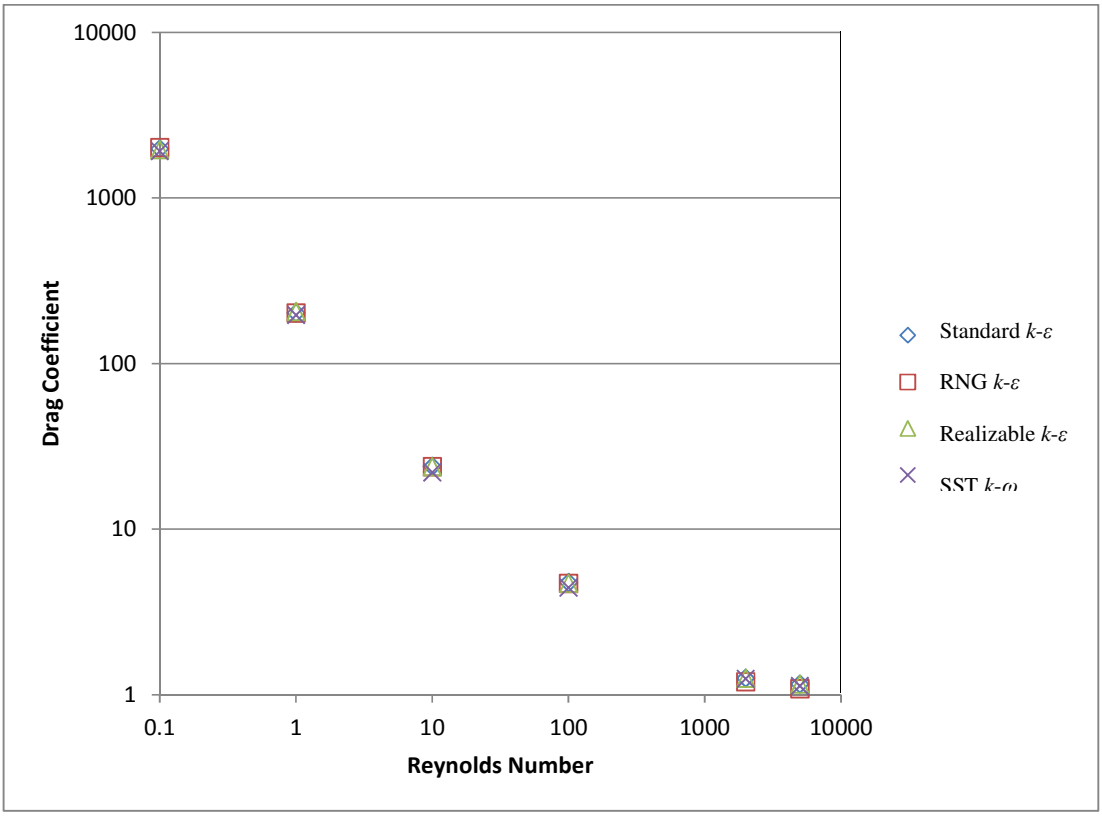

Figure 5.7. Comparison of RANS turbulence models for simulated drag coefficient values.

It can be noted that the simulated drag coefficients and pressure drop values are consistent with each other. Almost similar results were obtained for all the turbulence models employed with the difference of less than 9% as compared among the four turbulence models. This is probably due to the use of *k-ε* turbulence models. It is identified that *k-ε* turbulence models are isotropic turbulence models in which these models are not able to perform well at turbulent flow regimes i.e. high Reynolds number (Reddy and Joshi 2008). As expected, the drag coefficients decrease as the Reynolds number increases as can be seen in Figure 5.7 whereas the pressure drop value increases as Reynolds number increases as observed in Figure 5.8. This shows that all the turbulence models are able to predict the drag coefficients and pressure drop values consistently. This has implied that no best turbulence model is recommended for the prediction of drag coefficient and pressure drop values of packed bed of spherical particles. Therefore, further work needs to be done for improvement by considering the use of higher order turbulence models such as RSM.

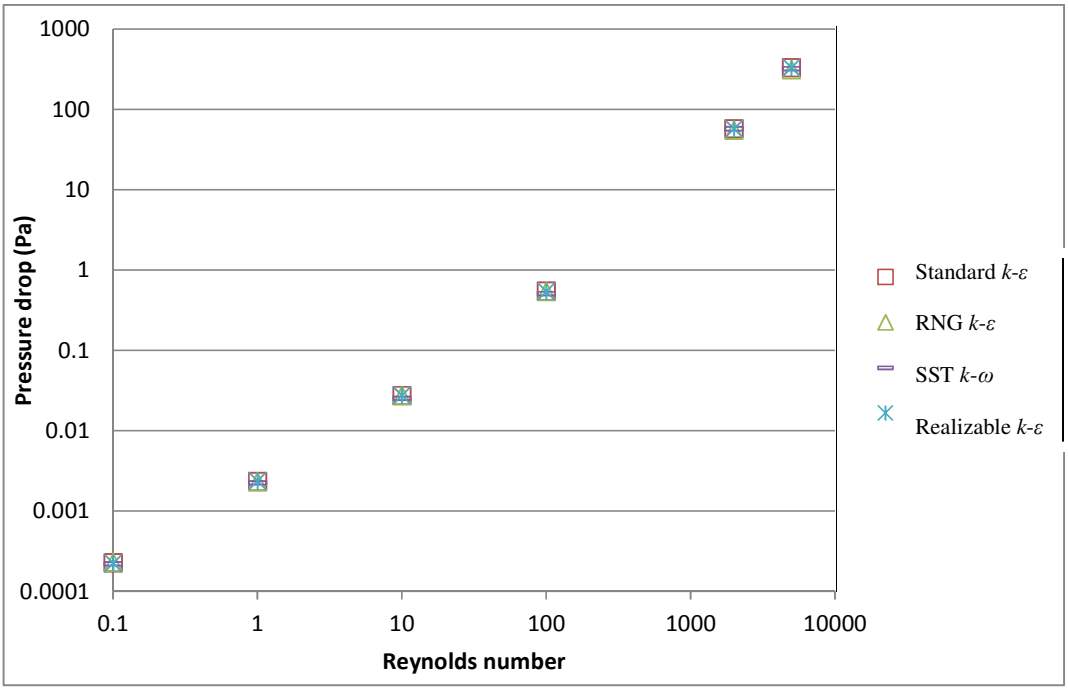

Figure 5.8. Comparison of RANS turbulence models for simulated pressure drop values.

5.7 The Effect of Bed Porosity on Drag Coefficients and Pressure Drop

The influence of bed porosity on the hydrodynamics of packed bed column was studied. It is noted that the parameters such as the height of the bed, the ratio between column to particle diameter, the particle size distribution and shape, the packing mode as well as the roughness of the particle surfaces can influence the bed porosity (Ribeiro et. al, 2010). In this current work, all the parameters were set as constant except for the bed porosity in order to observe the effect of bed porosity on the hydrodynamics in packed bed. The details of the geometry have been discussed in Chapter 3.

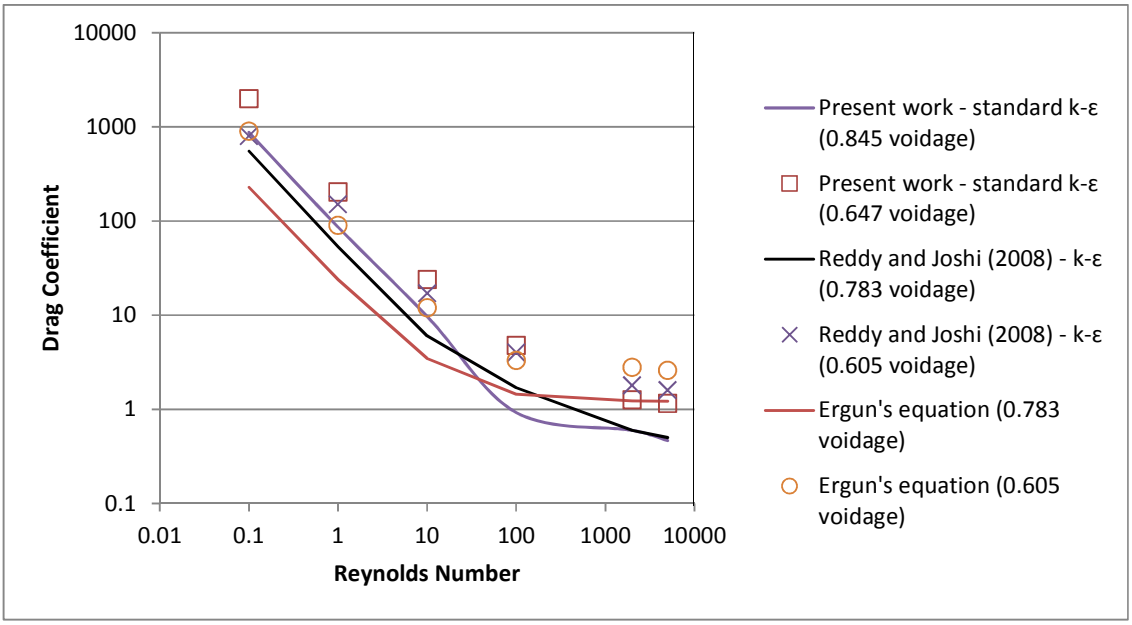

Figure 5.9. Comparison of simulated drag coefficient values for the effect of bed porosity.

Table 5.1. Percentage average error of the predicted pressure drop as compared to literature

	0.647 voidage		0.845 voidage	
Re	% error as compared to Reddy and Joshi (2008)	% error as compared to Ergun's equation	% error as compared to Reddy and Joshi (2008)	% error as compared to Ergun's equation
0.1	13	89	9	173
1	29	131	60	158
10	37	83	31	99
100	43	81	74	54
2000	42	70	33	65
5000	53	59	29	73

Figure 5.9 shows the simulated results of drag coefficient for bed voidage of 0.647 and 0.845 for the present work as compared with the literature data of Reddy and Joshi (2008) and Ergun's equation. As can be seen in Figure 5.9, the present work's bed voidage is 0.845 as compared to the literature that is 0.783. Although the bed voidage values are different but the bed geometry for the present work and the literature work are the same. It is also noted that despite the difference of bed voidage values, both packed beds are identical in dimension.

From Figure 5.9, it can be observed that the comparison with Reddy and Joshi (2008) is found to be in good agreement qualitatively. By referring to the percentage average error in Table 5.1, the simulated results for bed voidage of 0.647 is found to be closer to Reddy and Joshi (2008) especially for low Reynolds numbers. However, the percentage average error is found to be far overestimated as compared to Ergun's equation $Re < 1$. It is clearly revealed that bed porosity can affect the drag coefficient across the bed. On the other hand, in the case of bed voidage 0.647, the current work has generated a packed bed of 128 spheres of 8 layers meanwhile Reddy and Joshi (2008) used packed bed of 105 spheres in 7 layers. Due to the difference of the geometry, the bed voidage values are also different.

For packed bed of 56 spheres of 6 layers (bed voidage = 0.845), the values of the drag coefficient are found to be lower than the values of simulation for packed bed of 128 spheres of 8 layers (bed voidage = 0.647). In comparison with both literature data, the present work has overestimated the drag coefficient for $Re < 10$ whereas underestimated the drag coefficient for transition and turbulent flow ($Re > 100$). When the voidage is decreased from 0.845 (56 spheres) to 0.647 (128 spheres), it is noted that the ratio (S_w/S_p) of surface area of wall (S_w) to the surface area of particles (S_p) is increased from 0.6165 to 0.6569. The change in the surface area for both packed beds can be calculated by using S_w/S_p which is depending on the dimension of the bed and also the number of particles in the bed. Thus, the contribution of wall area increases with a decrease in the voidage. This has shown that more wall friction found in creeping flow regime. Therefore, in the turbulent flow regime ($Re > 1000$), the predicted drag coefficient values were found to be low since the wall friction is restricted to small boundary layer (Reddy and Joshi 2008).

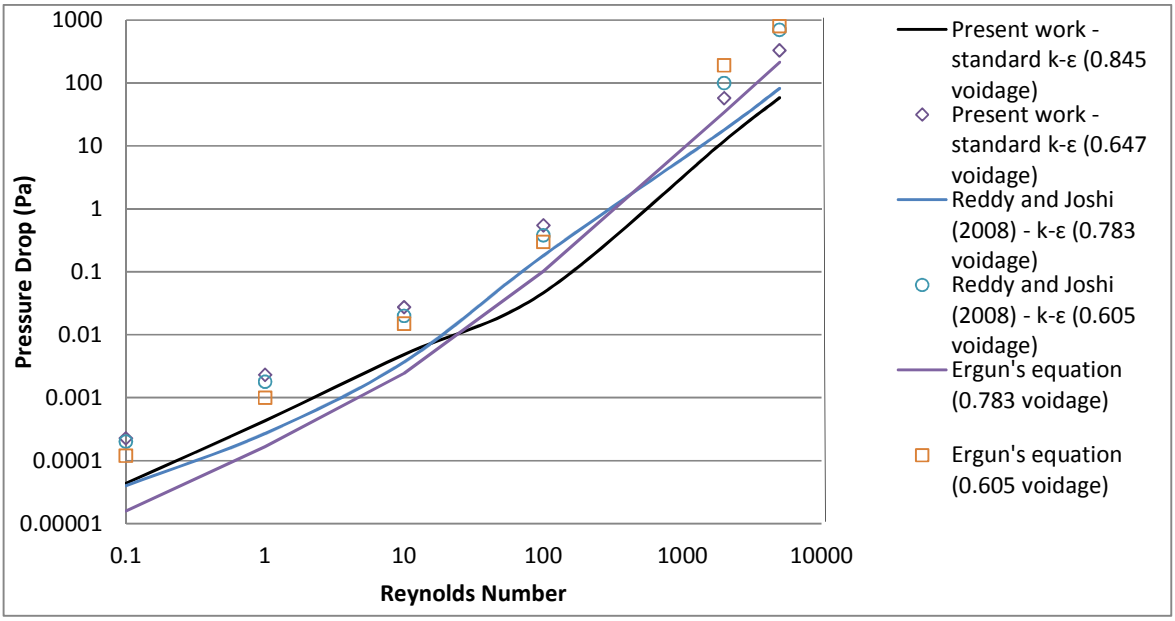

Figure 5.10. Comparison of simulated pressure drop values for the effect of bed porosity.

Table 5.2. Percentage average error of the predicted C_d as compared to literature

	0.647 voidage		0.845 voidage	
Re	% error as compared to Reddy and Joshi (2008)	% error as compared to Ergun's equation	% error as compared to Reddy and Joshi (2008)	% error as compared to Ergun's equation
0.1	147	120	59	284
1	35	125	63	262
10	41	100	62	180
100	19	44	46	36
2000	30	55	0	51
5000	28	55	7	62

Figure 5.10 shows the simulated results of pressure drop for bed voidage of 0.647 and 0.845 for the current work as compared to the literature data of Reddy and Joshi (2008) and Ergun's equation. Different from the results of drag coefficients, it is revealed that the values of the pressure drop for packed bed of 56 spheres of 6 layers (bed voidage = 0.845) are found to be higher than the values of simulation for packed bed of 128 spheres of 8 layers (bed voidage = 0.647). In comparison with both literature data, the present work has overestimated the pressure drop for $Re < 10$ with quite high percentage average errors (as seen in Table 5.2).

This may due to the unsuitability of turbulence models used in this study for laminar zone. Whereas the pressure drop for transition and turbulent flow ($Re > 100$) was underestimated. It is revealed that the predicted pressure drop for $Re > 100$ are found to be in good agreement with the literature with low percentage average errors (< 50%) as compared to $Re < 100$. The overall pressure drop may be affected by the wall friction and the channeling in the high void area near the wall. This is also found in the work of Reddy and Joshi (2008). It can be concluded that bed porosity can affect the pressure drop across the bed particularly due to the wall effects and the channelling near the wall.

CHAPTER 6 CONCLUSION AND RECOMMENDATION

The hydrodynamics studies of packed bed were investigated by using computational fluid dynamics. The commercially available code ANSYS FLUENT was used to predict the drag coefficients and pressure drop results. Four RANS turbulence models were compared to study their robustness in the system of supercritical carbon dioxide. It is revealed that SST k-ω turbulence model has the longest simulation period compared to the other model.

The predicted results of velocity, pressure drop and drag coefficient profiles for single sphere, packed bed of 56 spheres and 128 spheres were presented both qualitatively and quantitatively. For the flow distribution in single sphere, three flow regimes were observed and being investigated namely recirculation, recovery and near-wake. SST k-ω turbulence model was able to capture the recirculation region and near-wake of the sphere more clearly for both subcritical and supercritical conditions. As for the drag coefficient values, the predicted result by using RNG k-ε turbulence model was found to be the nearest to the literature in the transitional flow regime whereas SST k-ω turbulence model was found to be comparable to the literature data. It is also found that the C_p values for simulations by using SST k-ω turbulence model are the closest to the literature data and the pressure distribution curve is also consistent particularly for simulation of supercritical fluid. The lowest turbulent intensity has been predicted by using SST k-ω turbulence model although all simulations have predicted quite low turbulent intensity which is less than 1%.

For the validation works in single sphere study, it is revealed that the use of sensitivity analysis for SST k-ω and RNG k-ε turbulence models has resulted in good agreement for the predicted results of velocity profile in comparison with the literature data. The simulation results were found to be more promising as the values of the model parameters were increased. However, longer convergence time was detected as the values increased**.** The results also indicated that the predicted velocity profiles from the simulations were agreeable with the literature data of Dixon et al. (2011) with 10% and 6.77% average error respectively as compared to the use of sensitivity analysis for standard and realizable k-ε turbulence models. As for standard and realizable k-ε, in comparison with Clift et al. (1978), the percentage average errors were found to be 43.3% and 39.8%. Therefore, the results from the aforementioned study were implemented for packed bed of spherical particles due to non-

availability of literature data available for the validation of packed bed under supercritical fluid condition.

For packed bed of spherical particles of 56 spheres and 128 spheres, only four RANS turbulence models were being chosen to predict the hydrodynamics in packed bed columns namely standard, "Renormalization Group" RNG and realizable k-ε as well as SST k-ω. Similar trend was observed for the velocity profiles simulated by using four RANS turbulence models. Furthermore, the drag coefficient and pressure drop values simulated by using four RANS turbulence models were also quite similar. The isotropic k-ε turbulence models were unable to predict accurately the drag coefficient and pressure drop due to the imbalance on the turbulent length scales between the free stream and the wake region.

As for the effect of bed porosity, there is a good qualitative agreement as compared to literature data of Reddy and Joshi (2008) and Ergun's equation. The predicted drag coefficient values were found to be overestimated for both bed voidage of 0.647 (more spherical solids) and 0.845 (less spherical solids) in the laminar flow but it was underestimated for $Re > 100$. The predicted drag coefficient values were found to be low since the wall friction is restricted to small boundary layer. The results for pressure drop for both bed voidage of 0.647 and 0.845 were also found to be overestimated for $Re < 10$ and underestimated for transition and turbulent flow. This may due to the wall friction between sphere surfaces and channeling in the different bed voidage. In term of the flow pattern, the strong vectors through the centre were also detected due to the large open gap between the spheres in the bed for bed voidage of 0.845 and the highest velocity was visible at the central layer area. However, future work may include more simulations at porosity other than 0.647 and 0.845 in order to comprehensively study the effect of bed porosity to the hydrodynamics in packed bed.

It is known that the modelling of packed bed of spherical particles is very difficult especially the meshing due to the complex geometry and computational constraints. The simulations period was also found to be longer for packed bed of spherical particles as compared to single sphere simulations. In the case of single sphere study, it is recommended to employ SST k-ω turbulence model since it is able to capture the flow pattern more clearly in the turbulent regime although the simulation time were found to be longer. As for the simulations of packed bed of spherical particles, all turbulence models have shown quite similar predictive performances. Therefore, no best turbulence model is recommended for the

hydrodynamics study of packed bed of spherical particles. Hence, to improve this work, future project may consider the use of higher order turbulence models such as RSM. This is because RSM is anisotropic model and it has seven extra equations. This model also takes into consideration of all the effects derived from rapid changes at the main strain tensor. Therefore, it is more rigorous than one or two equations of turbulence models.

To extend this work for unsteady and multiphase flow in which the flow will be more complex, therefore LES method can be employed. It is known that the simulations by using this approach are three dimensional and time dependent but the largest scale of motion can be represented explicitly while the smaller scales are being approximated. Furthermore, DES method can also be applied in future work to investigate the flow pattern for high Reynolds number wall bounded flows.

Future work may also include the investigation of heat and mass transfer in packed bed columns since the fluid flow is governed by the heat and mass transfer inside the bed. Therefore, this project can be extended to develop a model which also takes into consideration the coupling of fluid flow with mass transfer. Due to the present work is to investigate and analyse the flow behaviour, therefore the effect of heat and mass transfer has been neglected.

Since the present study has only taken into consideration the liquid-liquid extraction. Therefore, in the future, it is proposed to study the comparison of turbulence models in predicting the hydrodynamics for solid-liquid extraction due to its popular used in the palm oil industry particularly in Malaysia.

REFERENCES

Abbas, K. A., A. Mohamed, A. S. Abdulamir and H. A. Abas (2008). "A Review on Supercritical Fluid Extraction as New Analytical Method." American Journal of Biochemistry and Biotechnology **4**(4): 345-353.

Akanda, M. J. H., M. Z. I. Sarker, S. Ferdosh, M. Y. A. Manap, N. N. N. Ab Rahman and M. O. Ab Kadir (2012). "Applications of Supercritical Fluid Extraction (SFE) of Palm Oil and Oil from Natural Sources." Molecules **17**(2): 1764-1794.

Al-Dahhan, M. H., F. Larachi, M.P. Dudukovic and A. Laurent (1997). "High-Pressure Trickle-Bed Reactors: A Review." Industrial and Engineering Chemistry Research **36**(8): 3292-3314.

Anderson, J. D. (2007). "Fundamentals of Aerodynamics." 4th Edition. New York: McGraw Hill.

Atmakidis, T. and E. Y. Kenig (2009). "CFD-based analysis of the wall effect on the pressure drop in packed beds with moderate tube/particle diameter ratios in the laminar flow regime." Chemical Engineering Journal **155**(1–2): 404-410.

Augier, F., F. Idoux and J. Y. Delenne (2010). "Numerical simulations of transfer and transport properties inside packed beds of spherical particles." Chemical Engineering Science **65**(3): 1055-1064.

Bahadori, A., H. B. Vuthaluru and S. Mokhatab (2009). "New correlations predict aqueous solubility and density of carbon dioxide." International Journal of Greenhouse Gas Control **3**(4): 474-480.

Bai, H., J. Theuerkauf, P. A. Gillis and P. M. Witt (2009). "A Coupled DEM and CFD Simulation of Flow Field and Pressure Drop in Fixed Bed Reactor with Randomly Packed Catalyst Particles." Industrial & Engineering Chemistry Research **48**(8): 4060-4074.

Baker, M. J. and G. R. Tabor (2010). "Computational analysis of transitional air flow through packed columns of spheres using the finite volume technique." Computers & Chemical Engineering **34**(6): 878-885.

Baker, M. J., P. G. Young and G. R. Tabor (2011). "Image based meshing of packed beds of cylinders at low aspect ratios using 3d MRI coupled with computational fluid dynamics." Computers & Chemical Engineering **35**(10): 1969-1977.

Bakic, V. V., M. Schmid and B. Stankovic (2006). "Experimental Investigation of Turbulent Structures of Flow around a Sphere." Thermal Science **10**(2): 97-112.

Bardina, J. E., P. G. Huang and T. J. Coakley (1997). "Turbulence Modeling Validation, Testing and Development." NASA Technical Memorandum 110446.

Berna, A., A. Tárrega, M. Blasco and S. Subirats (2000). "Supercritical CO2 extraction of essential oil from orange peel; effect of the height of the bed." The Journal of Supercritical Fluids **18**(3): 227-237.

Bingjie, S., Z. Weidong, Z. Zeting and Y. Enping (2002). "Hydrodynamics and Mass Transfer Performance in Supercritical Fluid Extraction Columns." Chinese Journal of Chemical Engineering **10**(6): 696-700.

Błaszczyński, T., A. Ślosarczyk and M. Morawski (2013). "Synthesis of Silica Aerogel by Supercritical Drying Method." Procedia Engineering **57**: 200-206.

Breuer, M (1998). "Large Eddy simulation of the Subcritical Flow Past a Circular Cylinder: Numerical and Modeling Aspects." International Journal for Numerical Methods in Fluids **28**(9): 1281-1302.

Brucato, A., F. Grisafi and G. Montante (1998). "Particle drag coefficients in turbulent fluids." Chemical Engineering Science **53**(18): 3295-3314.

Brunazzi, E. and A. Paglianti (1997). "Mechanistic pressure drop model for columns containing structured packings." AIChE Journal **43**(2): 317-327.

Buchmayr, M., J. Gruber, M. Hargassner and C. Hochenauer (2016). "A computationally inexpensive CFD approach for small-scale biomass burners equipped with enhanced air staging." Energy Conversion and Management **115**: 32-42.

Burström, P. E. C., V. Frishfelds, A. Ljung, T. S. Lundström and B. D. Marjavaara (2017). "Modelling heat transfer during flow through a random packed bed of spheres." Heat and Mass Transfer **53**(352): 1-21.

Byrappa, K., S. Ohara and T. Adschiri (2008). "Nanoparticles synthesis using supercritical fluid technology – towards biomedical applications." Advanced Drug Delivery Reviews **60**(3): 299-327.

Cabezón, D., E. Migoya and A. Crespo (2011). "Comparison of turbulence models for the computational fluid dynamics simulation of wind turbine wakes in the atmospheric boundary layer." Wind Energy **7**(14): 909-921.

Calis, H. P. A., J. Nijenhuis, B. C. Paikert, F. M. Dautzenberg and C. M. van den Bleek (2001). "CFD modelling and experimental validation of pressure drop and flow profile in a novel structured catalytic reactor packing." Chemical Engineering Science **56**(4): 1713-1720.

Campardelli, R., G. Della Porta and E. Reverchon (2012). "Solvent elimination from polymer nanoparticle suspensions by continuous supercritical extraction." The Journal of Supercritical Fluids **70**: 100-105.

Campregher, R., S. S. Mansur and A. Silveira-Neto (2006). Numerical Simulation of the Flow Around a Sphere Using the Immersed Boundary Method for Low Reynolds. Direct and Large-Eddy Simulation VI. E. Lamballais, R. Friedrich, B. Geurts and O. Métais, Springer Netherlands. **10**: 651-658.

Carrier, G. (1953). On slow viscous flow, DTIC Document.

Chalermsinsuwan, B., T, Chanchuey, W. Buakhao, D. Gidaspow and P. Piumsomboon (2012). "Computational fluid dynamics of circulating fluidized bed downer: study of modeling parameters and system hydrodynamic characteristics." Chemical Engineering Journal **189-190**: 314-335.

Choong, Y. Y., K. W. Chou and I. Norli (2018). "Strategies for improving biogas prodduction of palm oil mill effluent (POME) anaerobic digestion: A critical review." Renewable and Sustainable Energy Reviews **82**: 2993-3006.

Clamen, A. and W. H. Gauvin (1969). "Effects of turbulence on the drag coefficients of spheres in a supercritical flow Ŕegime." AIChE Journal **15**(2): 184-189.

Clifford, T. (1969). "Fundamentals of supercritical fluids." Oxford University Press: New York.

Clift, R., J. R. Grace and M. E. Weber (1978). "Bubbles, Drops, and Particles." Academic Press: New York.

Constantinescu, G. and K. Squires (2004). "Numerical investigations of flow over a sphere in the subcritical and supercritical regimes." Physics of Fluids **16**(5): 1449-1466.

Coussirat, M., A. Guardo, B. Mateos and E. Egusquiza (2007). "Performance of stress-transport models in the prediction of particle-to-fluid heat transfer in packed beds." Chemical Engineering Science **62**(23): 6897-6907.

Daly, B. J. and F. H. Harlow (1970). "Transport Equations in Turbulence." Physics of Fluids (1958-1988) **13**(11): 2634-2649.

del Valle, J. M., J. C. de la Fuente and D. A. Cardarelli (2005). "Contributions to supercritical extraction of vegetable substrates in Latin America." Journal of Food Engineering **67**(1–2): 35-57.

Dixon, A. G. (1988). "Correlations for the wall and particle shape effects on fixed bed voidage." Canadian Chemical Engineering **66**(5): 705-708.

Dixon, A. G., M. Ertan Taskin, M. Nijemeisland and E. H. Stitt (2011). "Systematic mesh development for 3D CFD simulation of fixed beds: Single sphere study." Computers & Chemical Engineering **35**(7): 1171-1185.

Dixon, A. G., M. Nijemeisland and E. H. Stitt (2013). "Systematic mesh development for 3D CFD simulation of fixed beds: Contact points study." Computers & Chemical Engineering **48**: 135-153.

Dixon, A. G., G. Walls, H. Stanness, M. Nijemeisland and E. H. Stitt (2012). "Experimental validation of high Reynolds number CFD simulations of heat transfer in a pilot-scale fixed bed tube." Chemical Engineering Journal **200–202**: 344-356.

Dorn, M., F. Eschbach, D. Hekmat and D. Weuster-Botz (2017). "Influence of different packingmethods on the hydrodynamics stability of chromatography columns." Journal of Chromatography A **1516**: 89-101.

Dolamore, F., C. Fee and S. Dimartino (2018). "Modelling ordered packed beds of spheres: The importance of bed orientation and the influence of tortuosity on dispersion." Journal of Chromatography A **1532**: 150-160.

Eisenmenger, M. J. (2005). "Supercritical Fluid Extraction, Fractionation and Characterization of Wheat Germ Oil." Master of Science Master Thesis, Oklahoma State University.

Eppinger, T., K. Seidler and M. Kraume (2011). "DEM-CFD simulations of fixed bed reactors with small tube to particle diameter ratios." Chemical Engineering Journal **166**(1): 324-331.

Ergun, S. (1952). "Fluid flow through packed columns." Chemical Engineering Progress **48**: 89-94.

Fernandes, J., P. F. Lisboa, P. C. Simões, J. P. B. Mota and E. Saatdjian (2009). "Application of CFD in the study of supercritical fluid extraction with structured packing: Wet pressure drop calculations." The Journal of Supercritical Fluids **50**(1): 61-68.

Fernandes, J., R. Ruivo, J. P. B. Mota and P. Simões (2007). "Non-isothermal dynamic model of a supercritical fluid extraction packed column." The Journal of Supercritical Fluids **41**(1): 20-30.

Fernandes, J., P. C. Simões, J. P. B. Mota and E. Saatdjian (2008). "Application of CFD in the study of supercritical fluid extraction with structured packing: Dry pressure drop calculations." The Journal of Supercritical Fluids **47**(1): 17-24.

Ferreira, S. R. S. and M. A. A. Meireles (2002). "Modeling the supercritical fluid extraction of black pepper (Piper nigrum L.) essential oil." Journal of Food Engineering **54**(4): 263-269.

Fukushima, Y. (2000). "Application of Supercritical Fluids." R&D Review of Toyota CRDL **35**(1): 1-9.

García-González, C. A., M. C. Camino-Rey, M. Alnaief, C. Zetzl and I. Smirnova (2012). "Supercritical drying of aerogels using CO2: Effect of extraction time on the end material textural properties." The Journal of Supercritical Fluids **66**: 297-306.

Ghafoor, K., J. Park and Y. H. Choi (2010). “Optimization of supercritical fluid extraction of bioactive compounds from grape (*Vitis labrusca B.)* peel by using response surface methodology.” Innovative Food Science and Emerging Technologies **11**(3): 485-490.

Goldstein, S. and J. Burgers (1931). "The forces on a solid body moving through viscous fluid." Proceedings of the Royal Society of London. Series A, Containing Papers of a Mathematical and Physical Character. 198-208.

Griffin, J. S., D. H. Mills, M. Cleary, R. Nelson, V. P. Manno and M. Hodes (2014). "Continuous extraction rate measurements during supercritical CO2 drying of silica alcogel." The Journal of Supercritical Fluids **94**: 38-47.

Guardo A. (2007). "Computational Fluid Dynamics Studies in Heat and Mass Transfer Phenomena in Packed Bed Extraction and Reaction Equipment: Special Attention to Supercritical Fluids Technology". PhD Thesis, Universitat Politècnica de Catalunya.

Guardo, A., M. Coussirat, M. A. Larrayoz, F. Recasens and E. Egusquiza (2005). "Influence of the turbulence model in CFD modeling of wall-to-fluid heat transfer in packed beds." Chemical Engineering Science **60**(6): 1733-1742.

Haghshenas Fard, M., M. Zivdar, R. Rahimi and M. Nasr Esfahani (2009). "Numerical Simulation of Hydrodynamics Parameters of the Packed Columns: Effect of Geometrical Characteristics on Pressure Drop." World Applied Sciences Journal **7**: 1439-1445.

Haghshenas Fard, M., M. Zivdar, R. Rahimi, M. Nasr Esfahani, A. Afacan, K. Nandakumar and K. T. Chuang (2007). "CFD Simulation of Mass Transfer Efficiency and Pressure Drop in a Structured Packed Distillation Column." Chemical Engineering & Technology **30**(7): 854-861.

Heidaryan, E., T. Hatami, M. Rahimi and J. Moghadasi (2011). "Viscosity of pure carbon dioxide at supercritical region: Measurement and correlation approach." The Journal of Supercritical Fluids **56**(2): 144-151.

Herrero, M., J. A. Mendiola, A. Cifuentes and E. Ibáñez (2010). "Supercritical fluid extraction: Recent advances and applications." Journal of Chromatography A **1217**(16): 2495-2511.

Hoerner, S. (1935). “Tests of Spheres with Reference to Reynolds Number, Turbulence and Surface Roughness.” NACA Technical Memorandum 777: 32.

Hosseini, S. H., S. Shojaee, G. Ahmadi and M. Zivdar (2012). "Computational fluid dynamics studies of dry and wet pressure drops in structured packings." Journal of Industrial and Engineering Chemistry **18**(4): 1465-1473.

Ibrahim, A. H., S. S. Al-Rawi, A. M. S. Abdul Majid, N. N. Ab. Rahman, K. M. Abo-Salah and M. O. Ab Kadir (2011). “Separation and Fractionation of *Aquilaria Malaccensis* Oil Using Supercritical Fluid Extraction and the Cytotoxic Properties of the Extracted Oil.” Procedia Food Science **1**: 1953-1959.

Iliuta, I. and F. Larachi (2001). "Mechanistic Model for Structured-Packing-Containing Columns: Irrigated Pressure Drop, Liquid Holdup, and Packing Fractional Wetted Area." Industrial & Engineering Chemistry Research **40**(23): 5140-5146.

Iwai, Y., T. Nakashima and S. Yonezawa (2013). "Preparation of dye sensitized solar cell by using supercritical carbon dioxide drying." The Journal of Supercritical Fluids **77**: 153-157.

Jafari, A., P. Zamankhan, S. M. Mousavi and K. Pietarinen (2008). "Modeling and CFD simulation of flow behavior and dispersivity through randomly packed bed reactors." Chemical Engineering Journal **144**(3): 476-482.

Jenson, V. (1959). "Viscous flow round a sphere at low Reynolds numbers (< 40)." Proceedings of the Royal Society of London A: Mathematical, Physical and Engineering Sciences, The Royal Society.

Johnson, T. A. and V. C. Patel (1999). "Flow past a sphere up to a Reynolds number of 300." Journal of Fluid Mechanics **378**: 19-70.

Karimi, M., G. Akdogan, A. Dehghani and S. Bradshaw (2011). "Selection of Suitable Turbulence Models for Numerical Modelling of Hydrocyclones." Chemical Product and Process Modeling **38**(6):-.

Khosravi Nikou, M. R. and M. R. Ehsani (2008). "Turbulence models application on CFD simulation of hydrodynamics, heat and mass transfer in a structured packing." International Communications in Heat and Mass Transfer **35**(9): 1211-1219.

Klöker, M., E. Y. Kenig, R. Piechota, S. Burghoff and Y. Egorov (2005). "CFD-based Study on Hydrodynamics and Mass Transfer in Fixed Catalyst Beds." Chemical Engineering and Technology **28**(1): 31-36.

Koh, J.-H. and G. Guiochon (1998). "Effect of the column length on the characteristics of the packed bed and the column efficiency in a dynamic axial compression column." Journal of Chromatography A **796**(1): 41-57.

Launder, B. E. and D. B. Spalding (1974). "The numerical computation of turbulent flows." Computer Methods in Applied Mechanics and Engineering **3**(2): 269-289.

Le Clair, B. P., A. E. Hamielec and H. R. Pruppacher (1970). "A Numerical Study of the Drag on a Sphere at Low and Intermediate Reynolds Numbers." Journal of the Atmospheric Sciences **27**(2): 308-315.

Lehotay, S. J. (1997). "Supercritical fluid extraction of pesticides in foods." Journal of Chromatography A **785**: 289-312.

Leva, M. and M. Grummer (1947). "Pressure drop through packed tubes: part III prediction of voids in packed tubes." Chemical Engineering Progress **43**: 713-718.

Li, R., J. Zhang, Y. Yong, Y. Wang and C. Yang (2015). "Numerical simulation of steady flow past a liquid sphere immersed in simple shear flow at low and moderate Re." Chinese Journal of Chemical Engineering **23**(1): 15-21.

Lloyd, B. and R. Boehm (1994). "Flow and Heat Transfer around a Linear Array of Spheres." Numerical Heat Transfer, Part A: Applications **26**(2): 237-252.

Logtenberg, S. A. and A. G. Dixon (1998). "Computational fluid dynamics studies of fixed bed heat transfer." Chemical Engineering and Processing: Process Intensification **37**(1): 7-21.

Logtenberg, S. A., M. Nijemeisland and A. G. Dixon (1999). "Computational fluid dynamics simulations of fluid flow and heat transfer at the wall–particle contact points in a fixed-bed reactor." Chemical Engineering Science **54**(13–14): 2433-2439.

Lopes, R. J. G. and R. M. Quinta-Ferreira (2009). "Turbulence modelling of multiphase flow in high-pressure trickle-bed reactors." Chemical Engineering Science **64**(8): 1806-1819.

Magnico, P. (2009). "Pore-scale simulations of unsteady flow and heat transfer in tubular fixed beds." AIChE Journal **55**(4): 849-867.

Mahr, B. and D. Mewes (2007). "CFD Modelling and Calculation of Dynamic Two-Phase Flow in Columns Equipped with Structured Packing." Chemical Engineering Research and Design **85**(8): 1112-1122.

Mâncio, A. A., K. M. B. da Costa, C. C. Ferreira, M. C. Santos, D. E. L. Lhamas, S.A.P. da Mota, R. A. C. Leão, R. O. M. A. de Souza, M. E. Araújo, L. E. P. Borges and N. T. Machado (2017). "Process analysis of physicochemical properties and chemical composition of organic liquid products obtained by thermochemical conversion of palm oil." Journal of Analytical and Applied Pyrolysis **123**: 284-295.

Matsuyama, K. and K. Mishima (2009). "Preparation of poly(methyl methacrylate)–TiO2 nanoparticle composites by pseudo-dispersion polymerization of methyl methacrylate in supercritical CO2." The Journal of Supercritical Fluids **49**(2): 256-264.

Maxworthy, T. (1965). "Accurate measurements of sphere drag at low Reynolds numbers." Journal of Fluid Mechanics **23**(2): 369-372.

Mayo, A. S., B. K. Ambati and U. B. Kompella (2010). “Gene delivery nanoparticles fabricated by supercritical fluid extraction of emulsions.” International Journal of Pharmaceutics **387**(1-2): 278-285.

Mewes, D., T. Loser and M. Millies (1999). "Modelling of two-phase flow in packings and monoliths." Chemical Engineering Science **54**(21): 4729-4747.

Mezzomo, N., J. Martinez and S. R. S Ferreira (2009). “Supercritical fluid extraction of peach (*Prunus persica*) almond oil: Kinetics, mathematical modelling and scale-up.” The Journal of Supercritical Fluids **51**(1): 10-16.

Mohseni M. and M. Bazargan (2011). "Modification of low Reynolds number k-ε turbulence models for applications in supercritical fluid flows." International Journal of Thermal Sciences **50**(1): 1-12.

Montillet, A., E. Akkari and J. Comiti (2007). "About a correlating equation for predicting pressure drops through packed beds of spheres in a large range of Reynolds numbers." Chemical Engineering and Processing: Process Intensification **46**(4): 329-333.

Natarajan, R. and A. Acrivos (1993). "The instability of the steady flow past spheres and disks." Journal of Fluid Mechanics **254**: 323-344.

Neve, R. S. (1986). "The importance of turbulence macroscale in determining the drag coefficient of spheres." International Journal of Heat and Fluid Flow **7**(1): 28-36.

Neve, R. S. and T. Shansonga (1989). "The effects of turbulence characteristics on sphere drag." International Journal of Heat and Fluid Flow **10**(4): 318-321.

Nijemeisland, M. and A. G. Dixon (2004). "CFD study of fluid flow and wall heat transfer in a fixed bed of spheres." AIChE Journal **50**(5): 906-921.

Norberg, C. (2002). "Pressure Distributions around a Circular Cylinder in Cross-Flow." Symposium on Bluff Body Wakes and Vortex-Induced Vibrations (BBVIV3), Queensland, Australia.

Oseen, C. W. (1927). "Hydrodynamik." Akademische Verlagsgesellschaft, Leipzig: 97-107.

Özbakır, Y. and C. Erkey (2014). "Experimental and theoretical investigation of supercritical drying of silica alcogels." The Journal of Supercritical Fluids.

Özkal, S. G., U. Salgın and M. E. Yener (2005). "Supercritical carbon dioxide extraction of hazelnut oil." Journal of Food Engineering **69**(2): 217-223.

Patankar, S.V. (1980). "Numerical heat transfer and fluid flow." Hemisphere, New York.

Perakis, C., V. Louli and K. Magoulas (2005). “Supercritical fluid extraction of black pepper oil.” Journal of Food Engineering **71**(4): 386-393.

Perrut, M. (2000). "Supercritical Fluid Applications: Industrial Developments and Economic Issues." Industrial & Engineering Chemistry Research **39**(12): 4531-4535.

Proudman, I. and J. R. A. Pearson (1957). "Expansions at small Reynolds numbers for the flow past a sphere and a circular cylinder." Journal of Fluid Mechanics **2**(3): 237-262.

Quan. L., S. Li, S. Tian, H. Xu, A. Lin and L. Gu (2004). "Determination of Organochlorine Pesticides Residue in Ginseng Root by Orthogonal Array Design Soxhlet Extraction and Gas Chromatography." Chromatographia **59**(1-2): 89-93.

Rahbar-Kelishami, A. and H. Bahmanyar (2012). "New predictive correlation for mass transfer coefficient in structured packed extraction columns." Chemical Engineering Research and Design **90**(5): 615-621.

Rahimi, M. and M. Mohseni (2008). "CFD modeling of the effect of absorbent size on absorption performance of a packed bed column." Korean Journal of Chemical Engineering **25**(3): 395-401.

Raynal, L., C. Boyer and J.-P. Ballaguet (2004). "Liquid Holdup and Pressure Drop Determination in Structured Packing with CFD Simulations." The Canadian Journal of Chemical Engineering **82**(5): 871-879.

Raynal, L. and A. Royon-Lebeaud (2007). "A multi-scale approach for CFD calculations of gas–liquid flow within large size column equipped with structured packing." Chemical Engineering Science **62**(24): 7196-7204.

Reddy, R. K. and J. B. Joshi (2008). "CFD modeling of pressure drop and drag coefficient in fixed and expanded beds." Chemical Engineering Research and Design **86**(5): 444-453.

Reddy, R. K. and J. B. Joshi (2010). "CFD modeling of pressure drop and drag coefficient in fixed beds: Wall effects." Particuology **8**(1): 37-43.

Reverchon, E. and C. Marrone (1997). "Supercritical extraction of clove bud essential oil: isolation and mathematical modelling." Chemical Engineering Science **52**(20): 3421-3428.

Ribeiro, A. M., P. Neto and C. Pinho (2010). “Mean Porosity and Pressure Drop Measurements in Packed Beds of Monosized Spheres: Side Wall Effects.” International Review of Chemical Engineering **2**(1): 40-46.

Riefler, N., M. Heiland, N. Räbiger and U. Fritsching (2012). "Pressure loss and wall shear stress in flow through confined sphere packings." Chemical Engineering Science **69**(1): 129-137.

Rimon, Y. and S. Cheng (1969). "Numerical solution of a uniform flow over a sphere at intermediate Reynolds numbers." Physics of Fluids (1958-1988) **12**(5): 949-959.

Robbins, D. J., M. S. El-Bachir, L. F. Gladden, R. S. Cant and E. von Harbou (2012). "CFD modeling of single-phase flow in a packed bed with MRI validation." AIChE Journal **58**(12): 3904-3915.

Rocha, J. A., J. L. Bravo and J. R. Fair (1993). "Distillation columns containing structured packings: a comprehensive model for their performance. 1. Hydraulic models." Industrial & Engineering Chemistry Research **32**(4): 641-651.

Romkes, S. J. P., F. M. Dautzenberg, C. M. van den Bleek and H. P. A. Calis (2003). "CFD modelling and experimental validation of particle-to-fluid mass and heat transfer in a packed bed at very low channel to particle diameter ratio." Chemical Engineering Journal **96**(1–3): 3-13.

Rueda, M., L. M. Sanz-Moral, A. Nieto-Márquez, P. Longone, F. Mattea and Á. Martín (2014). "Production of silica aerogel microparticles loaded with ammonia borane by batch and semicontinuous supercritical drying techniques." The Journal of Supercritical Fluids **92**: 299-310.

Said, W., M. Nemer and D. Clodic (2011). "Modeling of dry pressure drop for fully developed gas flow in structured packing using CFD simulations." Chemical Engineering Science **66**(10): 2107-2117.

Sanz-Moral, L. M., M. Rueda, R. Mato and Á. Martín (2014). "View cell investigation of silica aerogels during supercritical drying: Analysis of size variation and mass transfer mechanisms." The Journal of Supercritical Fluids **92**: 24-30.

Senol, A. (2001). "Mass transfer efficiency of randomly-packed column: modeling considerations." Chemical Engineering and Processing: Process Intensification **40**(1): 41-48.

Shih, T.-H., W. W. Liou, A. Shabbir, Z. Yang and J. Zhu (1995). "A new k-ϵ eddy viscosity model for high reynolds number turbulent flows." Computers & Fluids **24**(3): 227-238.

Sihvonen, M., E. Järvenpää, V. Hietaniemi and R. Huopalahti (1999). "Advances in supercritical carbon dioxide technologies." Trends in Food Science & Technology **10**(6–7): 217-222.

Sohankar, A., C. Norberg and L. Davidson (1999). "Numerical Simulation of Flow Past a Square Cylinder." 3rd ASME/JSME Joint Fluids Engineering Conference, San Francisco, California, USA.

Sovová, H., A. A. Galushko, R. P. Stateva, K. Rochová, M. Sajfrtova and M. Bártlová (2010). "Supercritical fluid extraction of minor components of vegetable oils: β-Sitosterol." Journal of Food Engineering 101(2): 201-209.

Spalart, P. and S. Allmaras (1992). "A one-equation turbulence model for aerodynamic flows." 30th Aerospace Sciences Meeting and Exhibit, American Institute of Aeronautics and Astronautics.

Stamenić, M. and I. Zizovic (2013). "The mathematics of modelling the supercritical fluid extraction of essential oils from glandular trichomes." Computers & Chemical Engineering **48**: 89-95.

Steinberger, E. H., H. R. Pruppacher and M. Neiburger (1968). "On the hydrodynamics of pairs of spheres falling along their line of centres in a viscous medium." Journal of Fluid Mechanics **34**(4): 809-819.

Stichlmair, J., J. L. Bravo and J. R. Fair (1989). "General model for prediction of pressure drop and capacity of countercurrent gas/liquid packed columns." Gas Separation and Purification **3**(1): 19-28.

Stokes, G. G. (1851). "On the Effect of the Internal Friction of Fluids on the Motion of Pendulums." Cambridge Philosophical Transactions **9**: 8-106.

Subramanian, K., S. Paschke, J. U. Repke and G. Wozny (2009). "Drag Force Modelling in CFD Simulation to Gain Insight of Packed Columns." Chemical Engineering Transactions **17**: 561-566.

Taneda, S. (1978). "Visual observations of the flow past a sphere at Reynolds numbers between 104 and 106." Journal of Fluid Mechanics **85**(1): 187-192.

Theuerkauf, J., P. Witt and D. Schwesig (2006). "Analysis of particle porosity distribution in fixed beds using the discrete element method." Powder Technology **165**: 92-99.

Teaters, L. (2012). "A Computational Study of the Hydrodynamics of Gas-Solid Fluidized Beds." Master of Science Thesis, Virginia Polytechnic Institute and State University.

Tomboulides, A. G. (1993). "Direct and large-eddy simulation of wake flows: flow past a sphere." PhD Thesis, Princeton University.

Towler, G. and R. K. Sinnott (2013). "Chemical Engineering Design: Principles, Practice and Economics of Plant and Process Design", Elsevier.

Van Der Merwe, D. F. and W. H. Gauvin (1971). "Velocity and Turbulence Measurements of Air Flow Through a Packed Bed." AIChE Journal **17**(3): 519-528.

Wadsworth, J. (1958). Nat. Res. Council, Nat. Aeron. Estab. Rep. MT-39.

Wagner, I., J. Stichlmair and J. R. Fair (1997). "Mass Transfer in Beds of Modern, High-Efficiency Random Packings." Industrial and Engineering Chemistry Research **36**(1): 227-237.

Wen, X., S. Akhter, A. Afacan, K. Nandakumar and K. T. Chuang (2007). "CFD modeling of columns equipped with structured packings: I. Approach based on detailed packing geometry." Asia-Pacific Journal of Chemical Engineering **2**(4): 336-344.

Wentz, C. A. and G. Thodos (1963). "Total and form drag friction factors for the turbulent flow of air through packed and distended beds of spheres." AIChE Journal **9**(3): 358-361.

Wong, B., S. Yoda and S. M. Howdle (2007). "The preparation of gold nanoparticle composites using supercritical carbon dioxide." The Journal of Supercritical Fluids **42**(2): 282-287.

Yang, J., J. Wu, L. Zhou and Q. Wang (2016). "Computational study of fluid flow and heat transfer in composite packed beds of spheres with low tube to particle diameter ratio." Nuclear Engineering and Design **300**: 85-96.

Yu, D., M. Peng and Z. Wang (2015). "CFD study on the supercritical carbon dioxide cooled pebble reactor." Nuclear Engineering and Design **281**: 88-95.

Zaidul, I. S. M., N. A. Nik Norulaini, A. K. Mohd Omar and R. L. Smith Jr (2007). "Supercritical carbon dioxide (SC-CO2) extraction of palm kernel oil from palm kernel." Journal of Food Engineering **79**(3): 1007-1014.

Zaidul, I. S. M., N. A. N. Norulaini, A. K. M. Omar and R. L. Smith Jr (2006). "Supercritical carbon dioxide (SC-CO2) extraction and fractionation of palm kernel oil from palm kernel as cocoa butter replacers blend." Journal of Food Engineering **73**(3): 210-216.

Zheng, D., X. He and D. Che (2007). "CFD simulations of hydrodynamic characteristics in a gas–liquid vertical upward slug flow." International Journal of Heat and Mass Transfer **50**(21–22): 4151-4165.

Zobel, N., T. Eppinger, F. Behrendt and M. Kraume (2012). "Influence of the wall structure on the void fraction distribution in packed beds." Chemical Engineering Science **71**: 212-219.

APPENDIX A – CHAPTER 4 RESULTS

Appendix A1 – Wall shear stress in subcritical and supercritical regimes for single sphere studies by using realizable *k*-ε turbulence model

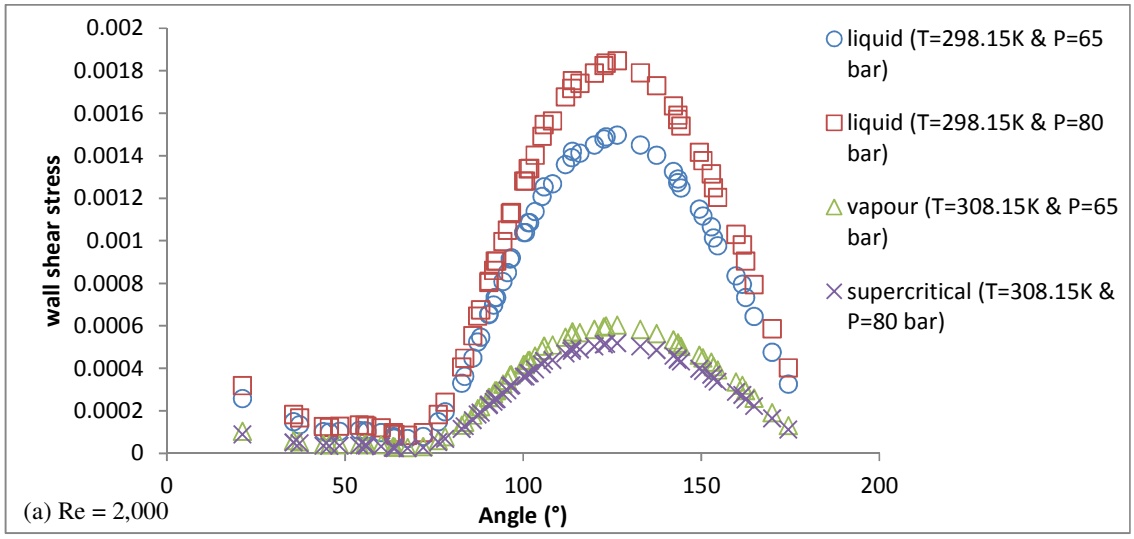

(a) Re = 2,000

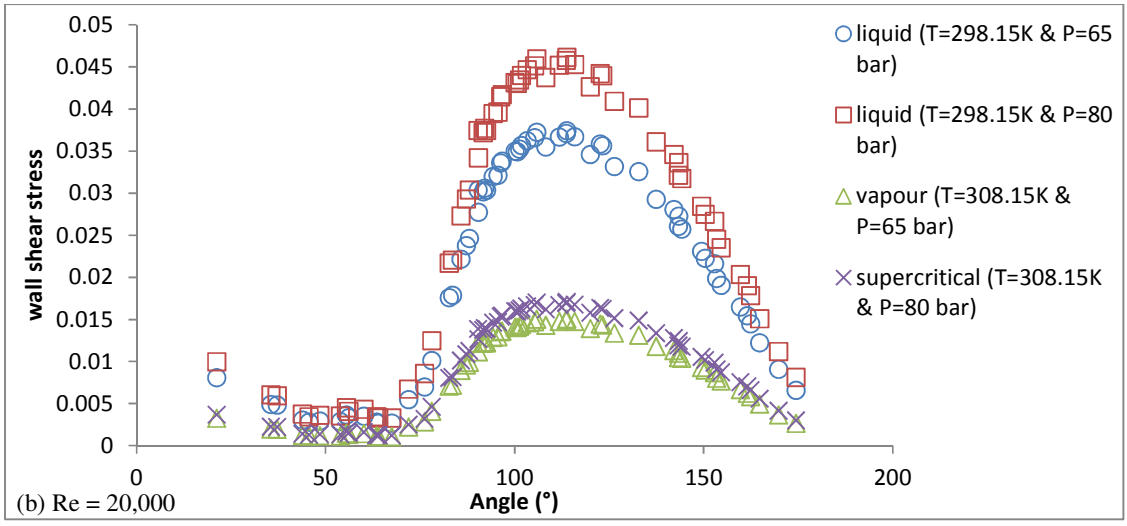

(b) Re = 20,000

Appendix A2 – Wall shear stress in subcritical and supercritical regimes for single sphere studies by using RNG *k*-*ε* turbulence model

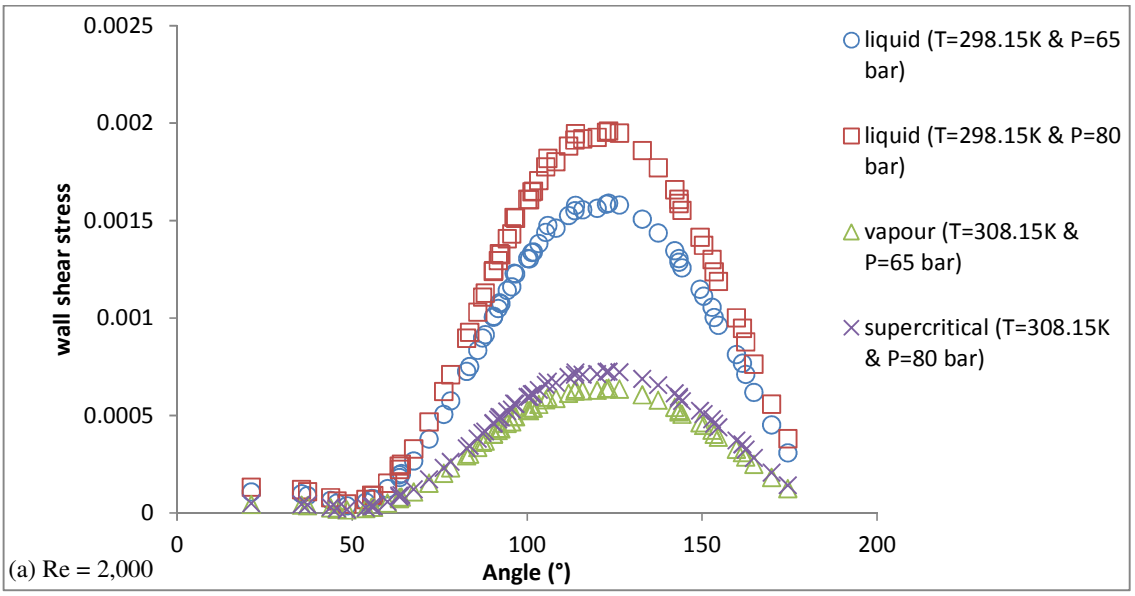

(a) Re = 2,000

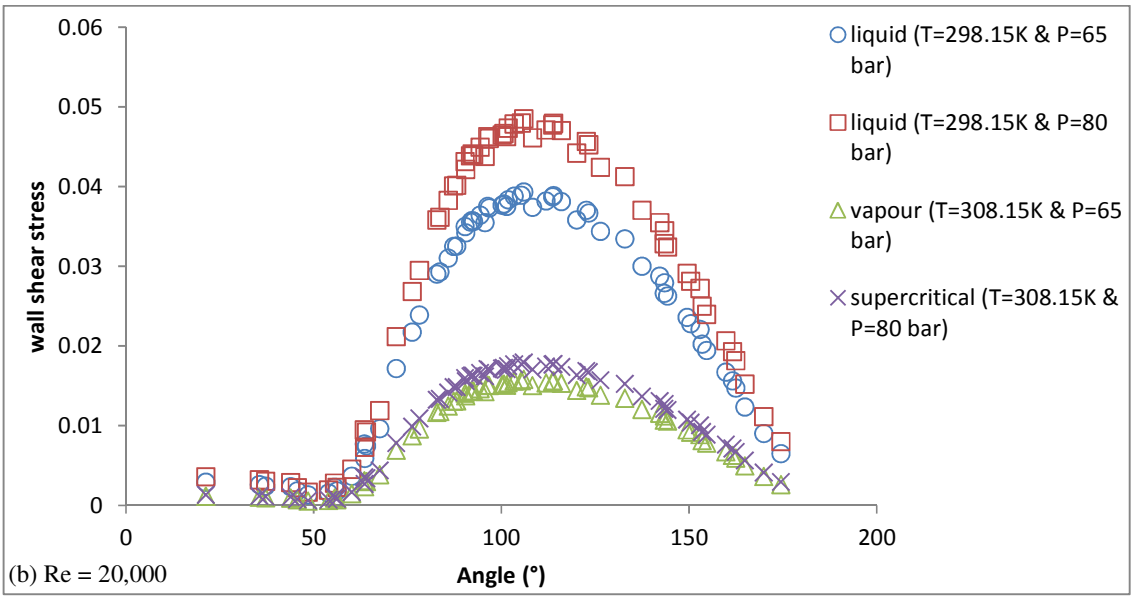

(b) Re = 20,000

Appendix A3 – Wall shear stress in subcritical and supercritical regimes for single sphere studies by using standard *k*-*ε* turbulence model

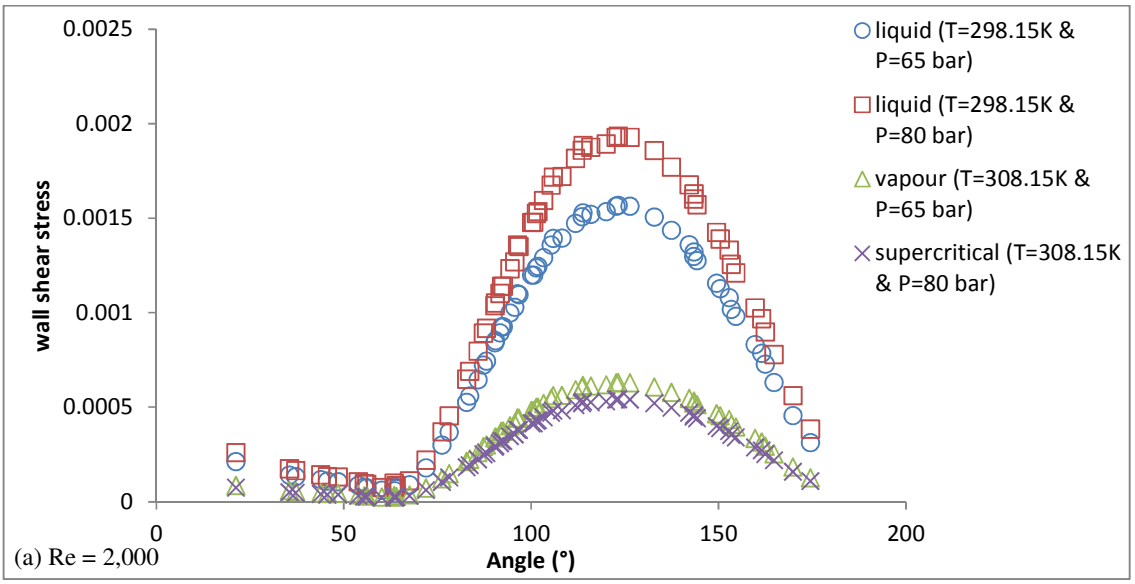

(a) Re = 2,000

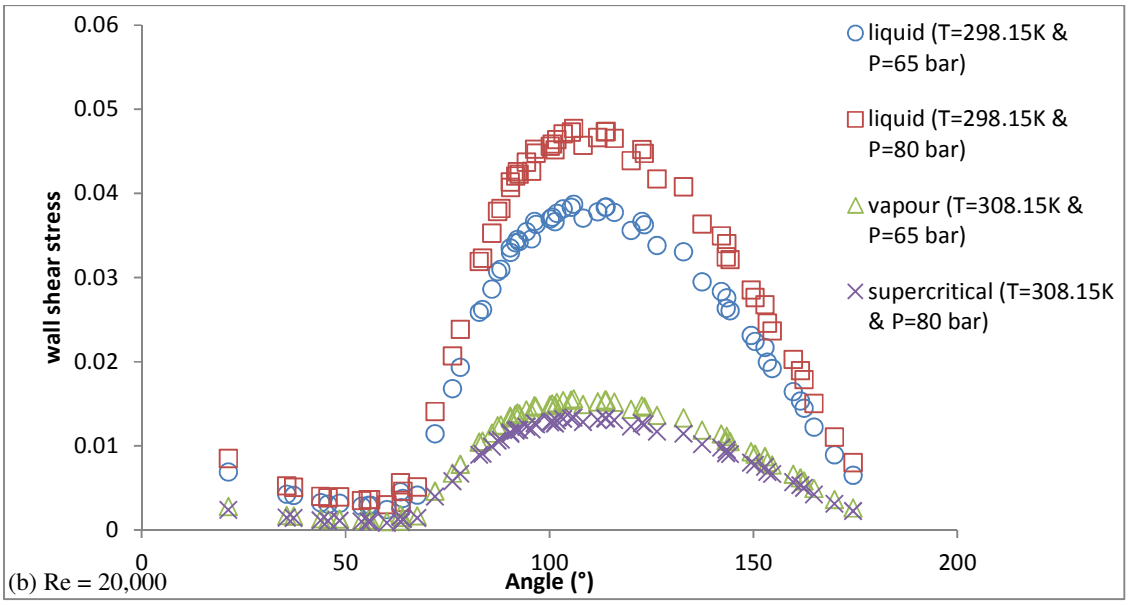

(b) Re = 20,000

Appendix A4 –Wall shear stress in subcritical and supercritical regimes for single sphere studies by using SST *k-ω* turbulence model

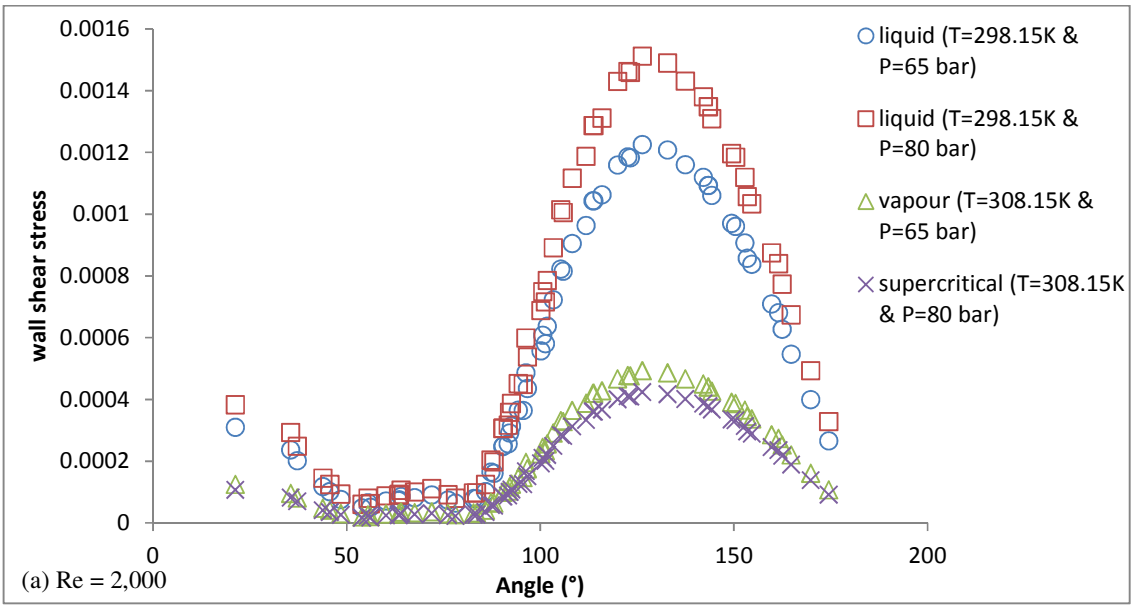

(a) Re = 2,000

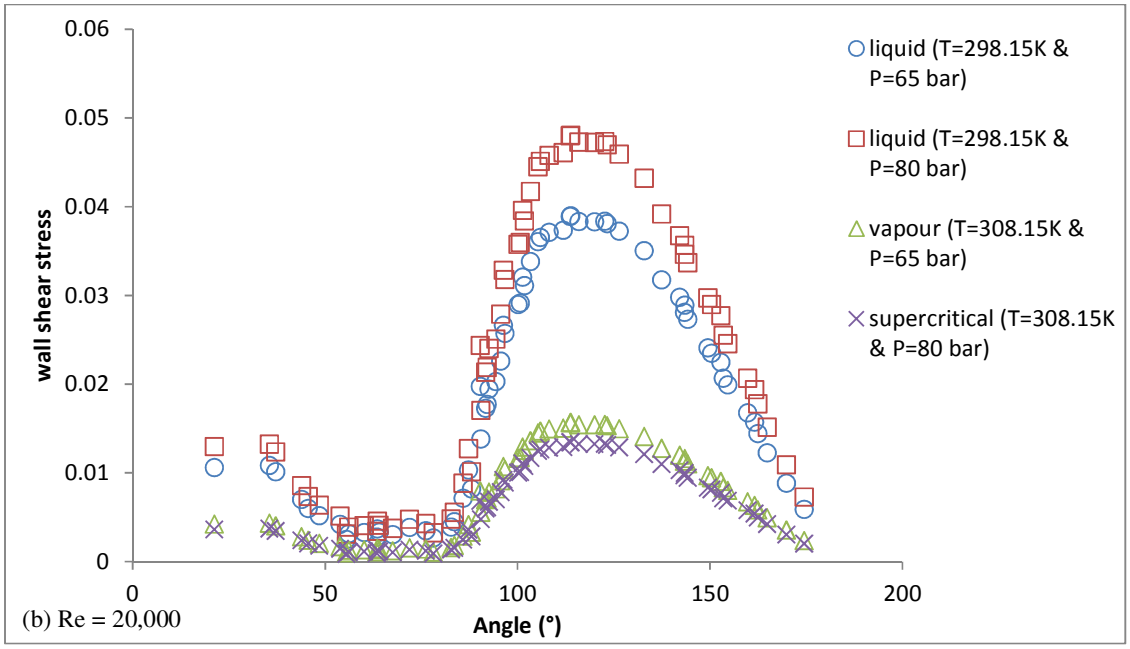

(b) Re = 20,000

APPENDIX B – CHAPTER 4 RESULTS

Appendix B1 – Contours of velocity profiles for *Re* = 2,000 by using realizable *k*-*ε* turbulence model.

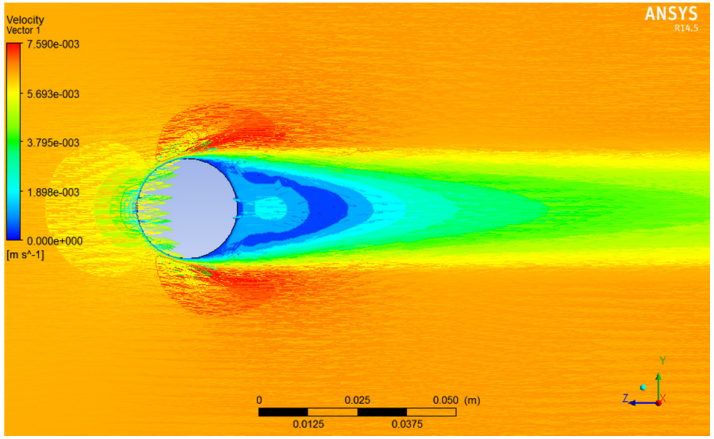

T = 298.15K, P = 65bar

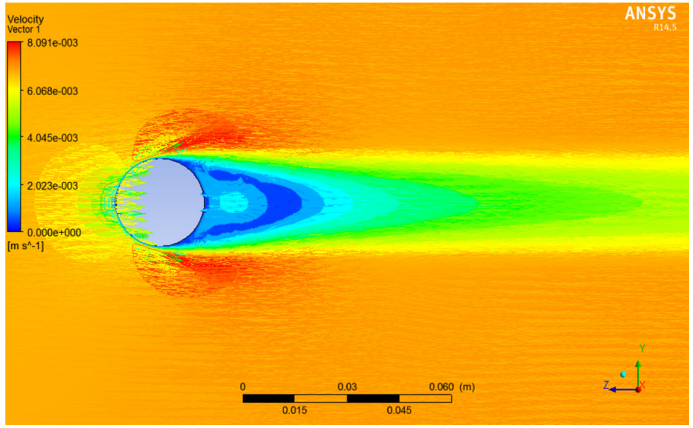

T = 298.15K, P = 80bar

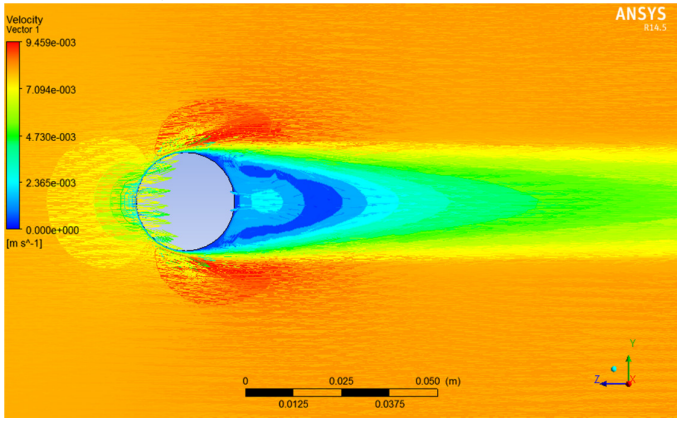

T = 308.15K, P = 65bar

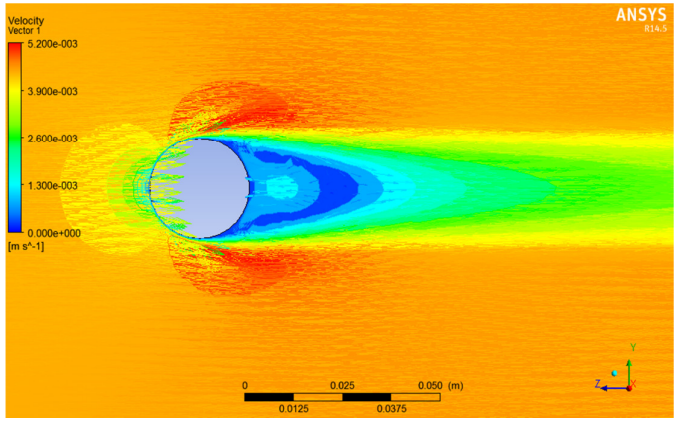

T = 308.15K, P = 80bar

Appendix B2 – Contours of velocity profiles for *Re* = 20,000 by using realizable *k*-*ε* turbulence model.

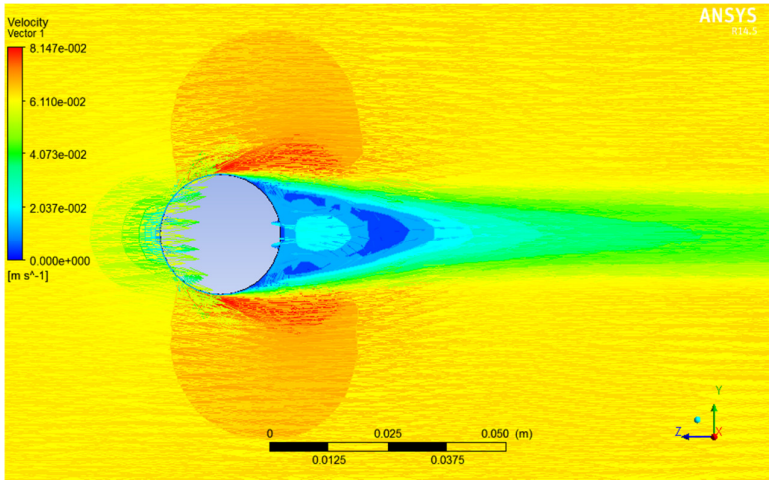

T = 298.15K, P = 65bar

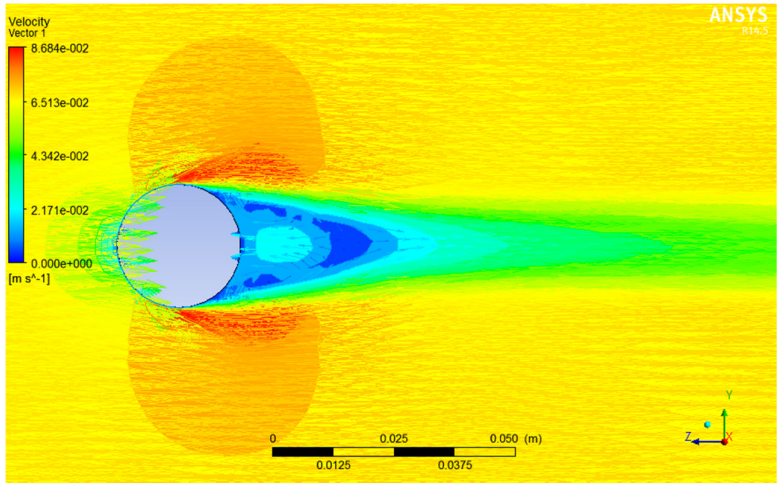

T = 298.15K, P = 80bar

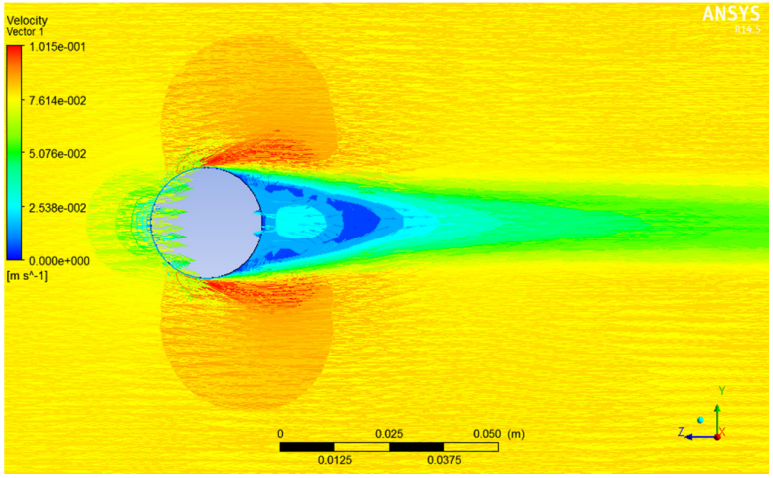

T = 308.15K, P = 65bar

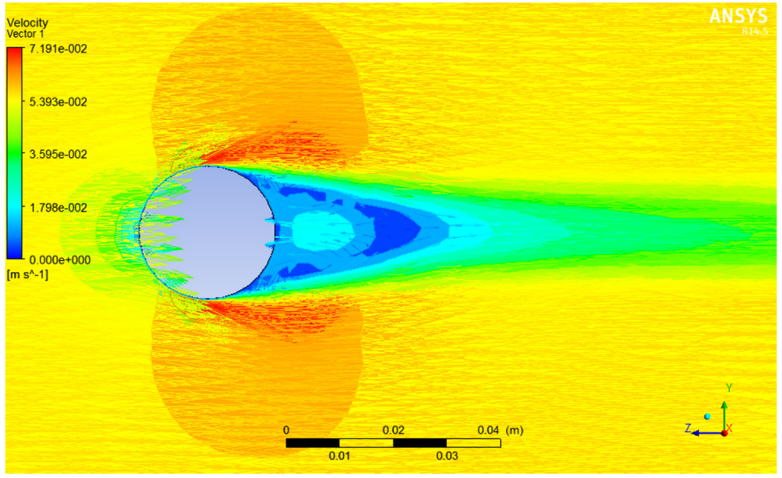

T = 308.15K, P = 80bar

Appendix B3 – Contours of velocity profiles for *Re* = 2,000 by using RNG *k*-ε turbulence model.

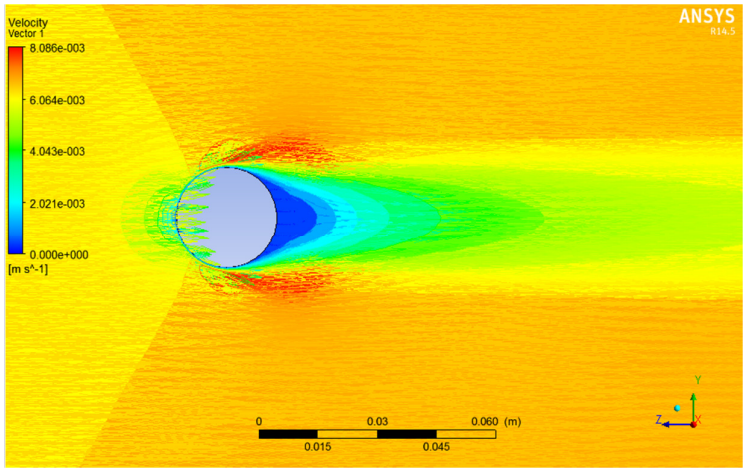

T = 298.15K, P = 65bar

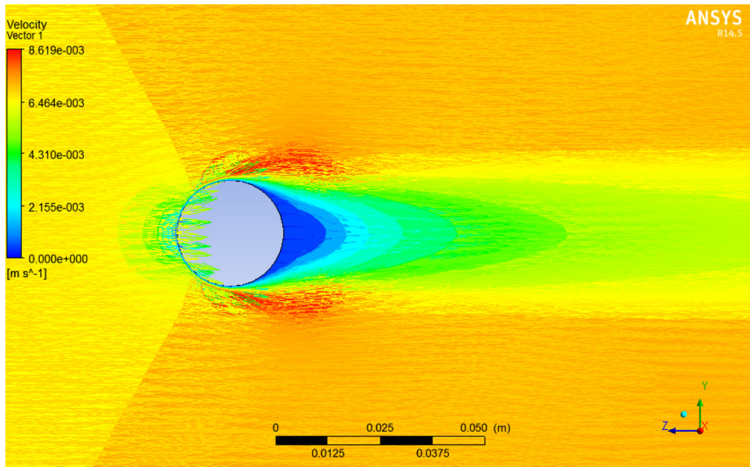

T = 298.15K, P = 80bar

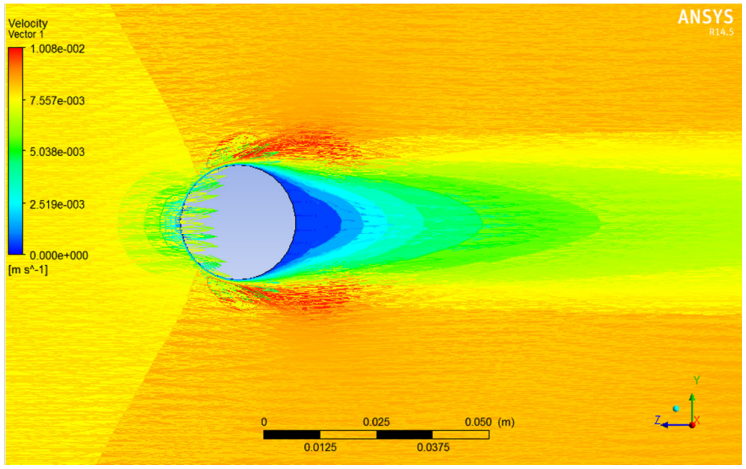

T = 308.15K, P = 65bar

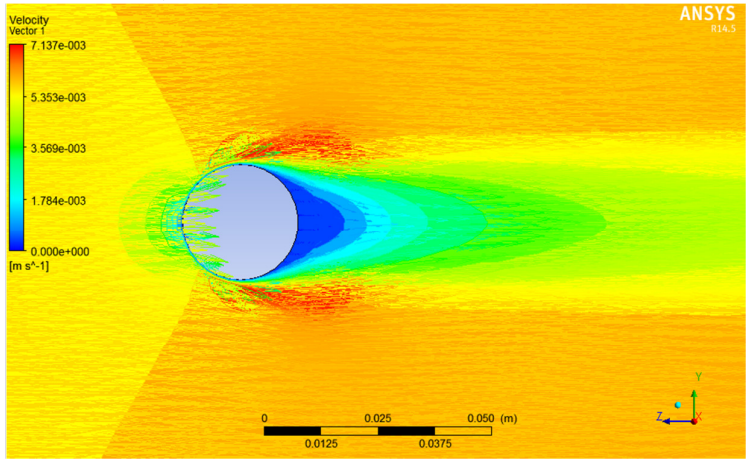

T = 308.15K, P = 80bar

Appendix B4 – Contours of velocity profiles for *Re* = 20,000 by using RNG *k*-ε turbulence model.

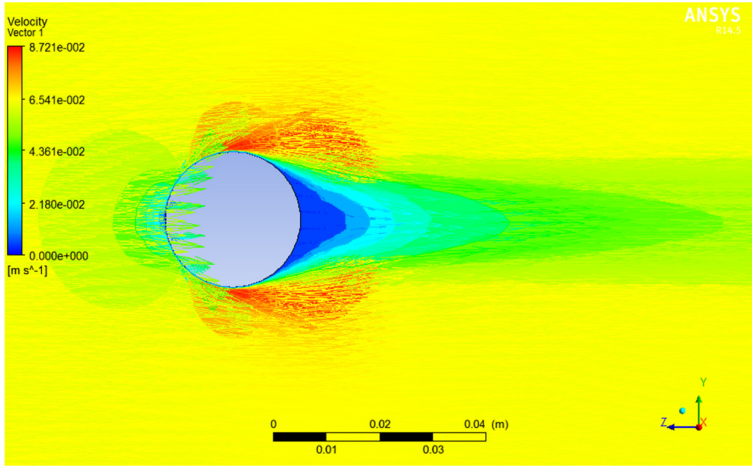

T = 298.15K, P = 65bar

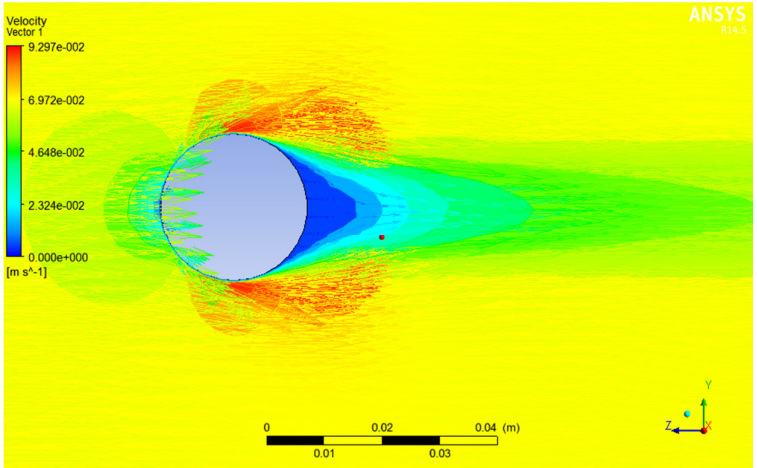

T = 298.15K, P = 80bar

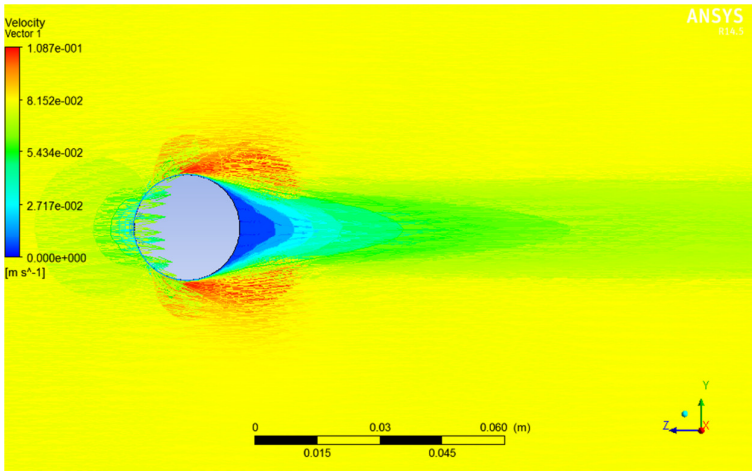

T = 308.15K, P = 65bar

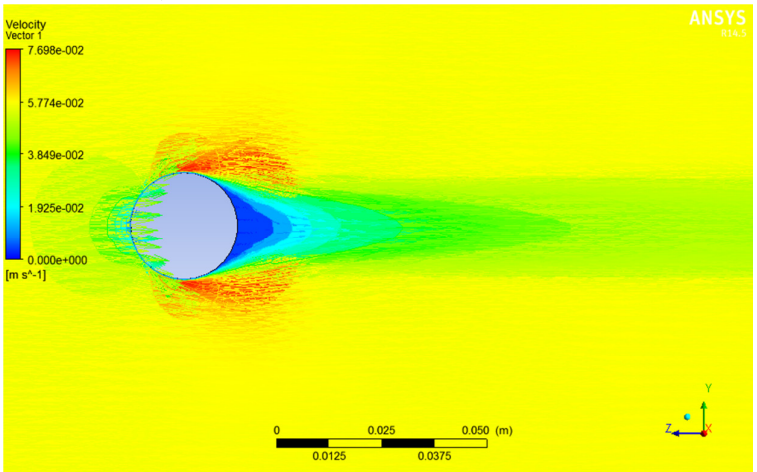

T = 308.15K, P = 80bar

Appendix B5 – Contours of velocity profiles for *Re* = 2,000 by using standard *k*-ε turbulence model.

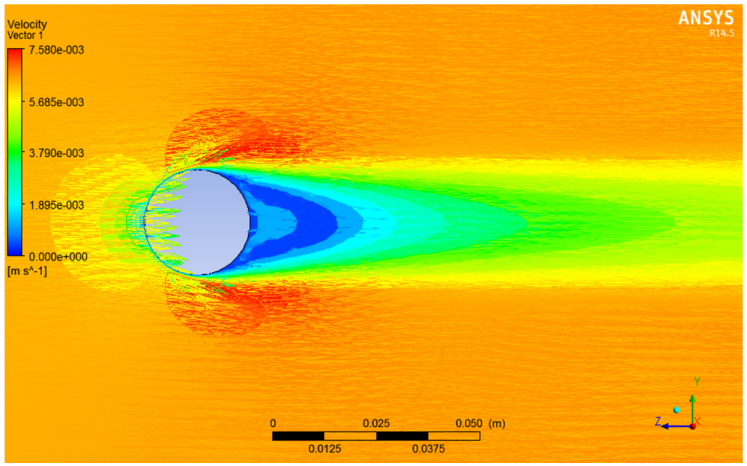

T = 298.15K, P = 65bar

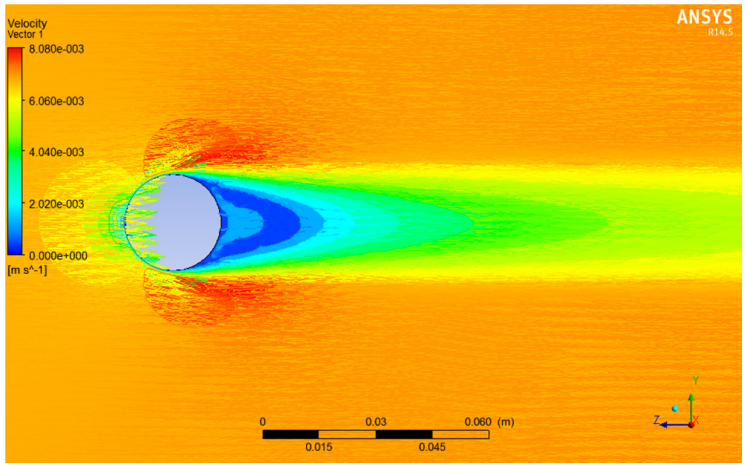

T = 298.15K, P = 80bar

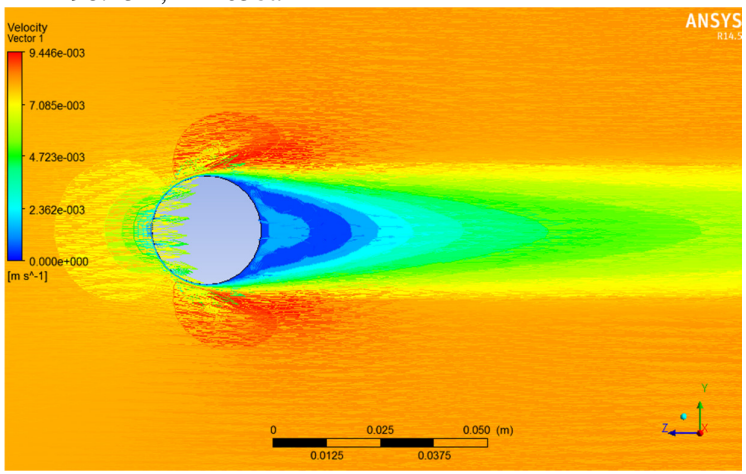

T = 308.15K, P = 65bar

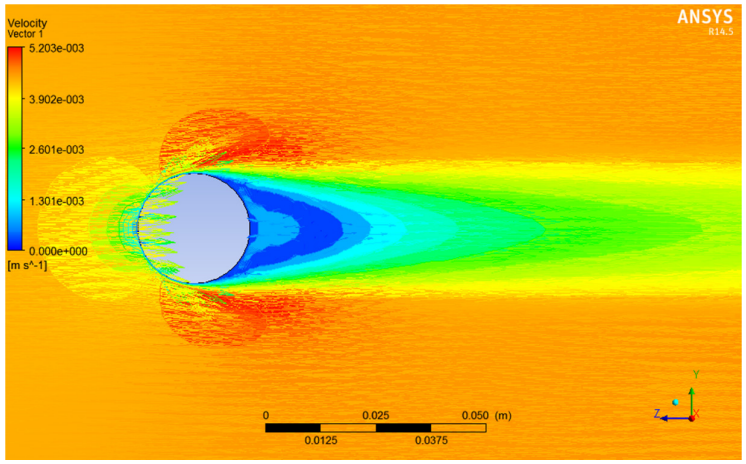

T = 308.15K, P = 80bar

Appendix B6 – Contours of velocity profiles for *Re* = 20,000 by using standard *k*-ε turbulence model.

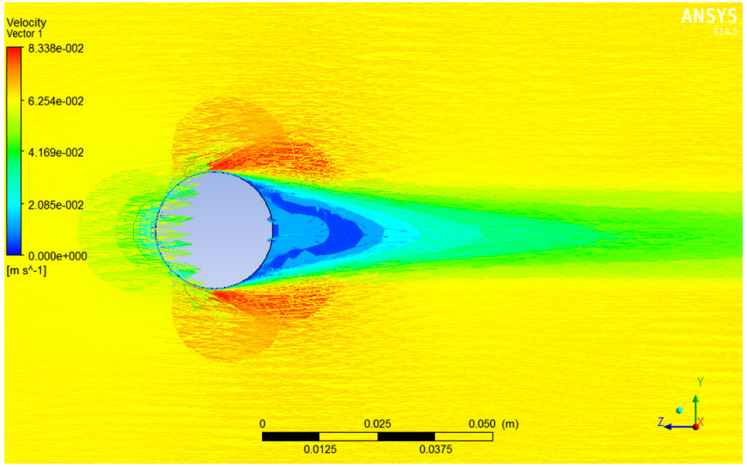

T = 298.15K, P = 65bar

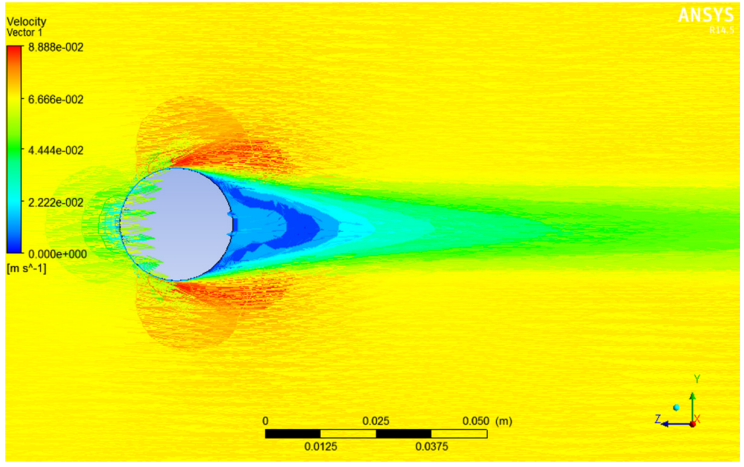

T = 298.15K, P = 80bar

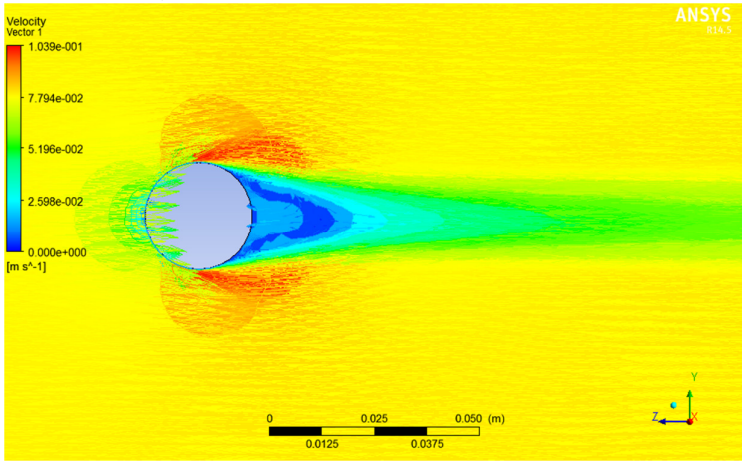

T = 308.15K, P = 65bar

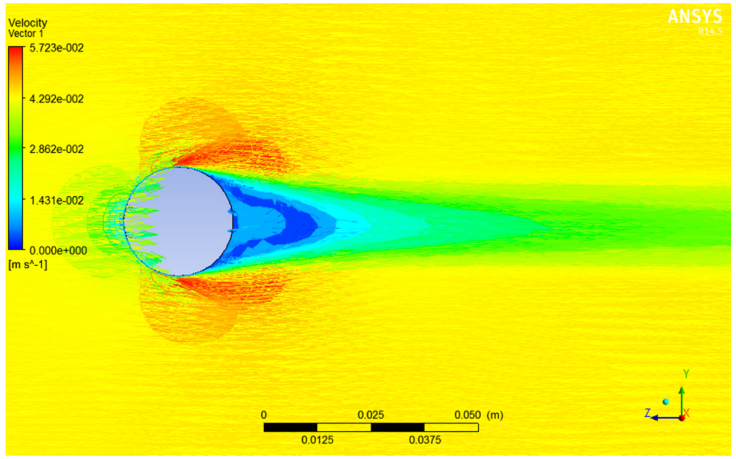

T = 308.15K, P = 80bar

Appendix B7 – Contours of velocity profiles for *Re* = 2,000 by using SST *k-ω* turbulence model.

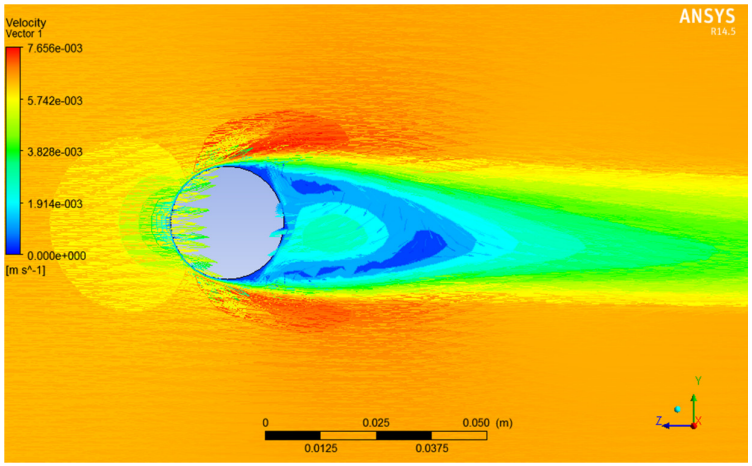

T = 298.15K, P = 65bar

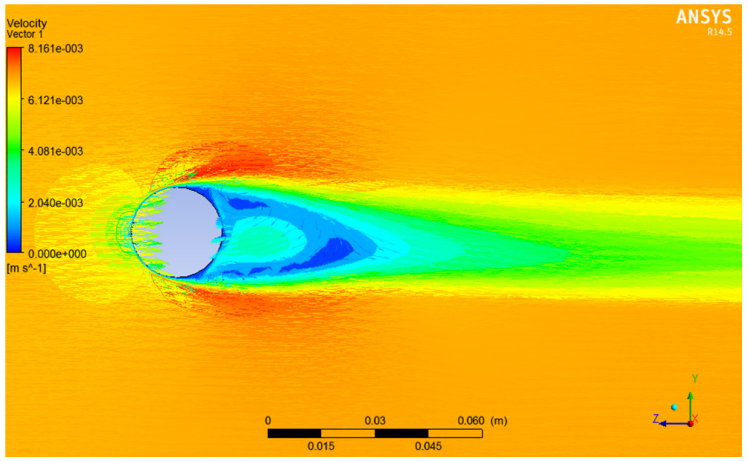

T = 298.15K, P = 80bar

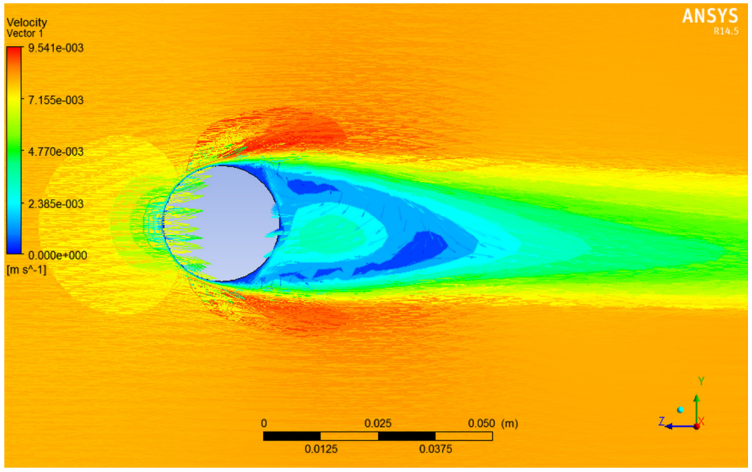

T = 308.15K, P = 65bar

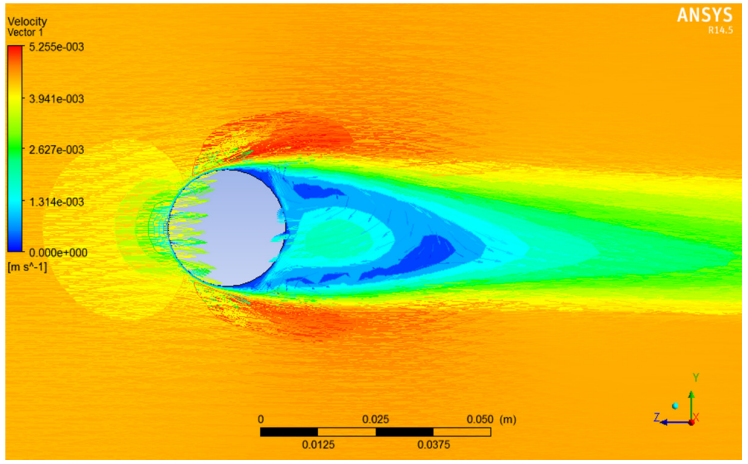

T = 308.15K, P = 80bar

Appendix B8 – Contours of velocity profiles for *Re* = 20,000 by using SST *k-ω* turbulence model.

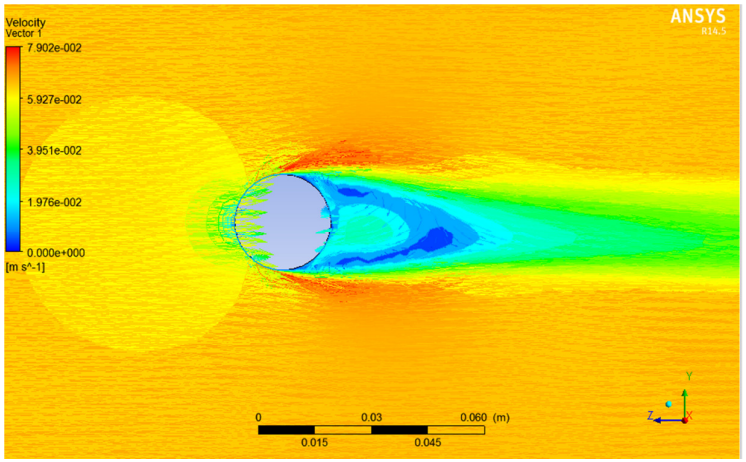

T = 298.15K, P = 65bar

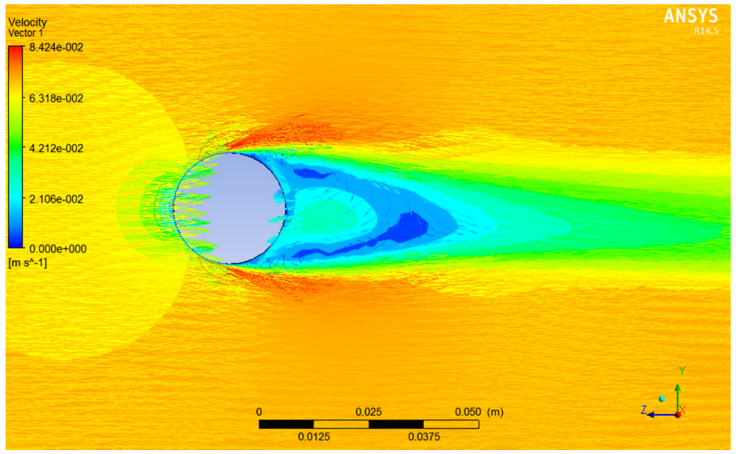

T = 298.15K, P = 80bar

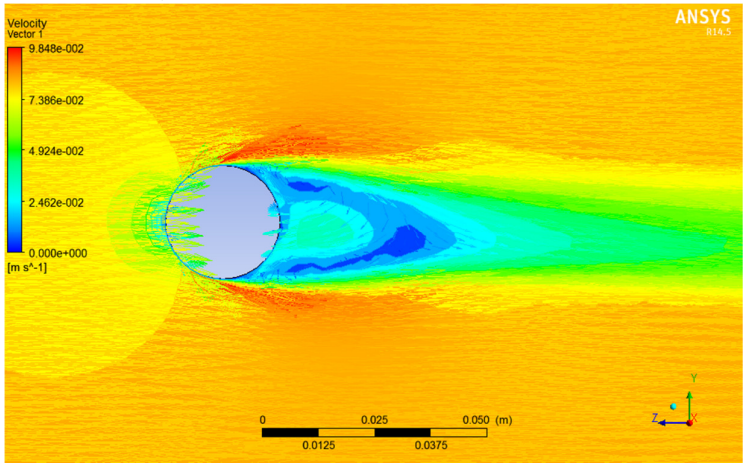

T = 308.15K, P = 65bar

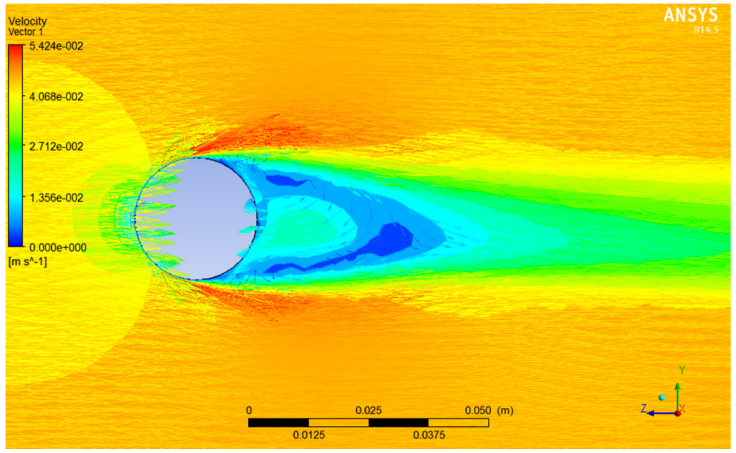

T = 308.15K, P = 80bar

APPENDIX C – CHAPTER 4 RESULTS

Appendix C1 – Contours of turbulent intensity for *Re* = 2,000 by using SST *k-ω* turbulence model.

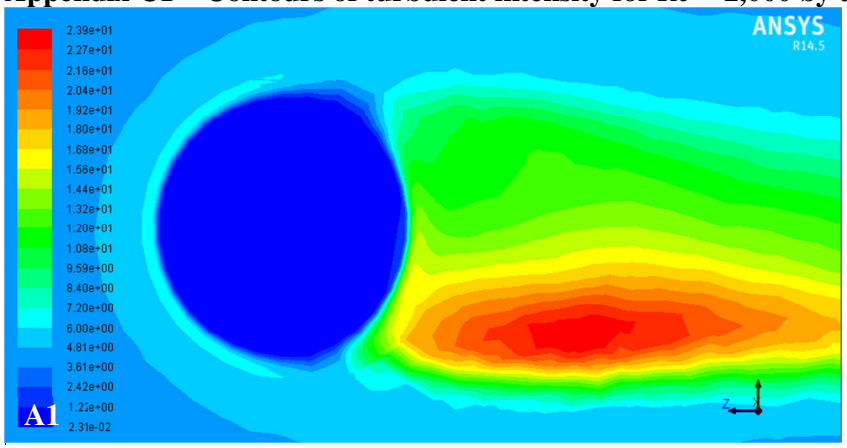

T = 298.15K, P = 65bar

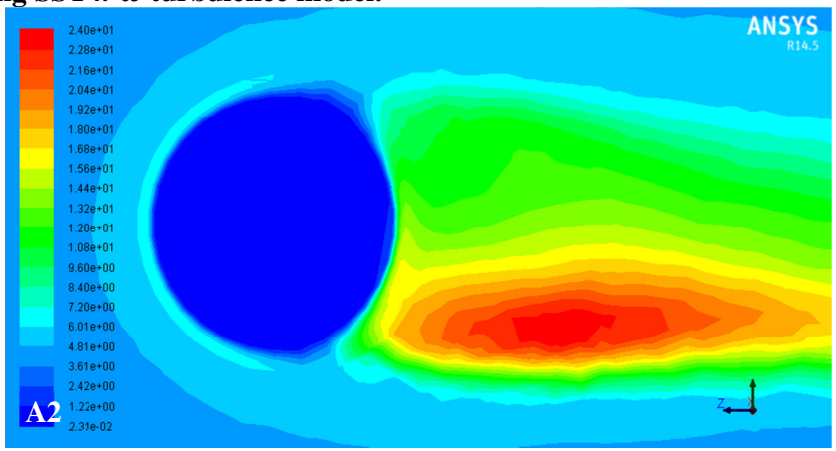

T = 298.15K, P = 80bar

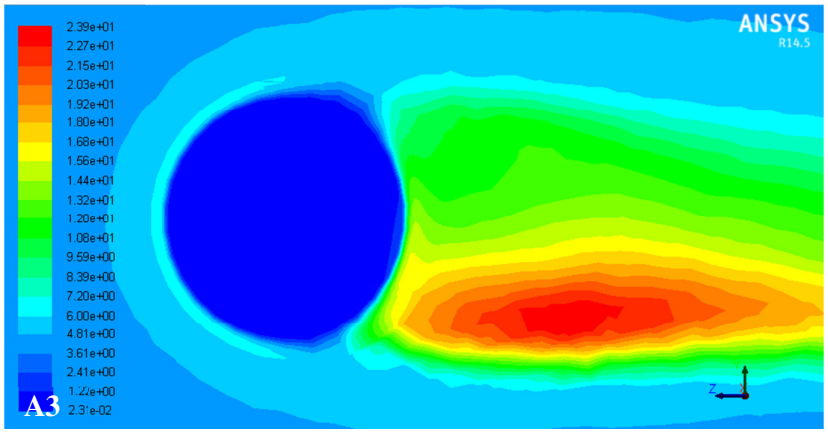

T = 308.15K, P = 65bar

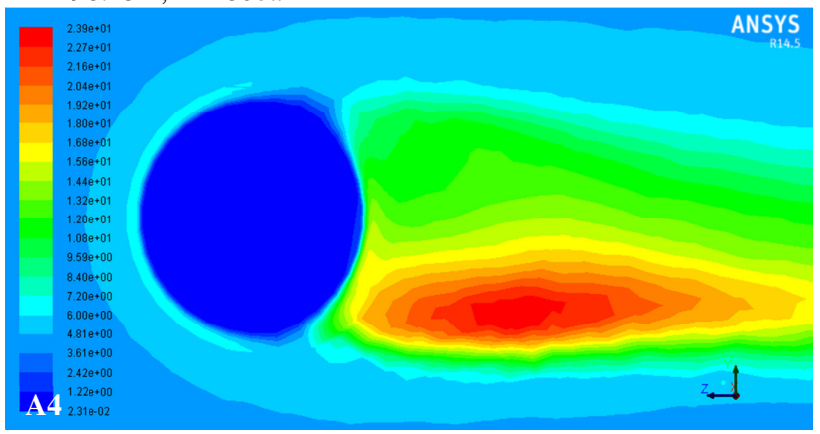

T = 308.15K, P = 80bar

Appendix C2 – Contours of turbulent intensity for *Re* = 20,000 by using SST *k-ω* turbulence model.

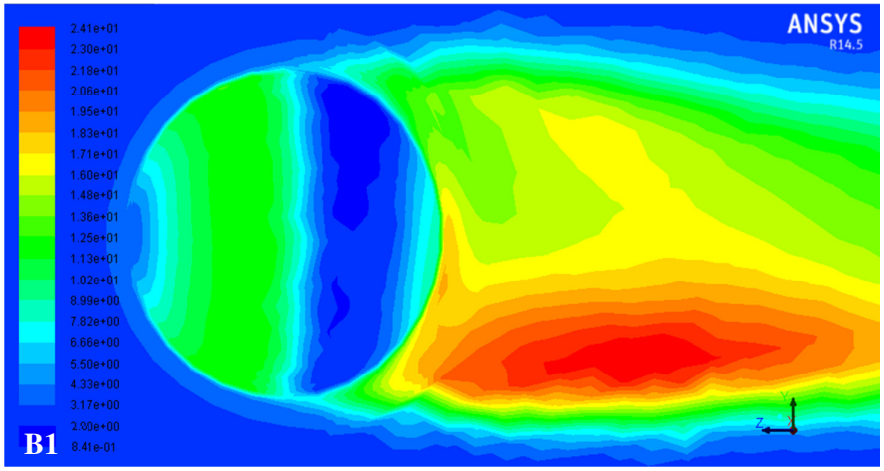

T = 298.15K, P = 65bar

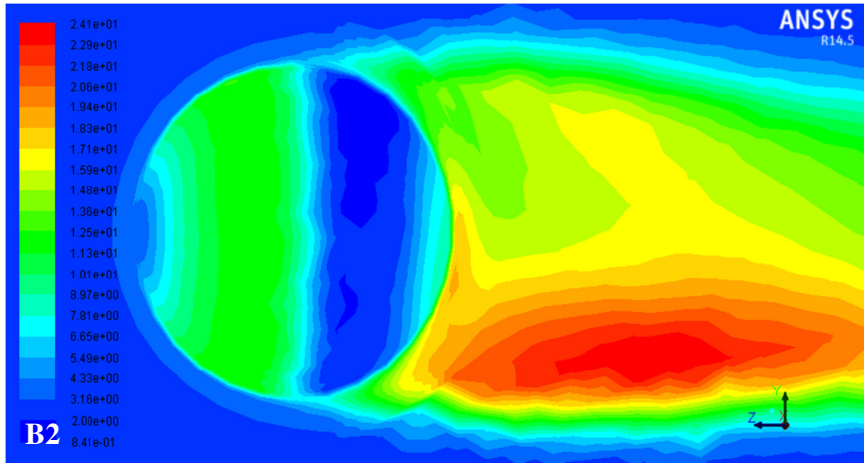

T = 298.15K, P = 80bar

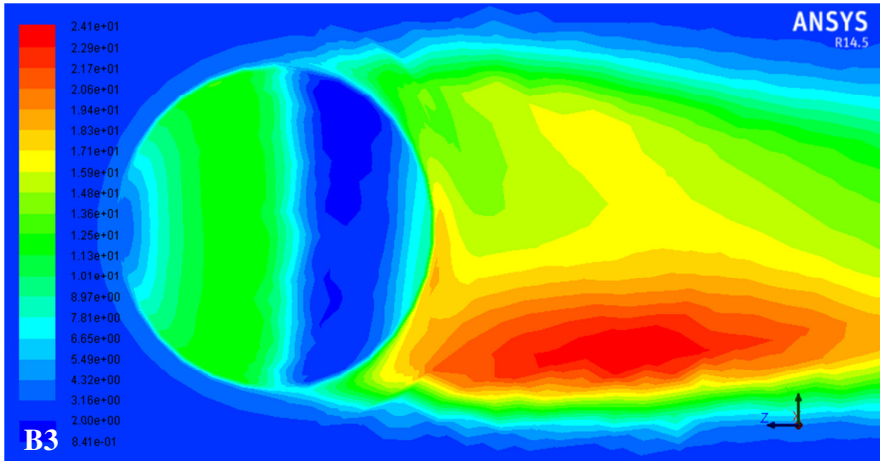

T = 308.15K, P = 65bar

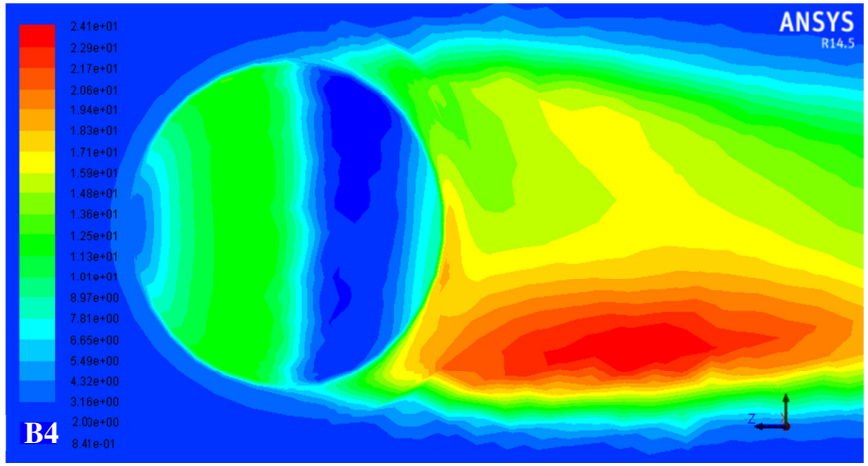

T = 308.15K, P = 80bar

Appendix C3 – Contours of turbulent intensity for *Re* = 2,000 by using realizable *k*-ε turbulence model.

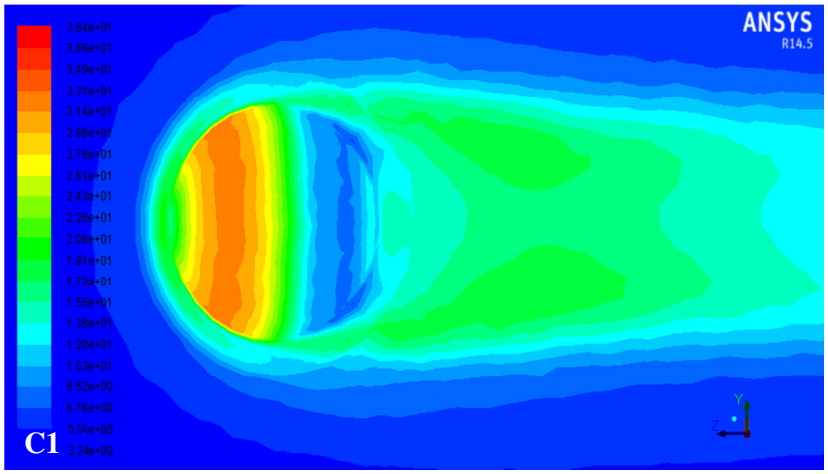

T = 298.15K, P = 65bar

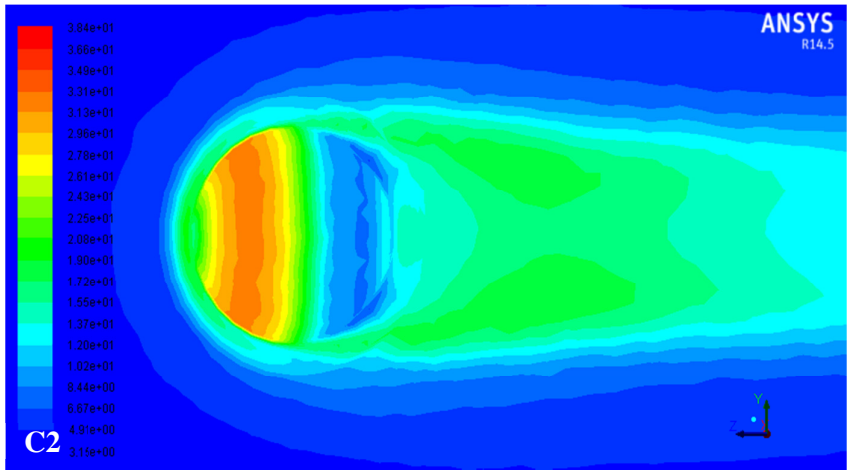

T = 298.15K, P = 80bar

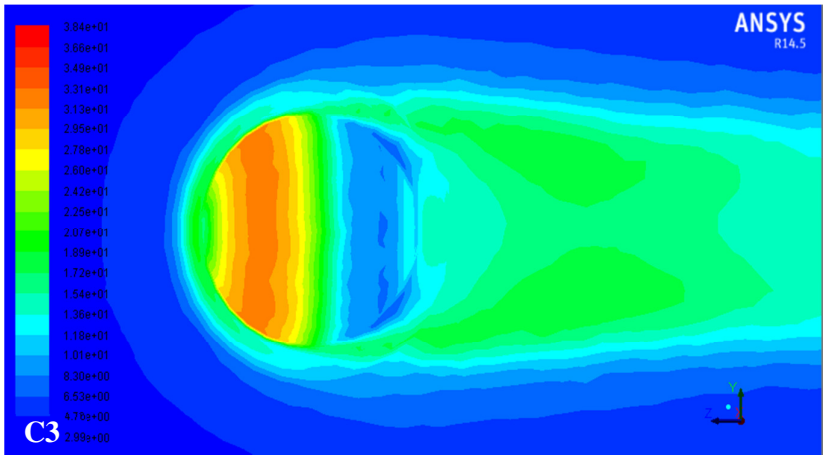

T = 308.15K, P = 65bar

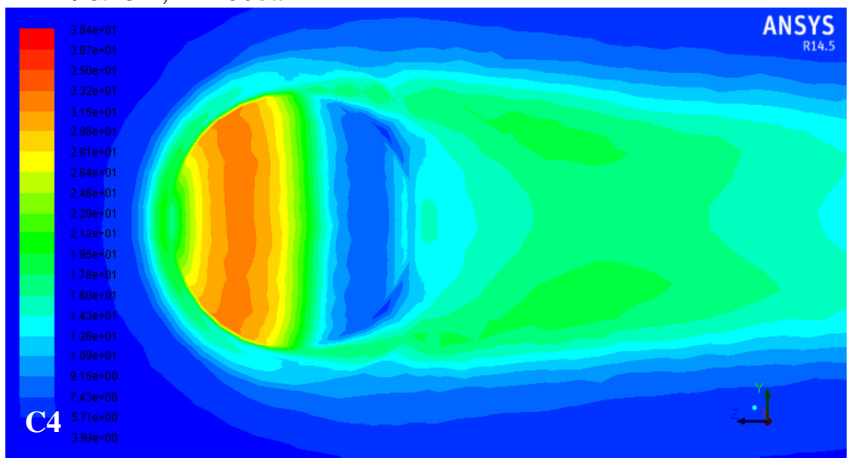

T = 308.15K, P = 80bar

Appendix C4 – Contours of turbulent intensity for *Re* = 20,000 by using realizable *k*-*ε* turbulence model.

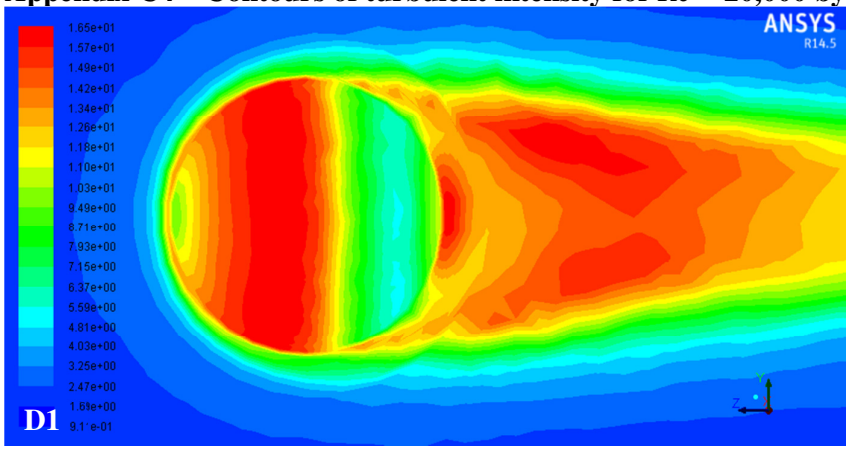

T = 298.15K, P = 65bar

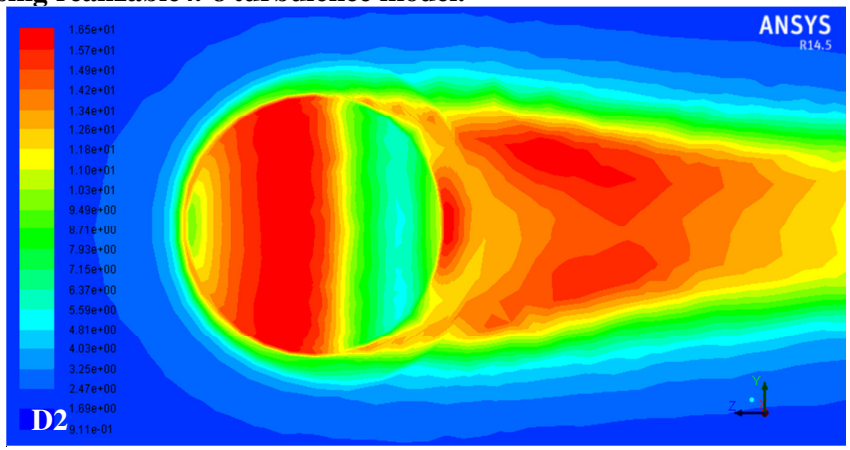

T = 298.15K, P = 80bar

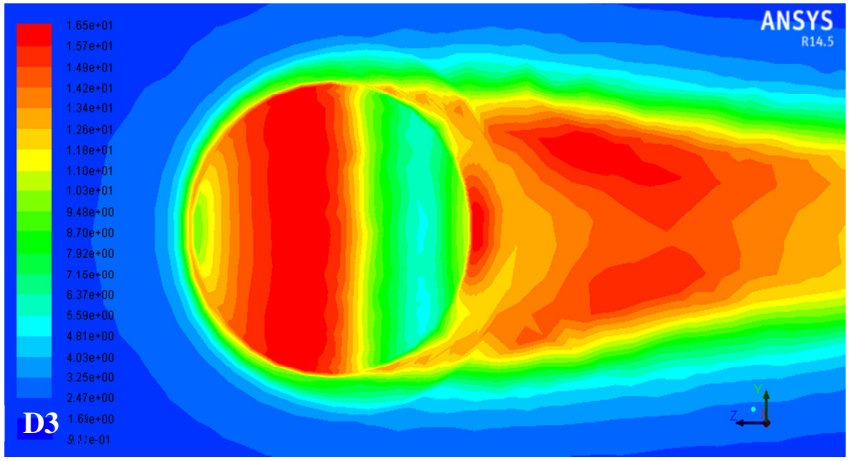

T = 308.15K, P = 65bar

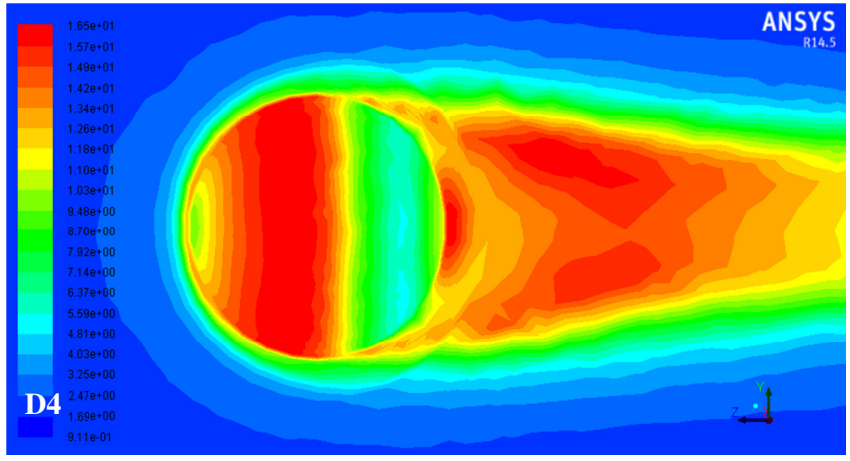

T = 308.15K, P = 80bar

Appendix C5 – Contours of turbulent intensity for *Re* = 2,000 by using RNG *k*-ε turbulence model.

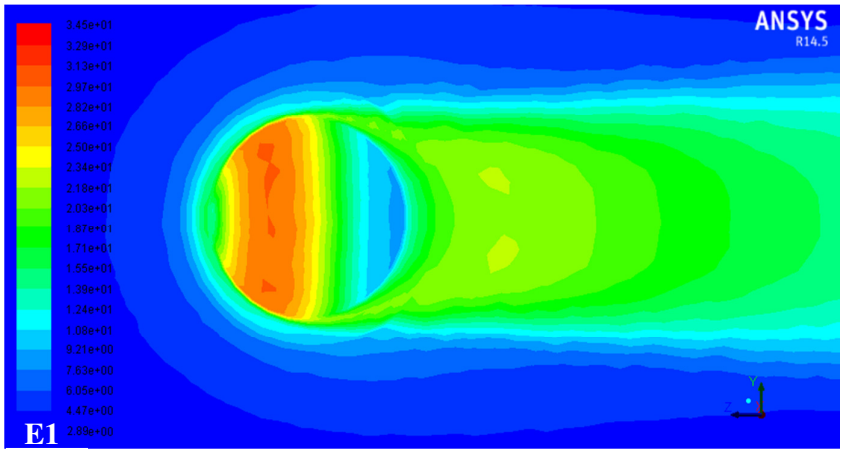

T = 298.15K, P = 65bar

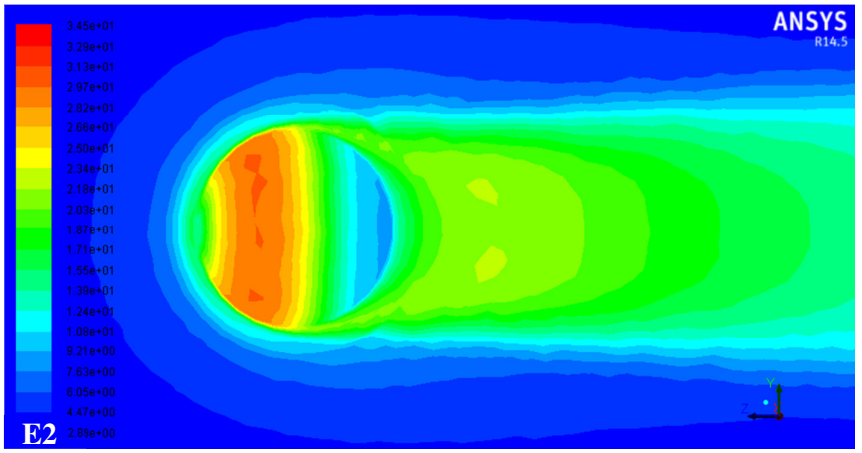

T = 298.15K, P = 80bar

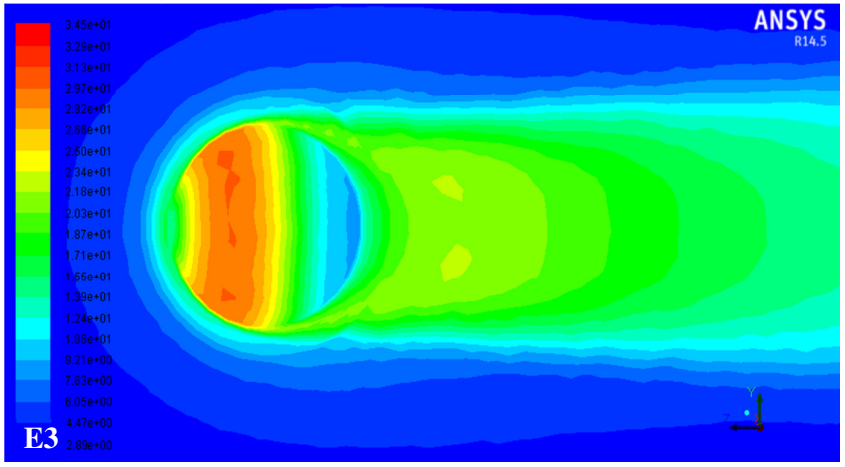

T = 308.15K, P = 65bar

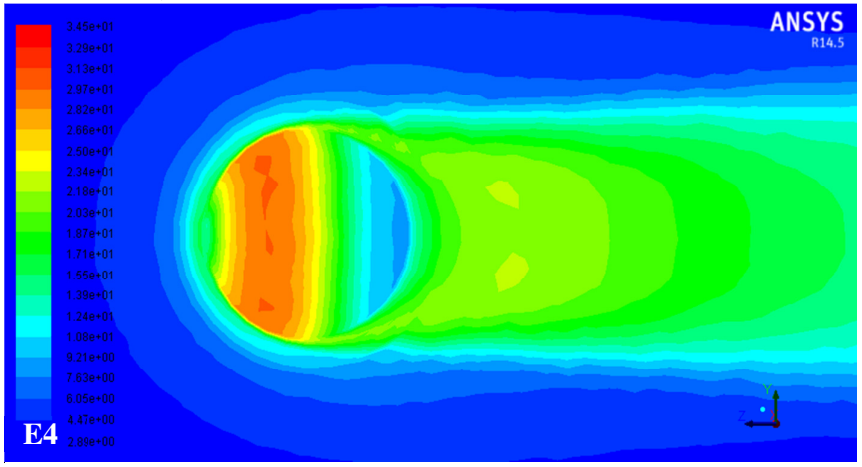

T = 308.15K, P = 80bar

Appendix C6 – Contours of turbulent intensity for *Re* = 20,000 by using RNG *k*-ε turbulence model.

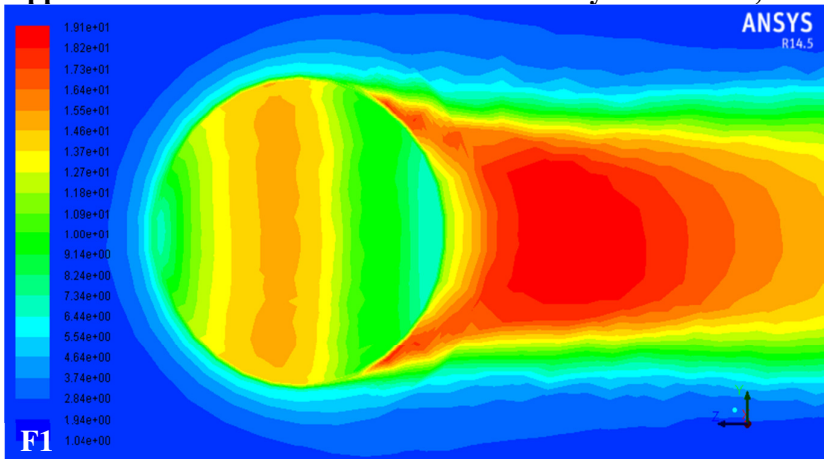

T = 298.15K, P = 65bar

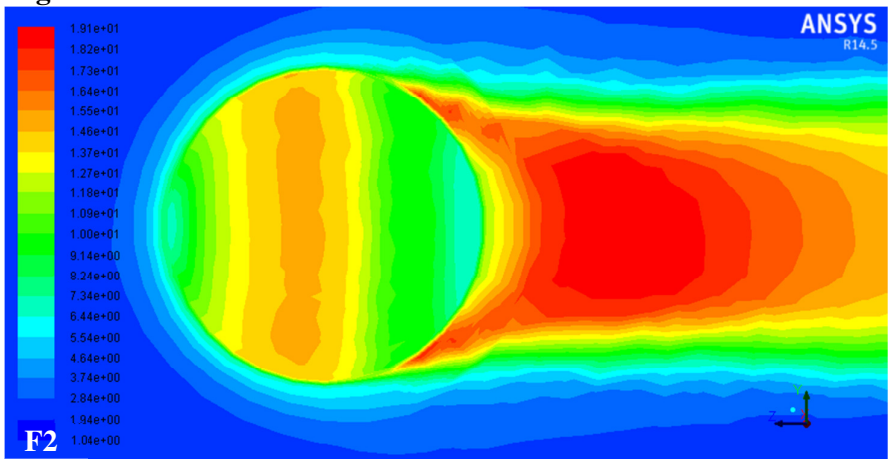

T = 298.15K, P = 80bar

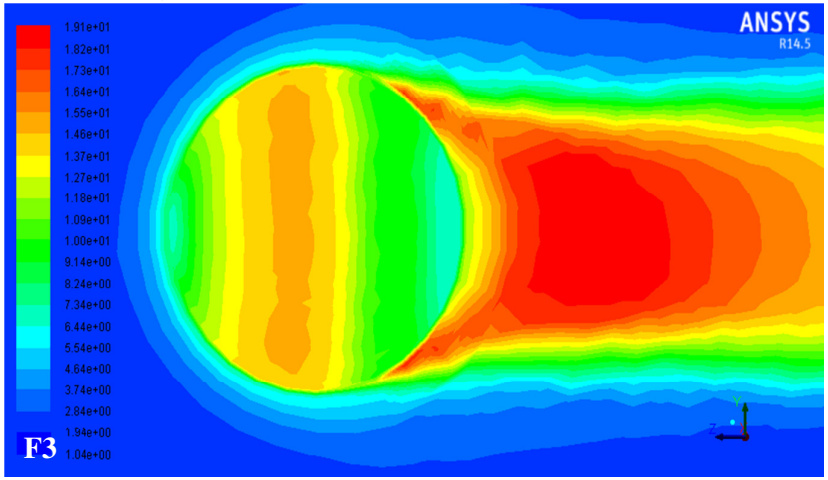

T = 308.15K, P = 65bar

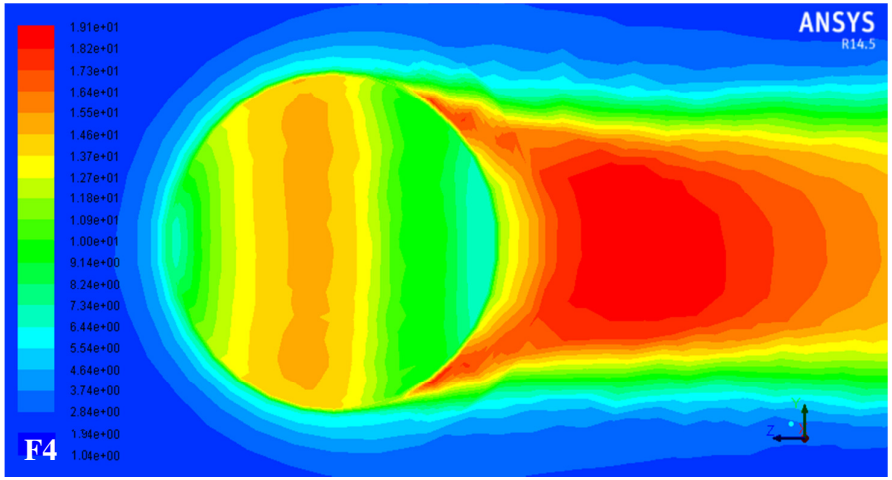

T = 308.15K, P = 80bar

Appendix C7 – Contours of turbulent intensity for *Re* = 2,000 by using standard *k*-ε turbulence model.

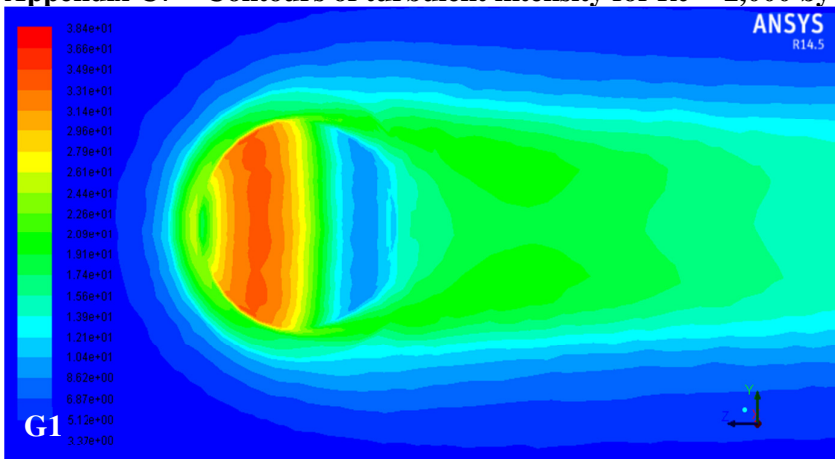

T = 298.15K, P = 65bar

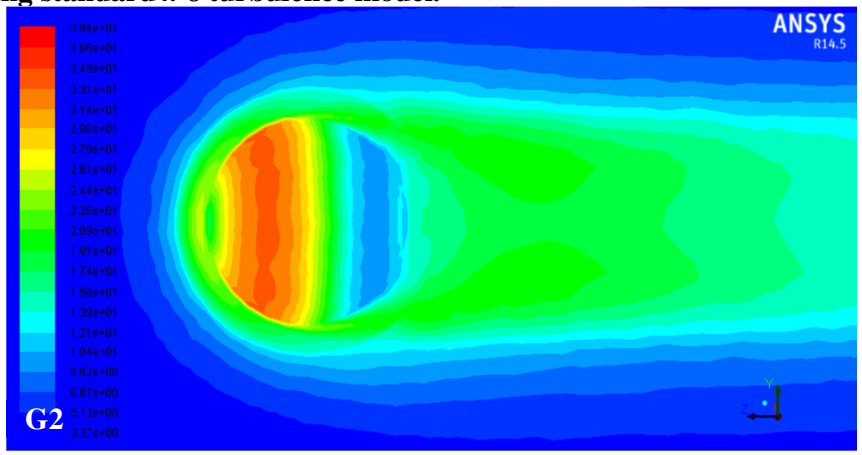

T = 298.15K, P = 80bar

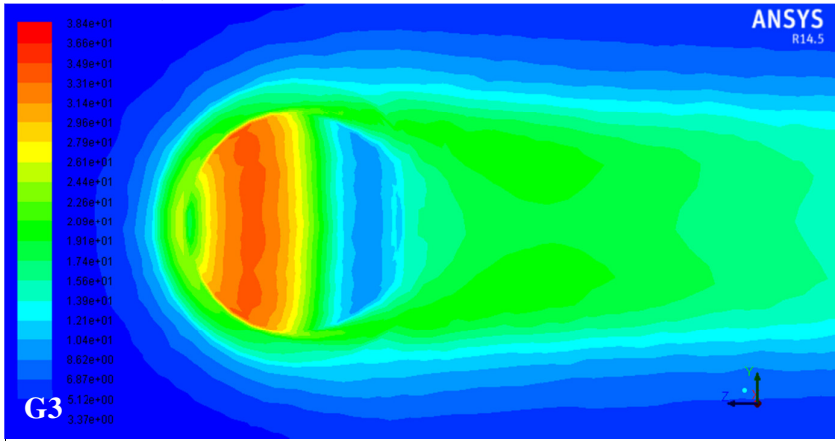

T = 308.15K, P = 65bar

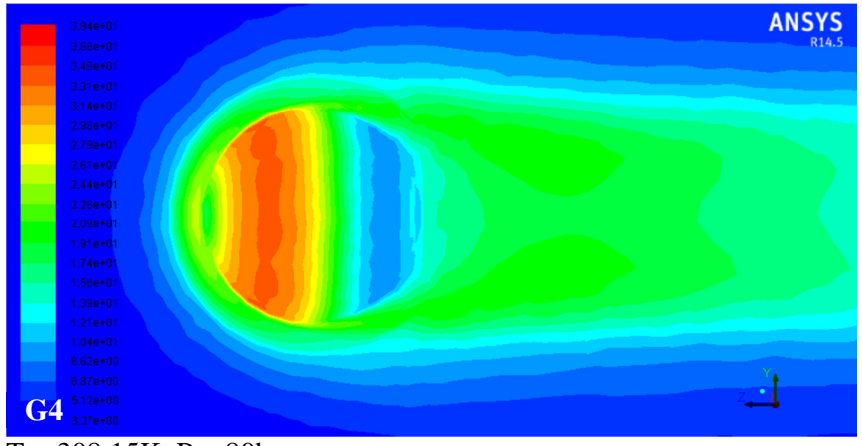

T = 308.15K, P = 80bar

Appendix C8 – Contours of turbulent intensity for *Re* = 20,000 by using standard *k*-*ε* turbulence model.

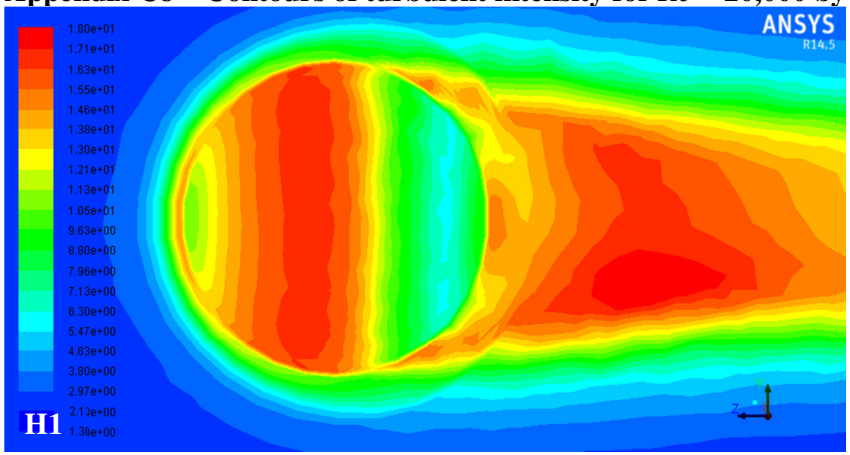

T = 298.15K, P = 65bar

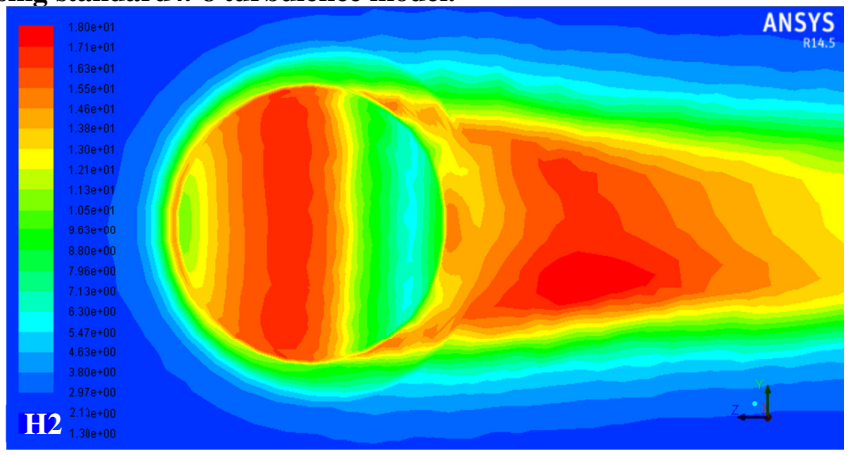

T = 298.15K, P = 80bar

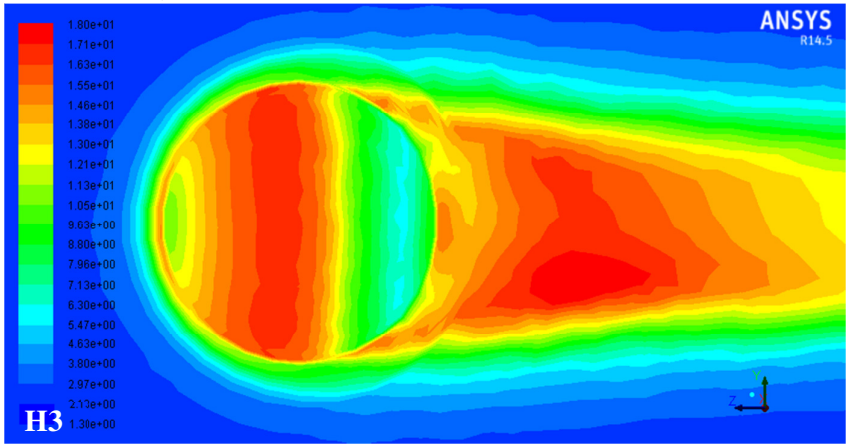

T = 308.15K, P = 65bar

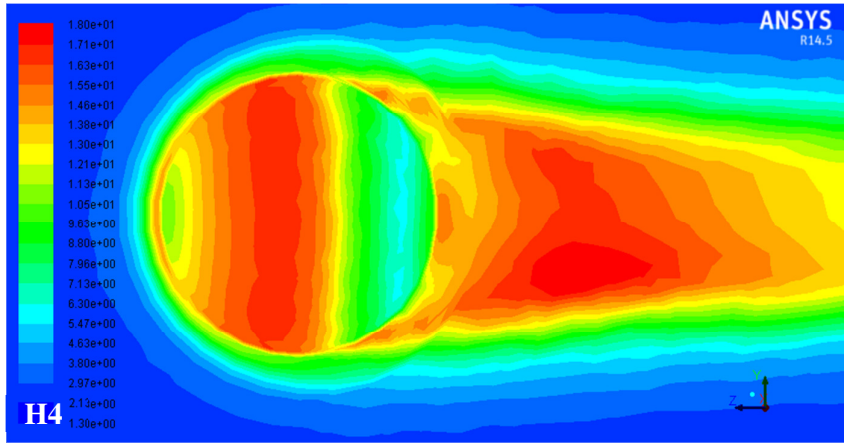

T = 308.15K, P = 80bar